

A Greenland-wide empirical reconstruction of paleo ice-sheet retreat informed by ice extent markers: PaleoGrIS version 1.0

Tancrède P.M. Leger¹, Christopher D. Clark¹, Carla Huynh², Sharman Jones³, Jeremy C. Ely¹, Sarah L. Bradley¹, Christiaan Diemont¹, Anna L.C. Hughes⁴

¹Department of Geography, University of Sheffield, Sheffield, S10 2TN, United Kingdom

²School of GeoSciences, University of Edinburgh, Drummond Street, Edinburgh, EH8 9XP, United Kingdom

³Aberystwyth University, Geography and Earth Sciences, Aberystwyth, SY23 3DB, United Kingdom

⁴Department of Geography, School of Environment, Education and Development, The University of Manchester, Manchester, M13 9PL, United Kingdom

Correspondence: Tancrède P. M. Leger (t.p.leger@sheffield.ac.uk): personal address: tankleger@gmail.com

Abstract. The Greenland Ice Sheet is a large contributor to global sea-level rise, and current mass losses are projected to accelerate. However, model projections of future ice-sheet evolution are limited by the fact that the ice sheet is not in equilibrium with present-day climate, but is still adjusting to past changes that occurred over thousands of years. Whilst the influence of such committed adjustments on future ice-sheet evolution remains unquantified, it could be addressed by calibrating numerical ice sheet models over larger timescales and, importantly, against empirical data on ice margin positions.

To enable such paleo data-model interactions, we need Greenland-wide empirical reconstructions of past ice-sheet extent that combine geomorphological and geochronological evidence. Despite an increasing number of field studies producing new chronologies, such a reconstruction is currently lacking in Greenland. Furthermore, a time-slice reconstruction can help: i) answer open questions regarding the rate and pattern of ice margin evolution in Greenland since the glacial maximum, ii) develop a standardised record of empirical data, and iii) identify [understudied](#) sites for [new](#) field campaigns. Based on these motivations, we here present PaleoGrIS 1.0, [the first](#) Greenland-wide isochrone reconstruction of ice-sheet extent evolution through the Late-Glacial and early-to-mid Holocene informed by both geomorphological and geochronological markers. Our isochrones have a temporal resolution of 500 years and span ~7.5 kyr from approximately 14 to 6.5 kyr BP. We here describe the resulting reconstruction of the shrinking ice sheet and conduct a series of ice-sheet wide and regional analyses to quantify retreat rates, areal extent change, and their variability across space and time. During the Late-Glacial and early-to-mid Holocene, we find the Greenland Ice Sheet has lost about one third of its areal extent (0.89 million km²). Between ~14 and ~8.5 kyr BP, it experienced a near constant rate of areal extent loss of 170 ± 27 km² yr⁻¹. We find the ice-sheet-scale pattern of margin retreat is well correlated to atmospheric and oceanic temperature variations, which implies a

high sensitivity of the ice sheet to deglacial warming. However, during the Holocene, we observe inertia in the ice-sheet system that likely caused a centennial to millennial-scale time lag in ice-extent response. At the regional scale, we observe highly heterogeneous deglacial responses in ice-extent evident in both magnitude and rate of retreat. We hypothesise that non-climatic factors, such as the asymmetrical nature of continental shelves and onshore bed topographies, play important roles in determining the regional-to-valley scale dynamics. PaleoGrIS 1.0 is an open-access database designed to be used by both the empirical and numerical modelling communities. It should prove a useful basis for improved future versions of the reconstruction when new geomorphological and geochronological data become available.

35

40

45

50

55

60

65

1 Introduction

The Greenland Ice Sheet holds an estimated ~ 7.4 m of global sea-level equivalent (Morlighem et al., 2017). It is currently experiencing mass loss at a rate of ~ 150 Gt yr^{-1} (over the 1992-2018 period; The IMBIE Team, 2019; Otosaka et al., 2023), making it a large contributor to current global mean sea-level rise. In a warming world, these losses are projected to accelerate (Meredith et al., 2019), with the latest Greenland Ice Sheet Model Intercomparison Project (ISMIP6) estimating a contribution to global mean sea-level rise of 32 ± 17 and 90 ± 50 mm by year 2100 for the RCP2.6 and RCP8.5 greenhouse gas concentrations scenarios, respectively (Goelzer et al., 2020). The robustness of such projections are limited by the short time span of instrumental evidence (10s to 100 years) used for verification and testing (Larsen et al., 2015). This is problematic because ongoing and future ice sheet mass losses are not exclusively a consequence of contemporary and future climate, but also represent adjustments to climate variations stretching further back in time (100s to 1000s of years; Rogozhina et al., 2011; Yang et al., 2022). As few models include the committed response to late-Quaternary environmental changes, current projection simulations might effectively be starting from ~~the wrong~~ a possibly unrealistic state, whose influence is thus far unquantified. Consequently, improved empirical reconstructions of late-Quaternary ice sheet evolution may be useful for refining future predictions of mass loss and global sea-level rise, by enabling the calibration of ice sheet models over larger timescales encompassing thousands of years (e.g. Lecavalier et al., 2014; Albrecht et al., 2020).

The response of the ice sheet to climate change during the Late-Quaternary likely contributes to major imbalances in its current state (Calov & Hutter, 1996), yet many key questions pertaining to this time remain unresolved. The position, rate, and pattern of ice margin retreat during the Late-Glacial and early-to-mid Holocene periods (between ~ 14 and ~ 6 kyr BP) remains ~~poorly~~ heterogeneously constrained in numerous regions. During that time, the ice sheet was responding to rapid and high-amplitude fluctuations in atmospheric and oceanic boundary conditions (e.g. the Bølling-Allerød Interstadial; Buizert et al., 2018), whilst also adjusting to fast rates of relative sea level change following the demise of other ice sheets ~~(e.g. during Meltwater Pulse 1A; Lin et al., 2021)~~. Consequent changes in ice sheet margin, volume, and surface mass balance were likely associated with modifications to the configurations of ice divides and to the position and discharge regimes of major ice streams (e.g. Franke et al., 2022). A key question concerns how far the ice sheet retreated behind its contemporary margin in response to the warming of the Holocene Thermal Maximum (10-5 kyr BP; Weidick et al., 2004; Cartapanis et al., 2022), a possible analogue to atmospheric warming expected in future decades (Funder et al., 2011). Calibrating model simulations against known Holocene margin positions around the full ice sheet perimeter might help answer this latter question.

The Greenland Ice Sheet has been subject to an increasing number of field studies reconstructing the deglacial evolution of the former ice-sheet margin, both on land and offshore. These typically use geomorphological, sedimentological, and geochronological dating analyses (e.g. Ten Brink & Weidick, 1974; Hjort, 1979; England, 1985; Bennike & Weidick, 2001;

Hughes et al., 2012; Briner et al., 2014; Larsen et al., 2014; Young et al., 2021; Garcia-Oteyza et al., 2022; Sbarra et al., 2022).

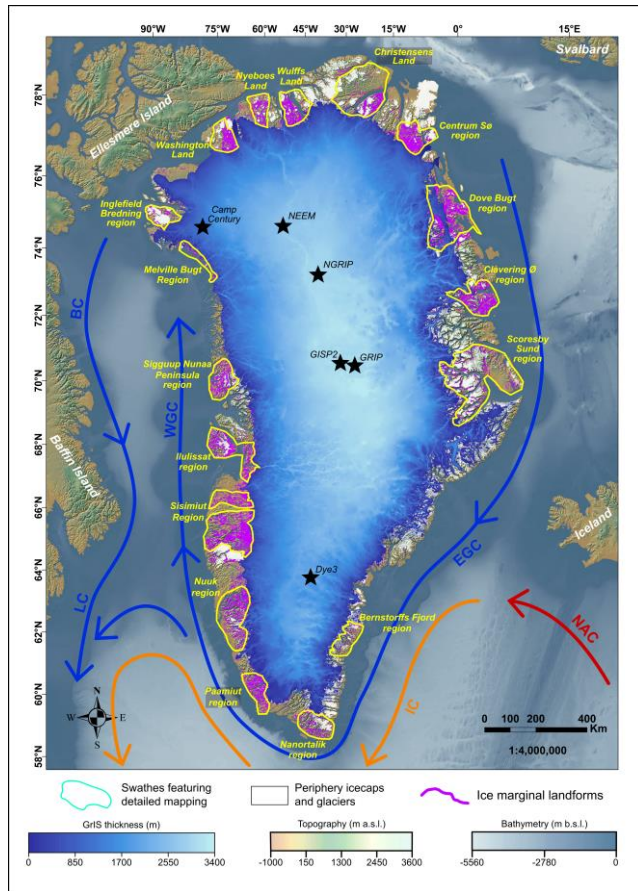
100 This growing library of geological evidence enables an improved understanding of the ice sheet response to deglacial climate change, at both regional and continental scale (Sinclair et al., 2016). However, to our knowledge, it appears that a Greenland-Ice-Sheet wide reconstruction with an open-access, reproducible database of geomorphological and geochronological evidence is lacking. Such a product would prove useful to both the modelling and empirical glaciology communities. It would enable ice-sheet scale analyses, help keep a standardised record of dating investigations, facilitate targeting ~~of understudied~~[new study](#) regions for future fieldwork, and provide a reconstruction for calibrating ice sheet model simulations. We note that ice-sheet wide summary datasets of accumulated evidence have played an essential and enabling role in advancing the understanding of other paleo ice sheets and in answering key glaciological questions on former ice dynamics (e.g. Dyke, 2004; Bentley et al., 2014; Hughes et al., 2016; Davies et al., 2020; Dalton et al., 2020; Clark et al., 2022).

110 Based on motivations outlined above, we present an ice-sheet wide isochrone reconstruction of the Greenland Ice Sheet's Late-Glacial and early-to-mid Holocene evolution informed by an ice-sheet scale dataset of geomorphological and geochronological ice extent markers, compiled in an open-access database. This reconstruction, hereafter referred to as PaleoGrIS 1.0, has a temporal resolution of 500 years, and spans 7.5 thousand years, between ~14 and ~6.5 kyr BP, the period bracketing most terrestrial landform evidence of ice margin change. This reconstruction represents a first attempt at combining both geochronological and geomorphological records to estimate the pattern and timing of the ice sheet deglacial retreat. In this manuscript, we describe our methodology in detail to make the reconstruction transparent and reproducible, with the hope that improved versions of PaleoGrIS can be produced as more empirical evidence arises. We use our isochrone reconstruction to conduct a series of ice-sheet wide and regional analyses to quantify the natural variation in retreat rates and areal extent change, and to address scientific questions on the nature and style of retreat dynamics in Greenland during the Late-Glacial to mid-Holocene period. We envisage that modellers can use this reconstruction to quantitatively compare deglacial simulations of the ice sheet with a vast quantity of empirical evidence. For example, the reconstruction (made available in both shapefile and NetCDF formats) could be used to quantitatively score model simulations ran as part of ensemble experiments, and/or to narrow down parameter spaces when conducting model sensitivity analyses, by testing the fit with margin extent and retreat pace (e.g. Patton et al., 2017; Ely et al., 2019; Pittard et al., 2022).

Field Code Changed

125

130



135
140
145
150
155

160 Figure 1. Greenland geographical context, present-day ice sheet thickness (BedMachine v4; Morlighem et al., 2017), and location of
 165 18 regions (boxes outlined in light green) where detailed ice-marginal landform mapping (displayed in purple) was conducted as
 part of this study. Note few areas were mapped in detail in the southeast due to relative lack of ice-free land. A simplified pattern of
 contemporary ocean circulation is represented, after Yang et al. (2016; Fig. 1); whereby red and orange arrows symbolize warmer
 Atlantic-origin water while blue arrows represent colder Arctic-origin water. NAC, IC, EGC, WGC, BC, and LC stand for North
 Atlantic, Irminger, East Greenland, West Greenland, Baffin, and Labrador Currents, respectively. The Digital Elevation Model
 (DEM) displaying both topographic and bathymetric data is from the GEBCO 2022 release (450 m resolution). Geographical extent
 of Greenland periphery icecaps and glaciers (white polygons) is from BedMachine v4. The locations of main Greenland ice cores
 (further mentioned in text) are shown by black stars. All data (here and in subsequent figures) are displayed projected to the WGS
 84 / NSIDC Sea Ice Polar Stereographic North coordinate reference system.

170

2 Methods

2.1 Geomorphological reconstruction of ice retreat patterns

175 Across Greenland's exposed land area there has been a rich but sporadic field collection of landform and sedimentary evidence
for former ice margin positions. These studies have been based on field investigation and mapping from aerial photographs or
satellite images (e.g. Weidick, 1968; 1971; Ten Brink & Weidick, 1974; van Tatenhove et al., 1996; Roberts et al., 2009; Levy
et al., 2012; Young et al., [2013](#)[2013b](#)), and more recently using Digital Elevation Models (DEM, e.g. Carrivick et al., 2017;
Pearce et al., 2018). Such investigations have typically mapped individual moraines, meltwater channels, and trimlines to
180 define former ice margin positions, which were then used to build local reconstructions of ice margin retreat. This information
covers a small fraction (<10%) of the land area leaving most of Greenland's ice marginal history unexplored. The release of
the 2m ArcticDEM (Porter et al., 2018) for the whole of Greenland provides a consistent dataset that has the potential to
revolutionise our understanding of Holocene ice retreat from the Greenland coast to the present-day ice sheet margin position.
Motivated by the availability of this new resource, we devised a mapping scheme and protocol that could capture the first-
185 order pattern of retreat for the whole of Greenland's terrestrial ice sheet periphery, an area of 430,500 km². We did not identify
and map every ice marginal landform from the ArcticDEM, as this would represent a decade-long task. Instead, we sampled
the area in sufficient detail to provide the first landform-based reconstruction.

2.1.1 Geomorphological mapping

190

We focussed our investigation on landforms indicating the position and shape of former Greenland-Ice-Sheet margins, paying
less attention to peripheral ice caps and mountain glaciers. To capture high-resolution details of ice marginal retreat across the
whole area and with a consistent approach is a challenge. To accomplish this, we adopted a sampling approach where for some
regions, that we called 'swathes', we investigated and mapped ice-marginal landforms in detail (e.g. Fig. 1-3). For the
195 intervening areas between swathes, we only identified the most prominent landforms that would permit us to connect paleo
ice margins across these areas, joining up swathe to swathe (see section 2.1.2). Eighteen swathes were chosen based on
presenting especially dense and well-preserved ice-marginal landforms (Fig. 1), to be positioned approximately evenly around
the ice sheet perimeter, and which covered ~60 % of Greenland's ice-free periphery. Although it was beyond the scope of this
continental-scale investigation to map all ice marginal landforms identifiable from the ArcticDEM, such an endeavour would

200 be a valuable future goal. We suggest the main focus should be to pursue mapping efforts in between the 18 swathes, which could contribute to updating future versions of the PaleoGrIS database.

All geomorphological mapping was conducted using remotely-sensed data. Identification of ice marginal landforms was carried out using the 2m ArcticDEM (Porter et al., 2018) and the 30m ALOS WORLD 3D (AW3D30) DEM¹. As recommended by Smith & Clark (2005), optimised orthogonal hillshaded relief models of 315° and 45° azimuth angles and 45° inclination were toggled between to minimise azimuth biasing and better identify landforms of interest. Moreover, to aid us in distinguishing glaciogenic sediments from bedrock features, Google Earth Pro software was used for consulting three-dimensional visualisations of satellite imagery (as recommended by Chandler et al., 2018). All mapped landforms were digitised manually as shapefiles in the WGS 84 / NSIDC Sea Ice Polar Stereographic North (EPSG code: 3413) reference coordinate system. To remain consistent throughout, and to avoid introducing bias from other investigators' landform interpretations, our mapping was conducted without input from previous mapping investigations. Furthermore, mapping was not conducted at a fixed spatial scale, but by zooming in or out to enable better visualization of spatially-variable landform details.

215 The main indicators of former ice extent were terminal and lateral moraine ridges, more expansive moraine complexes, hummocks and hummocky ridges, lateral meltwater channels and trimlines. These landforms were interpreted and identified based on their morphology and texture, their position in relation to the wider topographic setting, and following criteria for landform interpretation as detailed in Benn & Evans (2014), Chandler et al. (2018), Barr & Clark (2009), Rootes & Clark (2020), and Leger et al. (2020). The most numerous landforms were moraine ridges, which are typically discerned on DEM hillshades as arcuate, steep-sided, sometimes sinuous ridges with positive relief and often displaying sharp crests (e.g. Fig. 2). Given our aim of covering the entire landmass in a single pass with a small number of investigators, we did not individually map and classify landforms into their respective types (e.g. moraine ridge, meltwater channel). Instead, we captured and summarised information from these landforms by digitising lines all grouped into a single layer (shapefile) called 'ice marginal landforms' (Figs. 2,3). ~~Based on~~Due to a lack of pre-LGM ice margin chronologies across Greenland, and following the assumption that glaciogenic deposits relating to previous glaciations were overridden during the last glaciation (Funder et al., 2011) and ~~unlike~~thus less likely to be preserved; (with exceptions: i.e. Mejdahl & Funder, 1994; Kelly et al., 1999), we ~~consider~~adopt the assumption that our mapped ice-marginal landforms ~~to have been~~were deposited during the last deglaciation, between ~17 kyr BP and present.

230

¹ AW3D30: <https://www.Forc.jaxa.jp/ALOS/en/aw3d30/>

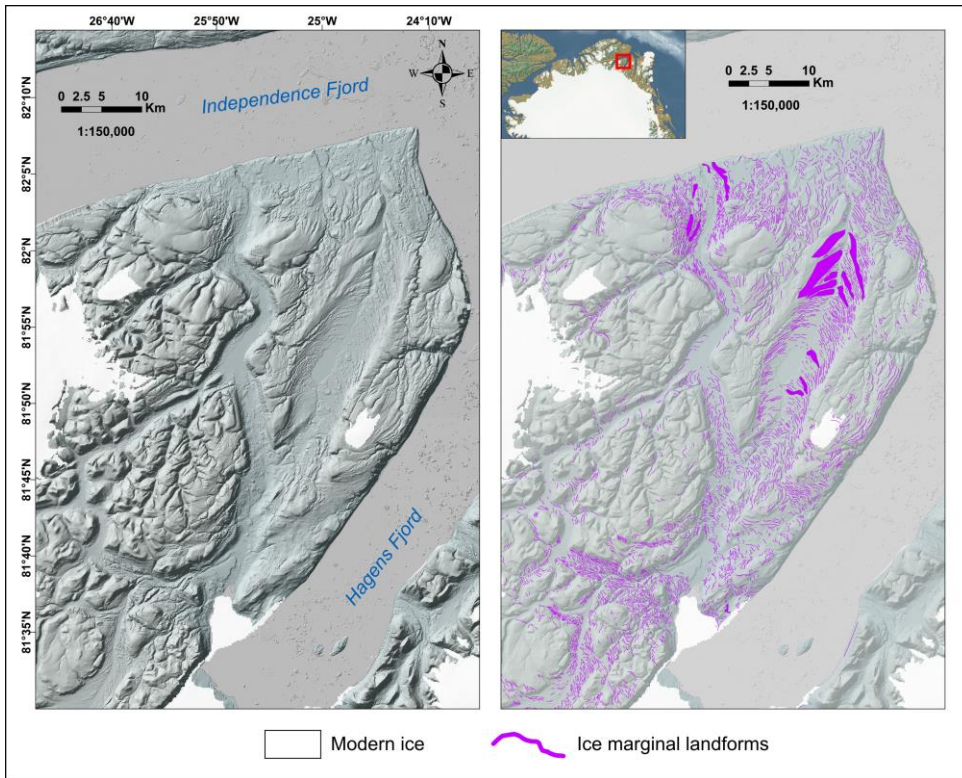


Figure 2. Comparison between DEM hillshade (light azimuth: 315°, incline: 45°) of the 2 m spatial resolution ArcticDEM (Porter et al., 2018) on the left-hand panel, and the same area with our ice-marginal landform mapping superimposed (right-hand panel). The area presented here is part of J.C. Christensen Land in North Greenland, as highlighted by the red box in figure inset. This region displays remarkable preservation and spatial density of terminal and lateral moraine rides, moraine complexes, lateral meltwater channels and trimlines.

235

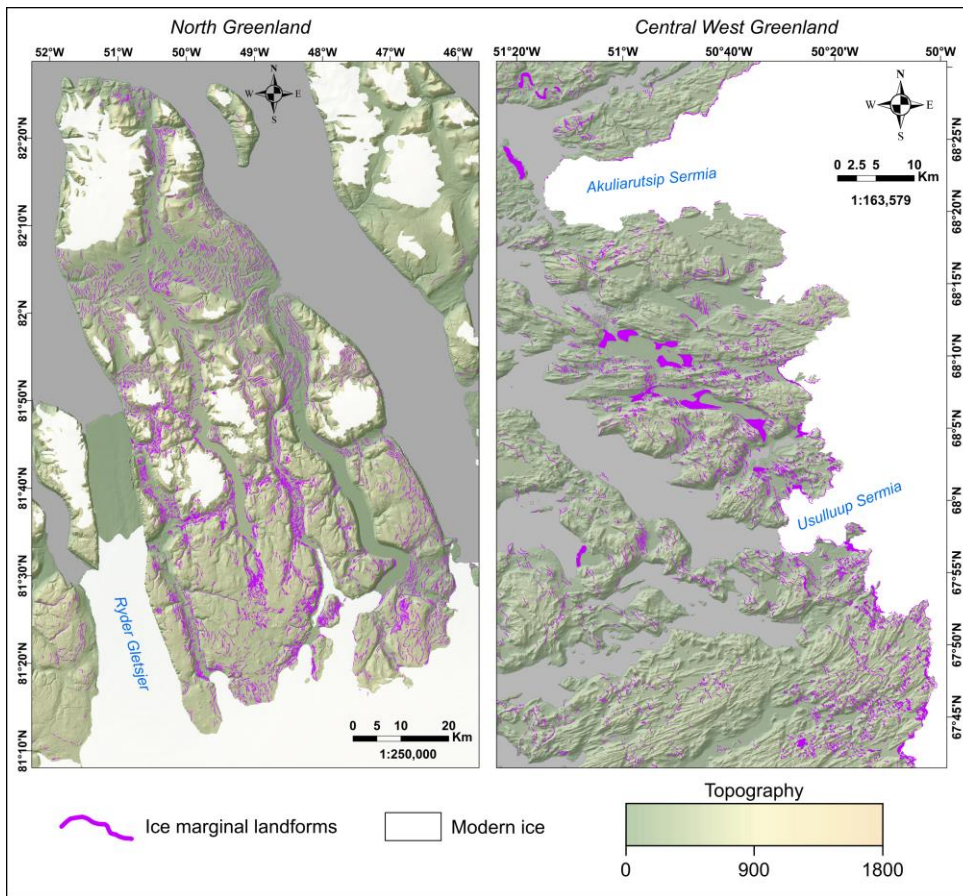
240

245 **2.1.2 Establishing an internally - consistent map of retreat pattern**

The high number (n = 194,302) of ice marginal landforms identified inhibited reconstruction at an ice sheet wide scale. Thus, the landform record underwent two stages of simplification/interpretation, to create a pattern of retreat, following the method employed by Clark et al. (2012). Firstly, ‘ice-marginal fragments’ were drawn to summarise the collective pattern where ice-marginal landforms could be reasonably linked in close proximity (thick black lines; Fig. 4). As a rule, ice-marginal fragments were mostly confined within the same valley unless the landform evidence was overwhelming for expanding beyond this scale. A further interpretive, and more speculative, step involved joining up these ice marginal fragments with ‘ice-marginal connectors’ (thick yellow lines; Fig. 4). These lines attempt to connect nearby ice-marginal fragments interpreted as being approximately time-synchronous. Such connectors are guided by less prominent or less dense spreads of landform evidence and by considering relationships between topography and plausible ice dynamics. As a result, the 18 swathes featuring more detailed mapping (Fig. 1) enable us to connect landforms with both ice-marginal fragments and connectors, while inter-swathe areas are mostly dominated by ice-marginal connectors. To interpolate ice marginal connectors across offshore areas, submarine topographic data was obtained from the 15 arc-second spatial resolution General Bathymetric Chart of the Oceans (GEBCO) 2022 release². Together, the ice marginal fragments and connectors depict the direction and relative age of ice marginal recession in undated time steps; the first-order pattern of ice marginal retreat (e.g. Fig. 4). The underlying assumption behind our first-order retreat pattern map is that retreat was generally considered to be monotonic unless there was geomorphological evidence for time-transgressive margins (e.g. cross-cutting moraines).

265

² https://www.gebco.net/data_and_products/gridded_bathymetry_data/



270 Figure 3. Examples of mapped ice-marginal landforms in two distinct regions displaying high density and preservation of ice-marginal glacial deposits. The mapped landforms are displayed overlaying topographic data from the AW3D30 DEM (30 m resolution). The left-hand panel presents mapping in a region of North Greenland (also referred to as Wulffs Land), while the right-hand panel focuses on the deglaciated region directly South of Disko Bay, in central West Greenland.

275

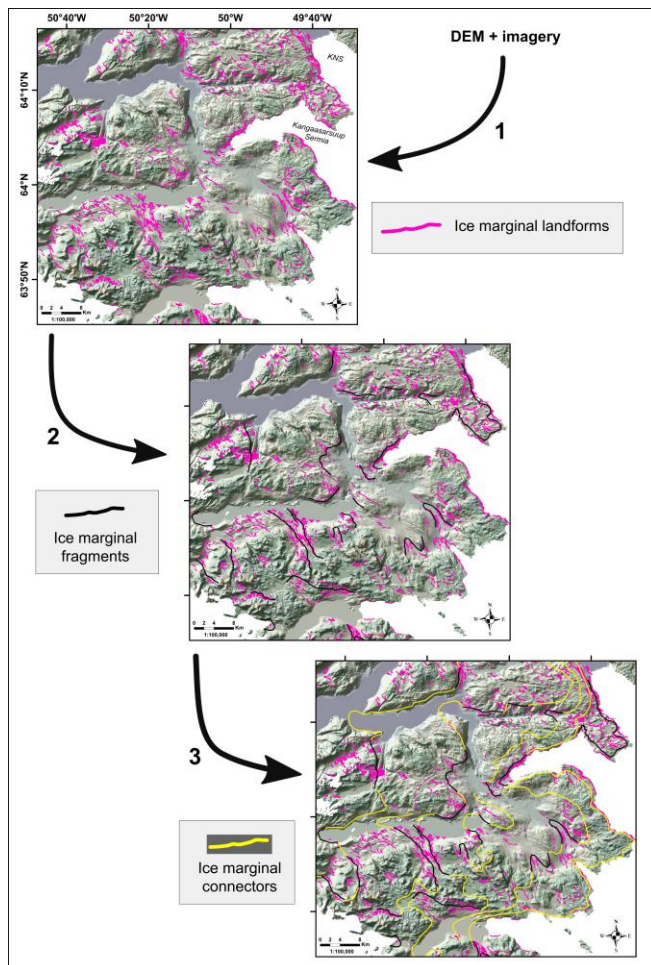


Figure 4. Visual and cartographic description of methodology followed to produce an ice-sheet-wide retreat pattern from DEM and imagery data. Our procedure involves three main steps of data generalization to incrementally summarise the “raw” topographic and imagery data, to near-continuous ‘ice marginal connectors’ interpreted as representing time-synchronous former ice sheet margins. The latter product is then used to inform our isochrone time-slice reconstruction, which involves adding geochronological information from our compilation of TCN and radiocarbon-derived event ages.

2.2 Compiling geochronological evidence

We attempt to compile published ages relating to the Greenland Ice Sheet grounded margin retreat from ~14 kyr BP through to the present-day for the entirety of the Greenland domain (Fig 1). We include ages from both Terrestrial Cosmogenic Nuclide (TCN) surface exposure dating and radiocarbon dating methods. Other dating methods (e.g. luminescence, lichenometry) were not included in this compilation as they have been applied much more sporadically for the specific objective of dating the former position of the ice-sheet margin in Greenland.

2.2.1 Terrestrial Cosmogenic Nuclide surface exposure ages

Compilation of ages

The geochronological component of the PaleoGrIS 1.0 database compiles published TCN surface exposure ages, and associated metadata, produced with the aim of dating the deglacial and Holocene ice-extent fluctuations of the Greenland Ice Sheet. Such ages estimate the timing of moraine emplacement and stabilisation, deposition of glacial erratics, or the abandonment of ice from exposed bedrock surfaces, all relevant for constraining the timing of ice retreat. These exposure ages were extracted predominantly from the maintained ICE-D Greenland online database³. In addition, a complementary review of the existing literature was conducted to compile relevant studies not currently included in ICE-D Greenland. Exposure ages dating the former margin evolution of periphery ice caps and mountain glaciers were intentionally excluded from our collection. Any new data added to ICE-D and any new study published later than our census date of the 21st October 2022, are not included in the PaleoGrIS 1.0 database.

Age calibration and re-calculation

All ages were re-calculated using the online calculator formerly known as the CRONUS-Earth online calculator version 3 (Balco et al., 2008). We do not apply an erosion rate correction to our exposure age calculations. We use the LSDn scaling scheme (Lifton et al., 2014), and the ¹⁰Be West Greenland production rate (Young et al., 2013a) obtained from the ICE-D online calibration database (<http://calibration.ice-d.org/>). Furthermore, no corrections were applied for post-exposure isostatic and/or tectonic uplift or subsidence, which given the young nature of the ages (<14 kyr BP) and the relatively low magnitude of surface elevation change (50-120 m) related to glacial isostatic adjustment during the Holocene, is not thought to cause age offsets greater than analytical uncertainties in most Greenland regions (Jones et al., 2019). To remain consistent across the domain, no corrections were applied for post-exposure vegetation or snow cover. Final exposure ages are reported

³ ICE-D Greenland: <https://version2.ice-d.org/greenland/publications>

in calendar years (or kyr) before present (BP), with ‘present’ defined as the year of sampling. Nuclide concentrations and sample metadata were retrieved from ICE-D and/or from original publications when needed. When multiple ages were described by original publications as dating a single time-synchronous margin, these were here grouped and summarized by a ‘summary event age’ (Fig. 5) and uncertainty calculated using the population arithmetic mean and the 1σ standard deviation, respectively. No grouping of ages was applied if not clearly described in source study as dating the same event. While TCN exposure ages positioned on mountains can act as former ice thickness indicators (e.g. elevation dipstick models) they aren’t used directly by our isochrone reconstruction, but are included in the database as they may prove useful for comparing with modelled ice-sheet thickness predictions, for instance.

Age filtering and quality control

Stratigraphical and/or statistical outliers were removed from event-age calculations only when considered as such in original publications. The only exception to this is when sample coordinates provided in original publications were either missing or erroneous (e.g. plotting offshore or within the ice sheet). In this case, the age was considered an outlier and was not included in summary event age calculations. For a few more recent investigations (e.g. Søndergaard et al., 2020), in situ cosmogenic ^{14}C was also measured alongside ^{10}Be or ^{26}Al . When ^{14}C -derived exposure ages display younger exposure ages and are described by authors as presenting no or less nuclide inheritance than other nuclides, they were given priority in our summary event age calculations. Our database also includes the details of whether paired nuclide analysis on a given sample (e.g. $^{26}\text{Al}/^{10}\text{Be}$) suggests a complex exposure/burial history, and thus guides us to exposure ages that are likely too old to be considered in our Holocene retreat reconstruction. Furthermore, to help combine the geomorphological and geochronological evidence in a time-slice reconstruction of ice sheet evolution, TCN exposure ages compiled within PaleoGrIS 1.0 are provided a quality control rating and classified in three categories described as high, medium, and low confidence ages. The criteria list followed to apply this quality control is presented in Table 1, and is derived from the investigations of Hughes et al. (2016), Small et al. (2017), and Davies et al. (2020).

370

375

Table 1. Quality control assessment criteria list for TCN and radiocarbon summary event ages compiled in the PaleoGrIS 1.0 database. Criteria are adapted from Hughes et al. (2016), Small et al. (2017), and Davies et al. (2020) to fit the Greenland-specific context of numerical dating of former ice-sheet margin retreat.

Dating technique	Quality control rating	Criteria
Pre-requisites for all techniques	n/a	<ul style="list-style-type: none"> - All metadata required for age re-calculation/calibration is provided, including AMS standards for TCN exposure ages - Publication clearly indicates when multiple ages from a site date an event (i.e. map, table with groups, stratigraphic age model etc) - Details of geologic and stratigraphic context is provided - Analytical errors are provided and <10% of age
TCN exposure	High confidence	<ul style="list-style-type: none"> - Multiple (at least 3) ages dating an event, post outlier removal - Exposure ages dating single event display little scatter: acceptable reduced Chi-square statistic - No evidence of complex exposure/burial history - No indication of major nuclide inheritance or post-depositional disturbance signals
	Medium confidence	<ul style="list-style-type: none"> - Only 2 samples dating an event, but showing consistent ages (post outlier removal) - Only 1 sample but for which the ¹⁴C radionuclide was also measured, and it displays a consistent or younger exposure age than obtained with other nuclides - Only 1 sample reported to date an event, but located near other samples (< ~10 km) displaying summary event ages consistent with stratigraphic order of events
	Low confidence	<ul style="list-style-type: none"> - Only 1, geographically isolated sample dating an event (post outlier removal) - Multiple samples but highly scattered exposure ages - Multi-nuclide analysis shows complex exposure/burial history of sample(s) - Coordinates reported by author plot in odd location (e.g. at sea or on ice when study site is terrestrial), thus suggesting inaccurate geolocation measurement
Radiocarbon dating	High confidence	<ul style="list-style-type: none"> - 1 sample to date an event (post outlier removal) but terrestrial sample and species of macrofossil/microfossil is identified and clearly reported - Multiple (at least 2) consistent samples from a single location or stratigraphic sequence (post outlier removal) to date an event, and which include at least 1 terrestrial sample
	Medium confidence	<ul style="list-style-type: none"> - Multiple consistent ages to date an event but all marine radiocarbon ages - Dated material is clearly reported - 1 terrestrial sample to date an event but dated material is gyttja, peat, humic acid (soil related)
	Low confidence	<ul style="list-style-type: none"> - Only 1 terrestrial but bulk sediment sample to date an event - Only 1 marine radiocarbon age to date an event - Poor stratigraphic context with respect to studied event - Dated material isn't reported or specific enough to attribute a quality control rating - Coordinates reported by author plot in odd location (e.g. at sea or on ice when study site is terrestrial), thus suggesting inaccurate geolocation measurement

2.2.2 Radiocarbon ages

415

Compilation of ages

The PaleoGrIS 1.0 database also features a collection of Greenland-wide radiocarbon ages and associated metadata which provide minimum-limiting age estimates of organic deposition in ice-free conditions following ice retreat during the deglacial and Holocene periods. This collection of radiocarbon ages was assembled by consulting former ice-sheet-scale reviews by Bennike & Björck (2002), Dyke (2004), Sinclair et al. (2016), and Dalton et al. (2020). Other more regional reviews, including those by Rinterknecht et al. (2014), Dyke et al. (2014), Larsen et al. (2014), and Young et al. (2021), were also examined. Furthermore, a review of the existing literature was conducted with the aim of finding other relevant studies not included in the above. Any new radiocarbon date published after the 21st of October 2022, our census date, is not included in the PaleoGrIS 1.0 database.

425

Age calibration and re-calculation

All radiocarbon ages were consistently recalibrated using the IntCal20 curve (Reimer et al., 2020) for terrestrial samples, the Marine20 (Heaton et al., 2020) curve for marine samples, and the CALIB 8.2 online calibration software⁴. We report final calibrated ages and uncertainty as the midpoint \pm half of the calibrated age range at 95% probability (2σ). Calibrated ages are reported in calendar years (or kyr) before present (BP), with ‘present’ defined as year 1950 AD.

430

For marine samples, we apply a marine reservoir age correction protocol that attempts to consistently account for both spatial heterogeneity in the reservoir effect itself, and for variability between ΔR calibration sites. To do so, we calibrate all marine ages against the Marine20 curve using regional ΔR values obtained from the maintained online Marine Reservoir Correction Database⁵ (Reimer & Reimer, 2001). For each sample and location, a final ΔR value is obtained by computing the weighted mean of the 10 nearest available ΔR calibration sites, determined directly from the correction database. The reported final uncertainty following this calculation is the maximum of the standard deviation of ΔR and the weighted uncertainty in mean of ΔR (Bevington, 1969). Following this protocol, ΔR values in our database range from -113 to 73 years, while ΔR uncertainties range from 36 to 150 years. We note these ΔR values mostly overlap with the newest Greenland-specific marine reservoir age correction assessment of Pearce et al. (*in review*, submitted after our compiled ages were re-calculated). We acknowledge that for polar latitudes ($>50^\circ\text{N}$), calibrating marine radiocarbon ages against the Marine20 curve may be problematic, due to greater variability in ocean ventilation and air-sea gas exchange caused by fluctuations in sea ice extent

435

440

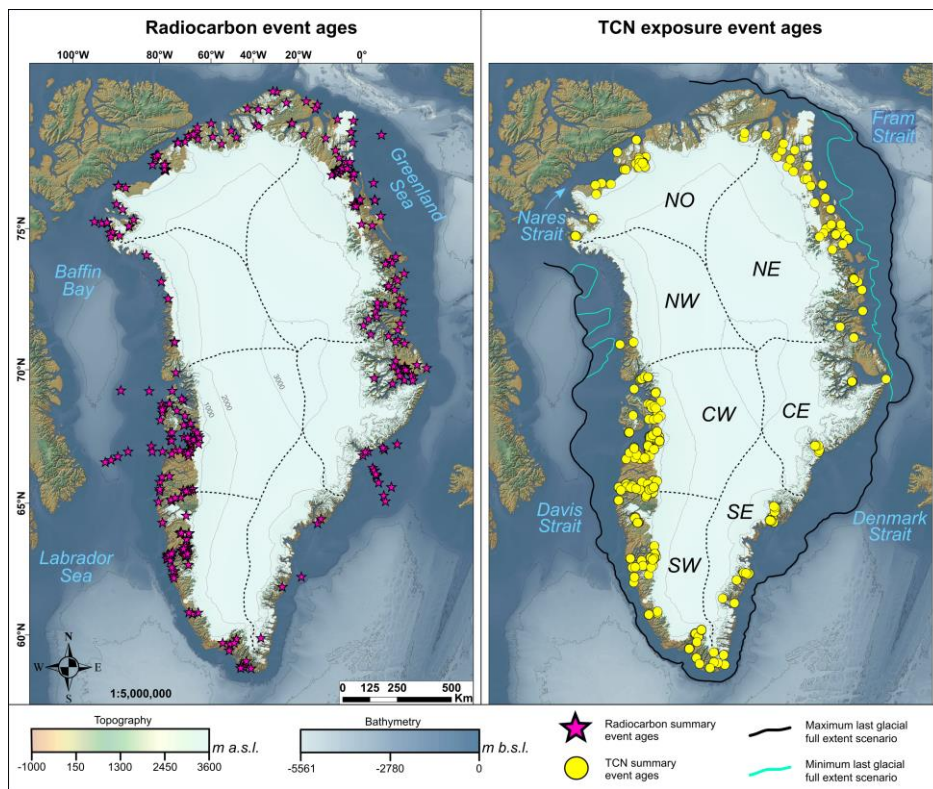
⁴ CALIB: <http://calib.org/calib/calib.html>

⁵ <http://calib.org/marine/>

and wind strength, leading to increased and more time-variable marine reservoir effects (Butzin et al., 2005; Heaton et al., 2022). However, this is more likely to be problematic during glacial periods (Reimer et al., 2020). For polar samples dating to the Holocene (11.5-0 kyr BP), Heaton et al. (2022) recommend calibrating directly against Marine20. Since the PaleoGrIS 1.0 reconstruction spans the Late-glacial and early-to-mid Holocene (14-6.5 kyr BP) period, and because 90% of the calibrated radiocarbon ages compiled in our database are younger than 11 kyr BP, we choose to treat all samples the same, for consistency.

Age filtering and quality control

Previous reviews and published studies were systematically filtered so that only radiocarbon dates produced with the aim to constrain the evolution of the ice sheet margin through time were compiled. Following this logic, only dated events that present a clear stratigraphic link to the evolution of the former ice sheet extent are incorporated in the database. In Greenland, a common example of such dates are multiple radiocarbon dates down a core of lacustrine sediments featuring a clear sedimentological transition from subglacial (e.g. till) to proglacial (e.g. silts and clays) deposits. In the latter case, and for any deglacial chronologies presenting multiple radiocarbon ages from a single core or single location, the oldest age of the sequence was considered the closest age estimate of ice-free conditions and organic deposition following ice retreat, and was thus retained as the summary event age (following Hughes et al., 2016; Small et al., 2017; Dalton et al., 2020) (Fig. 5). The data were also filtered so that radiocarbon ages dating the evolution of Greenland periphery ice caps and mountain glaciers were not included in this collection. Stratigraphical and/or statistical outliers were not included in the summary event age compilation when described as such in original publications. Samples featuring missing or erroneous geographical coordinates were also considered as outliers. Radiocarbon ages compiled within PaleoGrIS 1.0 are given a quality control rating and are classified in three categories described as high, medium, and low confidence ages. The criteria list followed to apply this quality control consistently through the dataset are displayed in Table 1.



480 **Figure 5. Spatial distribution of radiocarbon - derived (left-hand panel) and TCN exposure age - derived (right-hand panel)**
 485 **summary event ages (post filtering and statistics) used to produce the PaleoGrIS 1.0 isochrone reconstruction. Topographic and bathymetric data (GEBCO 2022 release) is overlaid with 1000 m interval contour lines. The dashed line shows our division scheme of the ice-sheet in seven main drainage regions that we refer to throughout the paper and in associated quantitative analyses, after the drainage basin sampling scheme of Rignot & Mougint (2012), labelled on the right hand panel. The right-hand panel also features lines denoting our estimations of maximum and minimum scenarios of last full glacial Greenland Ice Sheet extent (grounded ice only), based on a review of the literature (see section 2.6), and which informs the mapping of our outermost isochrones.**

Table 2. List of publications and associated numbers of compiled ages in PaleoGrIS 1.0 for TCN surface exposure dating.

TCN exposure ages			
Publication	Number of ages compiled	Publication	Number of ages compiled
Andersen et al. (2020)	13	Lesnek et al. (2018)	24
Balter-Kennedy et al. (2021)	5	Levy et al. (2012)	9
Briner et al. (2013)	2	Levy et al. (2016)	16
Carlson et al. (2014)	29	Levy et al. (2018)	16
Ceperley et al. (2020)	71	Levy et al. (2020)	41
Corbett et al. (2011)	30	Nelson et al. (2014)	11
Corbett et al. (2013)	19	Philipps et al. (2017)	6
Corbett et al. (2015)	28	Reusche et al. (2018)	33
Cronauer et al. (2016)	11	Rinterknecht et al. (2009)	12
Dyke et al. (2014)	23	Rinterknecht et al. (2014)	7
Garcia-Oteyza et al. (2022)	39	Roberts et al. (2008)	12
Hakansson et al. (2007)	4	Roberts et al. (2009)	16
Hakansson et al. (2007b)	7	Roberts et al. (2013)	17
Hughes et al. (2012)	12	Skov et al. (2020)	25
Kelley et al. (2012)	2	Søndergaard et al. (2019)	3
Kelley et al. (2013)	12	Søndergaard et al. (2020)	27
Kelley et al. (2015)	18	Winsor et al. (2014)	17
Lane et al. (2014)	15	Winsor et al. (2015)	47
Larsen et al. (2014)	47	Young et al. (2013a)	47
Larsen et al. (2018)	28	Young et al. (2013b)	5
Larsen et al. (2020)	43	Young et al. (2020)	62
Larsen et al. (2021)	9	Young et al. (2021)	61
Larsen et al. (2022)	47		

520

Table 3. List of publications and associated number of compiled ages in PaleoGrIS 1.0 for radiocarbon dating.

Radiocarbon ages			
Publication	Number of ages compiled	Publication	Number of ages compiled
Bennike (1987)	2	Kelly and Bennike (1985)	1
Bennike et al. (1994)	3	Kelly and Bennike (1987)	1
Bennike et al. (1999)	2	Kelly and Bennike (1992)	7
Bennike (2000)	4	Kelly and Funder (1974)	3
Bennike (2002)	19	Kelly et al. (1999)	3
Bennike et al. (2002)	6	Kuijpers et al. (2003)	1
Bennike (2008)	1	Landvik et al. (2001)	3
Bennike and Björck (2002)	7	Larsen et al. (2014)	15
Bennike and Wagner (2012)	1	Larsen et al. (2021)	4
Bennike and Weidick (2001)	75	Levy et al. (2017)	7
Bick (1978)	1	Lloyd et al. (2005)	2
Björck et al. (1994)	1	Long and Roberts (2002)	4
Blake (1987)	4	Long and Roberts (2003)	5
Blake (1992)	1	Long et al. (1999)	12
Blake (1996)	1	Long et al. (2003)	1
Bücher and Bennike (1996)	1	Long et al. (2006)	5
Briner et al. (2010)	3	Long et al. (2008)	2
Briner et al. (2013)	4	Manley and Jennings (1996)	1
Christiansen et al. (2002)	1	Marienfeld (1990)	3
Crane and Griffin (1959)	1	McCarthy (2011)	1
Cremer et al. (2001)	1	Nichols (1969)	1
Davies et al. (2022)	2	Ó Cofaigh et al. (2013)	5
Delibrias et al. (1986)	1	Perner et al. (2013)	4
Donner and Junger (1975)	3	Puleo et al. (2022)	1
Dowdeswell et al. (1994)	1	Shotton et al. (1974)	1
Eisner et al. (1995)	1	Simonarson (1981)	1
Englund (1985)	5	Smith and Licht (2000)	9
Fredsköld (1972)	2	Søndergaard et al. (2019)	1
Fredsköld (1973)	2	Sparenbom et al. (2006)	3
Fredsköld (1983)	7	Storms et al. (2012)	6
Fredsköld (1985)	2	Sugden et al. (1972)	1
Fredsköld (1995)	1	Tauber (1966)	1
Funder (1978)	2	Tauber (1968)	1
Funder (1982)	7	Ten Brink and Weidick (1974)	3
Funder (1990)	4	Trautman (1963)	1
Funder and Abrahamsen (1988)	2	Trautman and Willis (1966)	1
Funder and Hansen (1996)	2	Van Tatenhove et al. (1996)	3
Gulliksen et al. (1991)	1	Wagner et al. (2000)	2
Hakansson (1974)	1	Wagner and Møller (2002)	2
Hakansson (1975)	1	Washburn and Stuiver (1962)	1
Hakansson (1976)	1	Weidick (1968)	1
Hakansson (1987)	1	Weidick (1972)	3
Hansen (2001)	4	Weidick (1975)	4
Hansen et al. (2022)	2	Weidick (1976)	22
Hjort (1979)	8	Weidick (1977)	2
Hjort (1981)	4	Weidick (1978)	6
Hjort (1997)	2	Weidick and Bennike (2007)	10
Ingólfsson et al. (1990)	5	Weidick et al. (1990)	1
Ingólfsson et al. (1994)	1	Weidick et al. (1996)	1
Ives et al. (1964)	1	Weidick et al. (2004)	1
Jennings et al. (2002)	1	Willemse (2000)	1
Jennings et al. (2014)	1	Williams (1993)	6
Kaufman and Williams (1992)	1	Williams et al. (1995)	1
Kelly (1973)	2	Young et al. (2011a)	1
Kelly (1979)	1	Young et al. (2011b)	4
Kelly (1980)	1	Young et al. (2013)	3

555

2.2.3 The PaleoGrIS 1.0 geochronological database format

TCN and radiocarbon ages compiled were entered in two respective Excel (.xlsx) spreadsheets, made available in the PaleoGrIS 1.0 database⁶. Both spreadsheets (one for TCN and one for radiocarbon) document sample information and source publication details (also in Tables 2,3), metadata relevant to age calibration and re-calculations, all event identification and summary event ages, and age quality control attributions. A subset of these details including sample names, locations, source publications, summary event ages and uncertainties, were used to generate point shapefiles for use with any geographic information system software (e.g. ArcMap or QGIS). Further details concerning the several shapefiles published alongside this manuscript are described in the *Read Me* files provided in the online database.

565

2.3 Producing Greenland Ice Sheet-wide isochrones

Within the context of reconstructing past ice sheet extent, isochrones are defined as time-stamped and spatially-continuous [perimeters/margins](#) highlighting changes in the former spatial extent of an entire ice sheet over time. Reconstructing such continuous perimeters is a challenge given a fragmentary evidence base. Geochronological and geomorphological data available to empirically reconstruct isochrones are either point data (ages) or fragments of line data (e.g. moraine mapping). Such data are characterised by highly variable temporal and spatial densities and are associated with uncertainties of their own. Therefore, the task of drawing time-stamped and spatially-continuous ice sheet perimeters involves interpolating between empirical evidence and extrapolating across blank areas of the map (e.g. Stroeven et al., 2016; Hughes et al., 2016). The following paragraphs describe the methods followed to produce isochrones that combine geomorphological and geochronological evidence while separately accounting for temporal and spatial uncertainties in empirical data.

575

2.3.1 Isochrone time span, temporal resolution, and uncertainty

For PaleoGrIS 1.0, we map isochrones that delineate grounded ice only (and not floating ice fronts) (Fig. 6). Since Greenland ice-free land areas were deglaciated mostly during the Late-Glacial and early-to-mid Holocene periods, there is a higher density

⁶ Data available under this link:

of terrestrial TCN and radiocarbon dates displaying ages of between 12 and 6.5 kyr BP (Fig. 7). ~~The~~ Following the Holocene Thermal Maximum, between 6.5 kyr BP and 2 kyr BP, the number of available dates drop significantly (Fig. 7). ~~between 6.5 kyr BP and 2 kyr BP, when~~ This coincides with the ice sheet reaching its minimum Holocene extent (between ~7 and ~4.5 kyr BP), which in most Greenland regions was responding to the Holocene Thermal Maximum (Fig. 7). ~~At this time, the ice sheet is thought to have~~ either been as extensive as today, or more retreated around most of its perimeter than today's margin position (Larsen et al., 2015; Briner et al., 2016). After ~5-4 kyr BP, the onset of Neoglacial cooling caused ice-sheet re-advances culminating in the Little Ice Age, which explains the small relative increase in the number of dates in our compilation after 2 kyr BP (Fig. 7). Consequently, the time period featuring enough terrestrial geochronological evidence for reconstructing past retreat at the ice sheet scale currently spans only 6-7 kyr. Recent methodological and technological improvements to TCN exposure and radiocarbon dating now enable the production of Holocene ages with analytical uncertainties that can be less than to 500 and 200 years (at 1σ), respectively. For these reasons, we chose to produce ice-sheet-wide isochrones at 500-year temporal resolution between 12 and 6.5 kyr BP.

Between 14 and 12 kyr BP, when it is thought the ice sheet margin was predominantly marine terminating, and when less data is currently available, we chose to draw isochrones at 1000-year temporal resolution. Prior to this, between the ice sheet's last full glacial extent and 14 kyr BP, the ice-sheet is thought to have been mostly grounded on the presently-submerged continental shelf (Dalton & Funder et al., 2020). A few offshore sampling studies provide geochronological constraints for the approximate location of the grounded ice margin during this time period (e.g. Smith & Licht, 2000; Kuijpers et al., 2003; Ó Cofaigh et al., 2013). However, we believe such studies are currently too scarce and spatially scattered to enable tracing ice-sheet-wide isochrones between the last full glacial extent and 14 kyr BP, and hope such improvements can be made with future versions of this reconstruction, as more data from understudied/less studied regions arise. The PaleoGrIS 1.0 reconstruction therefore features 14 isochrones (or time slices) between 14 and 6.5 kyr BP.

In an attempt to account for uncertainties inherent to TCN exposure and radiocarbon dating, we chose to allocate a time range to individual isochrones, and thus to each time slice of our reconstruction (Fig. 6). For instance, the youngest and innermost isochrone of PaleoGrIS 1.0 is here referred to as the '7-6.5 kyr BP isochrone.' This means that we estimate the former margin to have been near the location of that isochrone line at any time between ~7 and ~6.5 kyr BP. This line was thus drawn to connect, as much as possible, the landforms and summary event ages comprised between 7.0 and 6.5 kyr BP, when rounded to the nearest 100 years. This approach is different from previous time-slice reconstructions that attributed a single timestamp to isochrones, and choosing to represent the dating uncertainty spatially by differentiating minimum, maximum, and/or optimum positions for isochrones for a given time slice (e.g. Dyke & Prest., 1987; Hughes et al., 2016; Davies et al., 2020; Dalton et al., 2020; Clark et al., 2022). Contrastingly, the PaleoGrIS 1.0 approach aims to more clearly distinguish and separate the temporal from the spatial uncertainties inherent to isochrone reconstructions. Isochrone temporal uncertainty is exclusively associated with the analytical and calculation/calibration uncertainties of numerical dates (TCN or radiocarbon), while

isochrone spatial uncertainty instead results from spatially variable density of geochronological and geomorphological evidence. Here, the latter is treated by attributing various confidence levels along a single isochrone line (more details in section 2.3.5). Therefore, our approach allows comparing numerical ice-sheet model outputs to a single isochrone, while enabling model time to vary within our isochrone temporal error range, and thus account for analytical uncertainty in geochronological data. To help modellers use the PaleoGrIS 1.0 isochrones in their model-data comparison procedures, our online database includes details (*Read Me* files) on how various data formats could be used depending on model resolution and the type of experiment conducted.

625

2.3.2 Rules followed when drawing isochrones

To draw spatially-continuous isochrones as consistently as possible around the ice sheet's periphery, the following workflow and set of rules were applied:

630

- Using ArcMap 10.7.1 software, we displayed our landform mapping database accompanied by our synthesised pattern of retreat map.

635

- All TCN and radiocarbon summary event ages were displayed rounded to 100 years and featuring a traffic-light colour code relating to one of the three confidence level categories (Table 1).

- All information was displayed on a rendition of topography from the ALOS World 3D 30 m spatial resolution DEM, and bathymetry from GEBCO 2022 release.

640

- The location of contemporary grounded ice was displayed at all times using the raster mask of the IceBridge BedMachine Greenland version 4 dataset (Morlighem et al., 2017).

- Isochrones were interpreted and mapped working clockwise around the full Greenland perimeter, and sequentially following chronological order (starting from oldest). The process was conducted iteratively and with numerous adjustments as the position of an individual isochrone might depend upon the preceding and succeeding ones. Multiple authors re-interpreted and contributed to the final isochrones to try and ensure a consensus view of possible alternate behaviours.

645

- When the ice sheet was everywhere more extensive than present, isochrones were drawn around the whole of Greenland. However, during younger isochrone time-slices (*i.e.* 10-6.5 kyr BP), paleo ice sheet margins were likely similar to present-day positions, or in a more retreated position, for certain regions (Briner et al., 2010; Larsen et al., 2015). In such cases, isochrones

650

were not drawn around the full ice-sheet perimeter, but were instead interrupted where they meet the present-day margin. We do not attempt to map out the extent of ice where retreated inside of the present-day position as the position of the ice margin is largely undefined/unknown, even within regions where it is known to have occurred.

655

The precise method employed when drawing isochrone lines varied depending on the nature and spatial/temporal density of empirical data available. When both mapped ice marginal landforms and TCN or radiocarbon event ages coincided, the line was drawn through both sets of information. When only reliable event ages were available, the line was drawn to connect them while considering topography, bathymetry, and the spatial configuration of the modern ice sheet margin (e.g. Fig. 6). On the other hand, when only mapped ice marginal landforms were available, the line was drawn following the landforms and topography/bathymetry only. In the absence of any chronological constraints, the retreat pattern was assumed to be monotonic in nature, *i.e.* producing a decreasing extent that is spatially and temporally consistent. The resulting ice-margin isochrones are thus much more complex than a product of lines joining up geochronological point data (Fig. 6). Rather the PaleoGrIS 1.0 isochrones represent a qualitative reconciliation and interpretation of topographic, geomorphological, and geochronological data. Such a heuristic approach sometimes relies on soft knowledge of typical interactions between ice sheet margins and topography, including the lobate behaviour of outlet glaciers and the dynamics of ice flow around present-day Greenland. The isochrones therefore stand as an informed interpretation of successive ice margin positions, in places well constrained and in others much less so, and which are likely to require adjustment once further landform or geochronological data become available.

670

675

680

685

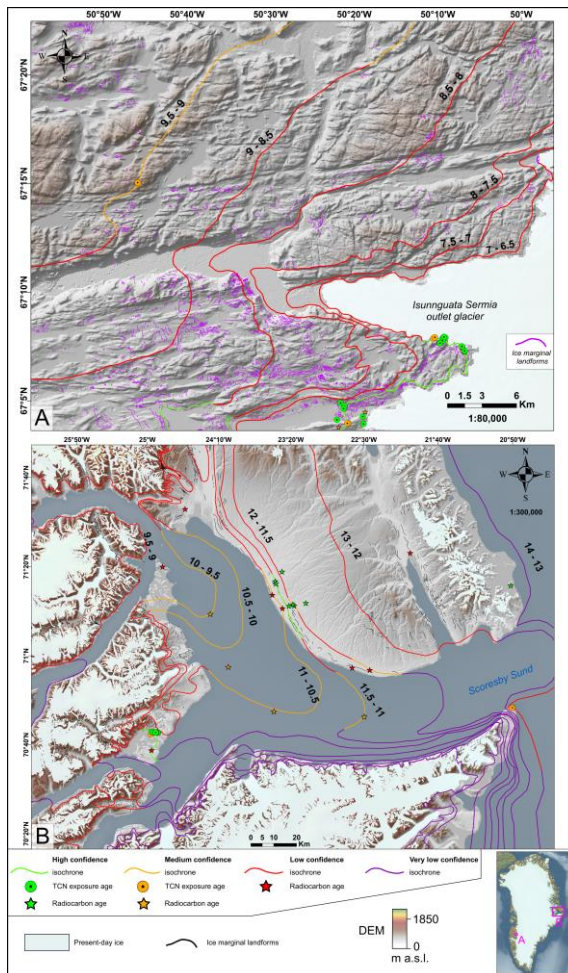


Figure 6. Example maps showing the details of the PaleoGrIS 1.0 isochrones in a land-dominated region of Central West Greenland (panel A) and a Fjord-dominated region of Central East Greenland (Scoresby Sund, panel B). The two examples highlight our choice of distinguishing isochrone temporal uncertainty (shown by time ranges labelled in bold black) from isochrone spatial uncertainty (shown by the four colour-coded confidence levels). The figure also displays the location of local event ages compiled in our database, here colour-coded based on our quality control assessment (Table 1). All data is displayed overlaying the AW3D30 DEM (30 m resolution).

2.3.3 Addressing periphery ice caps and glaciers

725

During the Late-glacial and early-to-mid Holocene, as the Greenland Ice Sheet margin receded, peripheral ice caps and mountain glaciers became separated from the main ice-sheet body. Ideally, a full reconstruction of the ice sheet Late-Glacial and Holocene evolution would also include the changing extent of these peripheral ice bodies. Future versions of PaleoGrIS could usefully be extended to include the development of such peripheral ice caps, but for this first version, we chose to exclusively reconstruct the retreat pattern of the main body of the ice sheet. Peripheral ice caps were thus either: i) included within the perimeter of the reconstructed Greenland Ice Sheet margin, when the latter was considered extensive enough; or ii) excluded from our reconstruction, after complete separation from the ice sheet was estimated to have occurred.

730

2.3.4 Connection with the Innuitian Ice Sheet

735

Ellesmere Island lies just 100 km to the NW of Greenland (Fig. 1) and along with much of the rest of the Canadian Arctic Archipelago it was covered by the Innuitian Ice Sheet, which is thought to have been connected to the Laurentide Ice Sheet until approximately 10.5-9.5 kyr BP (DaltonEngland et al., 20202006). Given such a close proximity it is deemed likely that the Greenland and Innuitian ice sheets coalesced over Nares Strait during glacial maxima (Dyke, 2004; Sinclair et al., 2016; Funder et al., 2011, Georgiadis et al., 2018; Dalton et al., 2020). We chose to make no inferences regarding the pattern of retreat associated with the margins of the Innuitian Ice Sheet. We thus draw isochrones that are consistent with the two ice sheets merging, but we interrupt them towards the point of deepest bathymetry between Greenland and Ellesmere Island, throughout the length of Nares Strait. The same method was applied to close polygon shapefiles over Nares Strait when measuring the ice sheet's areal extent and create time-slice maps.

740

745

2.3.5 Isochrone confidence levels

Geochronological and geomorphological evidence are spatio-temporally heterogeneous, causing each isochrone to feature spatially variable levels of reliability around its perimeter (e.g. Fig. 6). Given this uneven distribution of information, our mapping procedure was adapted accordingly. We split each isochrone line into four confidence-level categories referred to as 'high', 'medium', 'low', or 'very low' confidence isochrones, by applying the following set of rules:

750

- *High confidence isochrone sections*: Drawn when empirical evidence features both mapped ice marginal landforms and TCN or radiocarbon event ages deemed reliable, *i.e.* graded high or medium confidence.

755

• *Medium confidence isochrone sections*: Drawn when empirical evidence does not feature mapped ice marginal landforms but features reliable event ages, *i.e.* graded high or medium confidence.

760 • *Low confidence isochrone sections*: Drawn when empirical evidence features only ice marginal landforms, or only low reliability dates, *i.e.* ages graded low confidence.

• *Very low confidence isochrone sections*: Drawn in the absence of any mapped geomorphological or any geochronological evidence, but relying on topographic and/or bathymetric information exclusively.

765

2.3.6 Ages that could not reasonably be reconciled to isochrones

770 When building isochrones by integrating geochronological evidence from numerous published sources and locations, contradictory evidence can become challenging to resolve. For instance, this can occur when nearby event ages display high age variability while presenting similar levels of reliability, but also when they are found reversed relative to the general direction of presumed ice retreat, and/or relative to stratigraphic order of events in nearby valleys/regions.

775 For TCN exposure dating, misleading ages can result from nuclide inheritance causing too-old apparent ages, post-depositional disturbance causing too-young apparent ages, or laboratory contamination/errors potentially causing both (Dunai, 2010). [Such issues are in most cases reported in original publications enabling us to easily identify outliers.](#) In Greenland more specifically,

Late-Glacial and Holocene studies generally report nuclide inheritance to be the dominating cause of exposure age scatter (Larsen et al., 2021). For radiocarbon ages, delayed organic growth following ice retreat, or contamination by younger organics

780 (e.g. for bulk samples) can cause ages to be too young. This challenge is common in the Arctic, where post-deglaciation biodiversity establishment is relatively slow. For marine ages, an erroneous estimation of the marine reservoir effect can also cause calibrated ages to misrepresent the true deposition age. Moreover, in Greenland, numerous radiocarbon ages were produced to date the marine-to-freshwater transition of basins following isostatic uplift caused by ice retreat (Weidick et al., 2004). Delay in such uplift can increase the potential for radiocarbon ages underestimating the timing of deglaciation. The

785 misfit between our isochrone reconstruction and a specific event age may also be due to oversights in our age-filtering exercise.

In these challenging cases, drawing isochrones requires subjective decisions to either favour and/or ignore certain seemingly awkward or anomalous event ages, when weighed against our interpretation of the most representative timing of local deglaciation. Such interpretations were either based on a review of the region-specific literature, or on assessing the distance separating relevant isochrones in adjacent regions displaying more consistent geochronological constraints. Summary event

790

ages deemed challenging and ignored were identified and gathered post-mapping of isochrones in a separate shapefile available in the supplement. We acknowledge decisions to ignore event ages are necessarily subjective (see section 2.3.2).

795 2.3.7 Limitations and uncertainties in isochrone reconstruction

In regions of Greenland with high quality and density of geochronological and geomorphological constraints (e.g. the Sisimiut and Disko Bay regions), former ice margins can be reconstructed with reasonably high levels of confidence. Contrastingly, our reconstruction also features crude interpolations of ice margins over vast areas, due to the low density or absence of empirical evidence in numerous locations. Thus, the heterogeneous nature of our reconstruction's uncertainties, depicted by our four different confidence levels (section 2.3.5.), calls for caution. One must stress that the PaleoGrIS 1.0 isochrone reconstruction is not intended for use at the valley or regional scale, for which local investigations are likely more accurate (e.g. Pearce et al., 2018), but rather at continental scale. Caution should also be applied concerning the temporal resolution of our reconstruction, which aims to provide estimates of ice sheet margin positions every 1000-500 years. In fact, our reconstruction should be regarded as averaged or net retreat over such time intervals, and any short-lived re-advances or dynamic ice-sheet margin response (e.g. 10s to 100s years) are not captured in our reconstruction. In most locations, the PaleoGrIS 1.0 isochrones should not be considered precise enough to accurately depict the margin evolution of individual outlet glaciers, to predict the formation of small proglacial lakes and spillways, nor for reconstructing past meltwater pathways, for instance. The reliability of the reconstruction is of course dependent on the underpinning evidence, examination of which should guide a user away from more speculative areas. The continental-scale mapping approach can sometimes cause resulting ice configurations to be glaciologically unrealistic and inconsistent with a complex landscape at the valley scale (< 5 km spatial resolution), despite our efforts to consider the influence of local topography/bathymetry as much as possible.

Over the past 30 years, several offshore investigations have established the approximate location of the ice margin during initial deglaciation from its local full glacial position (~17-12 kyr BP), when the ice sheet was mostly marine-terminating (e.g. Smith & Licht, 2000; Nørgaard-Pedersen et al., 2008; Evans et al., 2009; Ó Cofaigh et al., 2004; 2013; Rasmussen et al., 2022; Hansen et al., 2022; Lloyd et al., 2023). Such studies remain scarce, and we find former grounding line positions remain largely understudied and undated. Readers should thus be aware that our oldest isochrones (*i.e.* between ~14 and ~12 kyr BP) are associated with crude interpolations across large offshore areas, thus presenting higher levels of uncertainty than we now have for the terrestrial areas.

We believe there is much scope for reducing isochrone uncertainty in future versions of the PaleoGrIS reconstruction, as more mapping and dating is conducted from less studied regions. We make suggestions as to what regions would most benefit from this attention in a later discussion section.

825

2.4 Estimating areal extent change of the Greenland Ice Sheet

To evaluate the former areal extent of the ice sheet (*i.e.* two-dimensional surface area) between ~14 and ~6.5 kyr BP, we produced a series of polygon shapefiles covering the area delineated by each isochrone perimeter and measured their areal extent using the ArcMap geometry calculator. To compare variations regionally, we divided the ice sheet into seven major hydrological basins, following the ice-divide sampling of Rignot & Mougnot (2012) and the IMBIE Team (2019) (Fig. 5). Region-dividing polylines were extended towards the outermost isochrones following topographic/bathymetric highs, while remaining as perpendicular to isochrones as possible. Therefore, for the exclusive purpose of subdividing the ice sheet into regions, the catchment areas were crudely assumed to remain similar from ~14 kyr BP onwards, as their paleo configurations remain unknown. Between the 14-13 and 10.5-10 kyr BP time slices, we consider our measurements as absolute estimates of areal extent. However, for time slices between 10-9.5 and 7-6.5 kyr BP, our measurements should be regarded as maximum-limiting estimates of ice-sheet areal extent. That is because empirical evidence suggests the ice sheet was as extensive or smaller than today in several regions during that time interval. In these cases, we chose not to guess the extent of retreat behind the current margin, and merged polygons representing more extensive margins with the contemporary ice sheet extent in data-free regions. Present-day ice sheet areal extent was computed from BedMachine Greenland version 4 (Morlighem et al., 2017), after removing peripheral glaciers.

We chose not to convert our ice sheet areal extent reconstruction into a volume and mass estimation. The Greenland Ice Sheet was characterised by very cold and arid conditions during extensive advance, and conversely significant increases in accumulation occurred during deglacial margin retreat. The relationship between areal extent and ice thickness is thus complex and not necessarily positively correlated across the ice sheet (Cuffey & Clow, 1997). To obtain a realistic deglacial volume reconstruction of the Greenland Ice Sheet requires extensive modelling experiments that take into account climate, surface mass balance, glacial isostatic adjustment, relative sea level change, calving, basal sliding (e.g. Bradley et al., 2018), and that conducts quantitative model-data comparisons. Our team is conducting such an experiment with the Parallel Ice Sheet Model (Winkelmann et al., 2011) and will thus present volume reconstructions in a separate publication.

855

2.5 Assessing rates of retreat and their variation

860 To quantitatively estimate the former retreat rates of outlet glaciers, 72 transects emanating from present-day outlets were drawn. Transects were traced from the outermost (14-13 kyr BP) to the innermost (7-6.5 kyr BP) PaleoGrIS 1.0 isochrone margins, following our estimate of the former glacier front central position at each time step, guided by topography. We thus follow the assumption that the approximate centre of former glacier termini (or grounding lines) was located near the point of lowest topography. Hence, such transects should not be interpreted as supraglacial flowlines, as these would have likely evolved through time with glacier catchments and ice divides potentially re-adjusting during deglaciation. The transects are made available in a polyline shapefile (see online database). Present-day outlet glacier names (preferably new Greenlandic, otherwise Danish) were obtained from the database of Bjørk et al. (2015), while distances along transects were measured for each isochrone spacing using ArcMap. As each isochrone is associated with a temporal uncertainty (*i.e.* 1000 or 500 yrs), both minimum and maximum retreat rates were calculated for each time-step. The reported retreat rate for each step is taken as the midpoint \pm half the range. For the purpose of evaluating former retreat rates only, the positions of isochrones are regarded as definite, and the reported error is exclusively temporal. For each transect, an 'overall retreat rate' (\pm temporal uncertainty) is also computed using the total distance divided by the minimum and maximum time span between outermost and innermost isochrones.

875

2.6 Where and when was Greenland's last full glacial extent?

Although we mostly focus on the terrestrial deglaciation from ~14 kyr BP onwards, it was important for positioning this outermost isochrone to have some knowledge of greater ice extents and indeed the maximum achieved extent in the last glacial. A review of Greenland's potential last full glacial extent (thought to occur around 18-16 kyr BP; Simpson et al., 2009) was conducted. We updated the full glacial margin drawn by Funder et al. (2011) after consulting publications contributing new empirical knowledge to that specific question (Möller et al., 2010; Ó Cofaigh et al., 2013; Arndt et al., 2017; Laberg et al., 2017; Jennings et al., 2017; Newton et al., 2017; Seidenkrantz et al., 2019; Sbarra et al., 2022; Couette et al., 2022; Rasmussen et al., 2022; Hansen et al., 2022). In several regions a debate prevails regarding whether grounded ice reached the outer continental shelf when in last full glacial configuration. We find that in all studied regions apart from offshore the Northeast Greenland Ice Stream (NEGIS; Rasmussen et al., 2022), more recent investigations tend to suggest a more extensive full glacial configuration than previously proposed, with grounded ice often argued to have reached the mid-to-outer shelf. For instance, in Central West Greenland, Ó Cofaigh et al. (2013) used a series of dated marine sediment cores and bathymetric subglacial landform mapping to show that the Uummanaq and Jakobshavn Isbræ ice streams remained grounded near the continental shelf edge until ~15 kyr BP. A similar interpretation was, for instance, proposed by Hansen et al. (2022), who argued that grounded ice in the Westwind Trough region (Northeast Greenland) was located towards the outer shelf during last full glacial

extent, and prior to 13.5 kyr BP. However, near the same site (79.5°N), Rasmussen et al. (2022) suggest that grounded ice did not reach the shelf edge during the last glacial. Such contrasts demonstrate the question remains open in this region. Vast areas of the Greenland continental shelf are still [understudied/data-scarce](#) for this purpose. We revise the limit of Funder et al. (2011) by considering two scenarios, a minimum and maximum last full glacial extent, with the aim of highlighting spatial uncertainties in debated [and understudied](#) regions (Fig. 5). These two full glacial extent scenarios are used to inform the mapping of our outermost isochrones, and are included here as shapefiles (see online database). The maximum extent scenario displays an ice sheet that reaches the shelf edge around the entire ice-sheet perimeter. The minimum extent scenario modifies the latter by following the outline of Funder et al. (2011) in the Central East and Northeast regions, except towards the Westwind Trough, where it accounts for new data by Hansen et al. (2022). The minimum extent scenario also displays a more retreated full glacial ice sheet in the Northwest region, where little data constrains whether a mid-shelf or outer shelf position was reached. We suppose that the grounding line was likely highly dynamic and that any maximum achieved last glacial extent configuration between these lines is feasible.

895

900

905

910

915

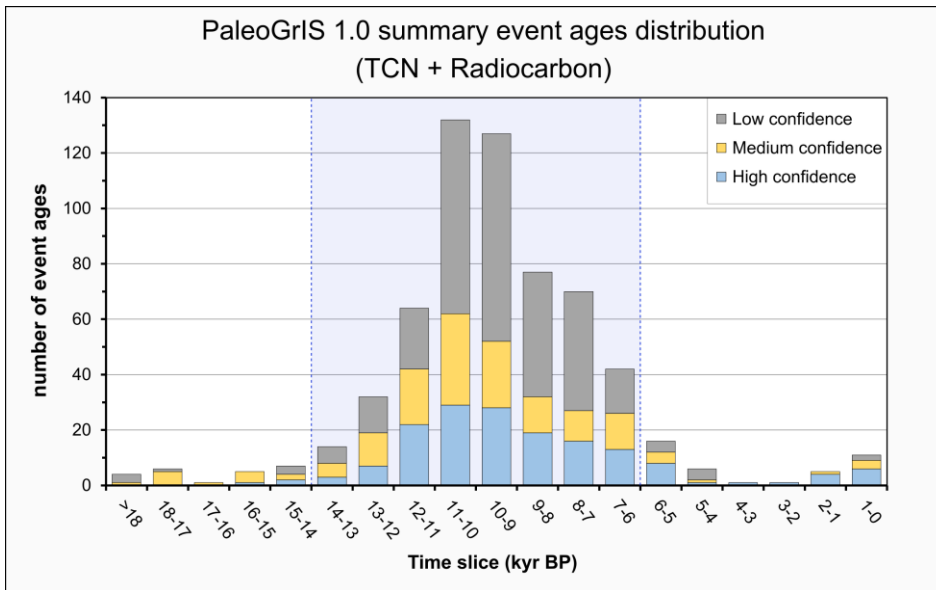


Figure 7. Histogram displaying the temporal distribution of all summary event ages calculated in the PaleoGrIS 1.0 database. Colour-coded relative proportions of the three quality control categories are shown for each thousand-year time slice bin. A light blue polygon highlights the time period covered by the PaleoGrIS 1.0 isochrone reconstruction. This Late-Glacial-to-mid-Holocene period (14-6.5 kyr BP) features the large majority (>90%) of compiled event ages dating the deglacial evolution of former Greenland Ice Sheet margins.

3 Results

940 3.1 The PaleoGrIS 1.0 geomorphological and geochronological database

3.1.1 Geomorphology

The PaleoGrIS 1.0 database contains a total of 194,302 ice-marginal landforms mapped over 430,500 km² of ice-free land
945 around Greenland. The distribution of landforms is relatively sparse in the Southeast (SE) and Northwest (NW) regions, where
the contemporary ice sheet terminates near to the coast. Consequently, the majority of ice-marginal landforms mapped as part
of this study are located in the Southwest (SW), Central West (CW), Central East (CE), Northeast (NE) and North (NO) regions
of ice-free Greenland. Interestingly, we find ice-marginal landforms are particularly abundant and well-preserved in NO
950 Greenland, increasing our confidence here in the retreat pattern relative to other regions. This abundance and pristine nature
of landforms might be due to the generally softer nature of subglacial bedrock (Pedersen et al., 2013) in this region enabling
greater sediment supply for moraine-building, a drier climate that could better promote landform preservation (Niwano et al.,
2021), or a potentially steadier and more monotonic retreat pattern of outlet glacier margins characterised by less dynamic
fluctuations and re-advances that cause erosion.

955 3.1.2 Geochronology

The PaleoGrIS 1.0 database features 1028 TCN exposure ages gathered from 45 studies and contains 423 radiocarbon ages
collected from 111 studies. Following the computation of summary statistics for age groups, and the removal of outliers, this
collection contains 251 TCN-derived summary event ages. This number excludes TCN exposure ages produced as past ice-
960 sheet thickness indicators (e.g. dipstick models). The radiocarbon age compilation features 370 summary event ages post age-
filtering. Therefore, a total of 621 summary event ages were directly used to inform our isochrone reconstruction. Details
regarding the temporal frequency distribution of summary event ages and their number per investigation are presented in
Figure 7 and Tables 2,3. We here acknowledge the possibility that relevant investigations and datasets may be missing from
our chronological database. It is our goal that such oversight can be corrected in future versions of PaleoGrIS.

965

In the PaleoGrIS 1.0 database, 90% (n = 558) of the summary event ages compiled are younger than 14 kyr BP and older than
6 kyr BP (Fig. 7). As a result, we chose to restrict our isochrone reconstruction to this time period (more justification for this
decision can be found in section 2.3.2). Following quality control assessment of summary event ages (Table 1), we find high
and medium confidence event ages each represent a quarter of the total (26 and 25%, respectively). Low confidence event ages

970 represent the largest proportion, *i.e.* 49% (Fig. 7). This is in part explained by numerous event ages resulting from a single
marine radiocarbon age, here attributed a low confidence rating due to large uncertainties in past marine radiocarbon reservoir
effects at high latitudes (Heaton et al., 2022) (see criteria list: Table 1). However, we stress that event ages described as “low
confidence” may still closely estimate the true timing of margin retreat and are by no means excluded from our isochrone
reconstruction. Our event age quality control assessment is merely an indicator utilised to inform challenging decisions made
975 when tracing isochrones.

Using our geochronological database, we analyse the spatial variability in event age reliability across Greenland and its
periphery. For TCN exposure ages, we find a higher relative concentration of medium-to-low confidence event ages in NO
Greenland, and more specifically from Inglefield Land, Inglefield Bredning, Washington Land and around Danmarks Fjord,
980 Hagen Fjord, Independence Fjords and the Centrumssø regions. Indeed, while studies that investigated these regions sampled
both bedrock and erratic surfaces, and have produced extensive datasets, their results often display old apparent ages (Ceperley
et al., 2020; Larsen et al., 2018; 2020; Søndergaard et al., 2019; 2020). It has been stated that this abundance of overestimating
exposure ages is most likely associated with high levels of nuclide inheritance in NO Greenland caused by insufficient
subglacial erosion of bedrock and transported clasts. Future studies producing exposure ages from these regions might thus be
985 inclined to also measure *in situ* cosmogenic ^{14}C alongside other radionuclides (e.g. ^{10}Be , ^{26}Al , ^{36}Cl), which may enable the
quantification of nuclide inheritance and more accurate estimation of Holocene deglacial exposure ages (e.g. Søndergaard
et al., 2020). We note that the ice-free region to the West of the Akuliarutsip Sermia and Inuppaat Quuat glaciers (67.3-68.3°N;
50.1-54°W), in Central West Greenland, also displays a high concentration of medium-to-low confidence TCN event ages
(Young et al., 2020). For radiocarbon ages, however, we do not observe any clear spatial patterns in the variability of summary
990 event age reliability.

3.2 Regional retreat patterns and timings

995 In this section we describe the PaleoGrIS 1.0 isochrone reconstruction, and the pattern and timing of ice-sheet margin retreat,
for selected regions, followed by a chronological description of the main deglacial events. This section also describes key
empirical constraints that inform our reconstruction. When found, new Greenlandic place and glacier names are preferably
used to describe the geography (e.g. after Bjørk et al., 2015). When not found, we refer to places, features and certain glaciers
using Danish or other foreign names.

1000

3.2.1 Ice sheet retreat in North Greenland, and the timing of Nares strait opening

1005

Towards the onset of the studied time period (*i.e.* 14-13 kyr BP), our reconstruction portrays the Innuitian (ice over Ellesmere Island) and Greenland Ice Sheets as connected, with grounded ice from both ice masses merging along Nares Strait, as supported by empirical evidence (e.g. Jennings et al., 2011; Georgiadis et al., 2018). For that timestep, we reconstruct the two connected ice sheets to feature marginal grounding lines on both southwestern and northeastern ends of Nares strait, with respective margins terminating into Baffin Bay and the Lincoln Sea (Fig. 8). Geochronological evidence of ice sheet extent suggests retreat of these two grounding lines occurred somewhat simultaneously on both ends of the Strait. This is supported by ages indicating onshore regions located closest to Nares Strait's openings (e.g. Inglefield Fjord and Wulffs Land) were progressively deglaciated earlier than regions located towards its centre, *i.e.* terrestrial regions adjacent to Kane Basin, such as Washington and Inglefield Lands (Fig. 8). Indeed, TCN exposure ages suggest grounded ice had retreated within Inglefield Fjord by around 11.5-11 kyr BP (Søndergaard et al., 2019). At the same time, deglacial radiocarbon ages (Funder, 1982; Kelly & Bennike, 1992) indicate ice from the Ryder, Steensby, and C.H. Ostenfeld basins had retreated towards the outermost present-day coastline of Nyeboes, Wulffs, and Nares Lands. After 11 kyr BP, we reconstruct grounding lines that retreated further within Nares Strait, and that reached the southwestern and northeastern edges of Kane basin by 9-8.5 kyr BP (Fig. 8). TCN ages produced from contemporary coastal regions of Inglefield Land (Søndergaard et al., 2020) and Washington Land (Ceperley et al., 2020) suggest regions adjacent to the Humboldt glacier lateral margins started deglaciating around 8.5-8 kyr BP. During that time, further East, evidence suggests the Petermann Glacier front was located towards the Fjord's mouth (Bennike, 2002). After ~8 kyr BP, in this region, we estimate that the ice sheet had retreated inland beyond present-day coastlines, except for offshore contemporary Humboldt glacier, where we map a grounding line that remained within ~100 km outside the present-day margin. Therefore, empirical data suggests the last ice bridge connecting the Innuitian and Greenland Ice Sheets over Nares Strait survived exclusively within the Kane basin, and until 8.5-8 kyr BP (although large uncertainties remain). We thus estimate the final deglacial opening of Nares strait to have occurred between 9 and 8 kyr BP (Fig. 8). Following this, further retreat caused the ice sheet margin to reach its present-day extent by 7.5-7 kyr BP on Inglefield Land, while shortly after (7-6.5 kyr BP) on Washington Land.

1030

In northernmost Greenland (>82.7°N), we reconstruct a margin retreat pattern characterised by a disconnection with glaciers and ice caps from Roosevelts Land that occurred at around 10-9.5 kyr BP. This estimation is however uncertain due to the low abundance of local geochronological constraints. Around 9-8.5 kyr BP, we estimate further retreat to generate ice sheet separation from the large Hans Tausen ice cap. Between 8.5 and 6.5 kyr BP, relatively slow retreat of more-extensive-than present ice margins was still occurring on inter-fjord regions of Wulffs, Adam Berings and Christensens Lands (Larsen et al., 2020). In the same regions, empirical evidence suggests outlet glaciers terminating in deep and wide fjords, such as

1035

Independence, Hagens, or Victoria Fjords, experienced faster retreat than those located on adjacent inter-fjord regions (Larsen et al., 2020).

1040

3.2.2 Ice sheet retreat in Northeast Greenland, and ice-margin evolution in the Nioghalvfjordsfjorden and Jøkelbugten regions

1045 In this section, we describe the PaleoGrIS 1.0 isochrone reconstruction in a region characterised by a ~300 km-long stretch of the coast in northeast Greenland belonging to King Frederick VIII Land, and which lies between Holms Land (79.8°N) and the Skærfjorden embayment (77.4°N). The largest contributor to ice flux in this region is the North East Greenland Ice Stream (NEGIS), which currently splits into three wide, marine-terminating and fast-flowing outlet glaciers displaying surface velocities in places > 1000 m yr⁻¹ (Joughin et al., 2018). These are, from north to south, the Nioghalvfjordsbrae (also referred as 79N) glacier, the Zachariae Isstrøm glacier, and the southernmost branch which splits in two sub-outlets, the Koføed-Hansen
1050 Bræ and Storstrømmen outlet glaciers (Fig. 9). In this region, a debate prevails regarding whether the grounded ice sheet advanced extensively on the wide continental shelf during last full glacial extent, or whether it was restricted to the inner shelf (Rasmussen et al., 2022). However, recent offshore investigations (e.g. Hansen et al., 2022), including soon to be published work (Ó Cofaigh et al., 2023), increasingly suggest a last full glacial ice sheet margin that was more extensive than previously
1055 drawn by Funder et al. (2011), and that likely reached the mid-to-outer continental shelf. However, whether the grounded ice sheet remained confined to the prominent bathymetric Westwind (north) and Norske (south) troughs, or instead also flowed eastwards over the mid-shelf bathymetric highland separating the two, the Northwind Shoal, is uncertain (Arndt et al., 2017; Pados-Dibattista et al., 2022). The large disparity between our minimum and maximum last full glacial extent scenarios reflects this debate in the literature (Fig. 9).

1060

To remain conservative, our reconstruction in this region features a very low confidence outermost isochrone (14-13 kyr BP) located closely inboard of our minimum last full glacial extent scenario, and depicting a grounded ice-sheet margin positioned towards the mid-shelf, while remaining confined within the Westwind and Norske troughs (Fig. 9). This 14-13 kyr BP extent is constrained in Westwind Trough by a marine radiocarbon deglacial chronology by Hansen et al. (2022). We then tentatively
1065 reconstruct an ice sheet margin that had monotonically retreated ~50 km westwards along the troughs by ~12-11.5 kyr BP, as suggested by offshore data by Davies et al. (2022). However, directly south of Norske trough, we reconstruct a less extensive ice sheet margin around the same time (12-11.5 kyr BP). This interpretation is based on TCN exposure ages by Larsen et al. (2018) indicating that by 11.5 kyr BP, the grounded ice had likely retreated West of Kap Amélie (77.5°N), into the Skærfjorde embayment, and had reached the Storøen and Ambolten Islands; a north-to-south oriented archipelago acting as a topographic
1070 barrier to ice flowing eastwards from the deep Jøkelbugten basin (Fig. 9).

Based on TCN-derived event ages from Bourbon Øer (Larsen et al., 2018) and Dove Bay (Larsen et al., 2022) located ~60 km further South, we reconstruct a margin that had retreated to the inner shores of Skærfjorden, and that was positioned ~55 km from the present-day ice front of Nioghalvfjærdsbrae, by ~11.5-11 kyr BP. Over the next two thousand years, our reconstruction suggests the ice sheet margin retreated relatively quickly westwards within the Jøkelbugten basin, through Lamberts Land, and within Nioghalvfjærdsfjorden, with a former margin that was positioned within ~15 km of the present-day ice sheet front in most locations of the region, by ~10-9.5 kyr BP. We estimate the next phase of retreat to be slower ($< 20 \text{ m yr}^{-1}$) with an ice-sheet margin remaining more extensive but near the present day one, until ~9-8.5 kyr BP. This is well supported by coeval TCN exposure ages from Bloch Nunatak, an Island located near Nioghalvfjærdsbrae's contemporary calving front, and from three sites situated ~3 km from the modern lateral margins of Zachariae Isstrøm glacier (Larsen et al., 2018). To the South of Nioghalvfjærdsbrae, and for a 300 km long stretch of the ice margin, we thus reconstruct an ice sheet margin that was as- or more- retreated than present by ~8.5 kyr BP. This contrasts with the mountainous region directly northwest of Nioghalvfjærdsbrae, however, where the predominantly land-terminating former ice sheet margin appears to have retreated more slowly and more steadily. This is supported by our mapping depicting a highly regular spacing of moraine ridges in this region. There, we reconstruct an ice-sheet margin that remained more extensive than present for two thousand years longer than further South, until ~7-6.5 kyr BP, as indicated by deglacial event ages by Bennike & Weidick (2001) and Larsen et al. (2018; 2020).

1075

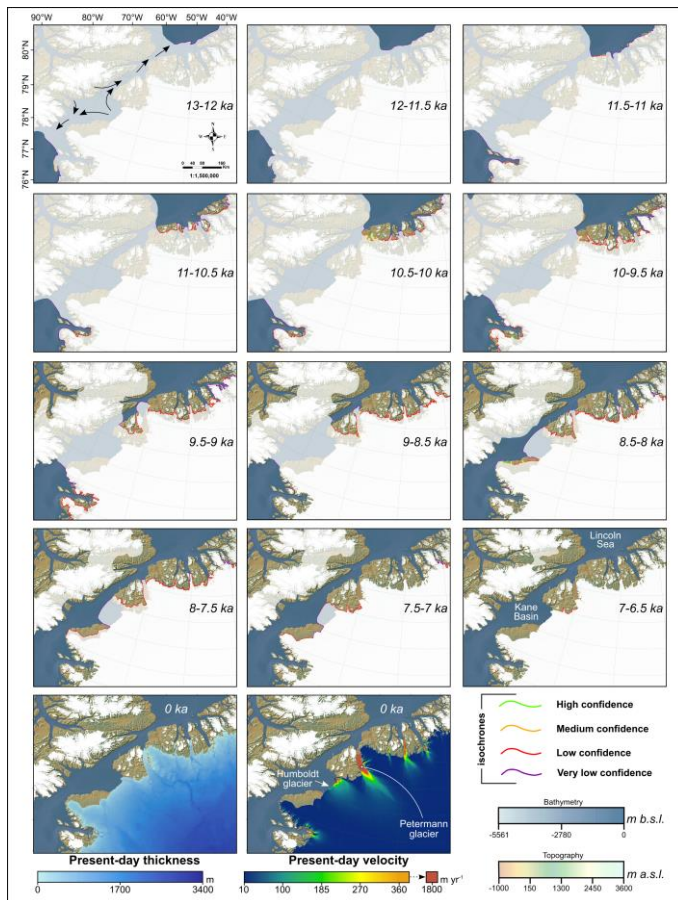
1080

1085

1090

1095

1100



1145 Figure 8. Time slice maps of the PaleoGrIS 1.0 isochrone reconstruction in Nares strait region. The reconstructed ice sheet areal
 1146 extent for each given time slice is displayed in each sub-panel as a white transparent polygon, while the underlying opaque white
 1147 layer is the present-day ice cover from BedMachine v4. The reconstructed ice sheet margins are highlighted by our isochrone
 1148 polylines, which feature different colour schemes relating to our four isochrone confidence levels (see section 2.3.5). We merge our
 1149 isochrones with the reconstruction of former ice extent over Ellesmere Island (Innuitian Ice Sheet) from Dalton et al. (2020). While
 1150 no modifications were applied to the margin extent of that dataset, the timing of Dalton et al. (2020) isochrones was in some cases
 modified (by less than 1 kyr at most) to match our reconstruction. Bottom panels also feature present-day ice-sheet thickness
 (Morlighem et al., 2017) and surface velocity data (Joughin et al., 2018). Topography and bathymetry are from the GEBCO 2022
 release.

1155

3.2.3 Ice sheet retreat in Central East Greenland, and ice-margin evolution in the Scoresby Sund and Kangerlussuaq regions

The central East (CE) region of the Greenland Ice Sheet is characterised by two major ice-drainage basins. The northernmost one is composed of ice streams and outlet glaciers flowing eastwards, and into Fjord systems that merge to form Scoresby Sund. The southernmost basin comprises three major ice streams flowing south-eastwards, the Kangerlussuaq, Christian IV, and Hutchinson Plateau Glaciers (Rignot & Mouginot, 2012; Bjørk et al., 2015). We here describe the general pattern and timing of retreat in these two key regions (Fig. 10).

1165 *The Scoresby Sund region*

At ~14-13 kyr BP, we reconstruct a grounded ice sheet margin positioned towards the inner continental shelf, near the mouth of Scoresby Sund and around the location of the underwater Kap Brewster moraine complex (Dowdeswell et al., 1994; Fig. 10). The timing of this specific extent is highly uncertain and exclusively based on a TCN-derived chronology from Kap Brewster, by Håkansson et al. (2007). For this time slice, we reconstruct the ice sheet as connected with ice caps from the Liverpool Land peninsula (Fig. 10). However, our reconstruction tentatively suggests disconnection between the two occurred shortly after, towards ~13-12 kyr BP. By ~12-11.5 kyr BP, deglacial radiocarbon ages (Bennike et al., 1999) indicate the Scoresby Sund outlet had retreated within the Fjord, with its northern lateral margin resting against the southwestern slopes of Jameson Land. Following further glacier retreat and thinning, we reconstruct the disconnection of ice flowing south-eastwards within Hall Bredning Fjord and ice flowing north-eastwards within Gaasefjord to occur between ~11.5 and ~10 kyr BP, based on radiocarbon deglacial chronologies by Marienfeld (1990), Ingólfsson et al. (1994) and Hansen (2001). We propose that progressive westward retreat and separation into three outlet glaciers retreating into Nordvest Fjord, Harefjord, and Føhnfjord, occurred between ~9.5 and ~8 kyr BP. After ~8 kyr BP, we estimate the grounded ice extent was similar or less than present in this region (Funder, 1978).

1180 *The Kangerlussuaq glacier region*

During the last full glacial configuration of the ice sheet, outlets of the southernmost basin in CE Greenland converged into one major lobe, commonly referred to as the Kangerlussuaq outlet glacier (Dowdeswell et al., 2010). This major outlet flowed south-eastwards and is thought to have likely reached the outer continental shelf during last full glacial extent (Mienert et al., 1992), although this remains uncertain. The deglacial pattern and timing of retreat of the Kangerlussuaq outlet has been studied by a relatively large number of offshore coring (e.g. Williams, 1993; 1995; Andrews et al., 1996; Smith & Licht, 2000) and onshore (e.g. Dyke et al., 2014) investigations. Based on findings from these empirical studies, we reconstruct a grounded ice margin reaching a mid-shelf position towards ~14-13 kyr BP in this area (Fig. 10). Between ~14 and ~10 kyr BP, our

reconstruction suggests the Kangerlussuaq outlet glacier retreated in a relatively slow and monotonic manner ($\sim 10 \text{ m yr}^{-1}$). Radiocarbon-dated marine sediment records (Smith & Licht, 2000) suggest faster retreat between ~ 10 and $\sim 9 \text{ kyr BP}$ ($\sim 70\text{--}40 \text{ m yr}^{-1}$) caused the outlet glacier to reach the Kangerlussuaq Fjord mouth by $\sim 9 \text{ kyr BP}$. We estimate later retreat within the Fjord to have been relatively quick ($\sim 60 \text{ m yr}^{-1}$), and a similar or more-retreated than present extent was likely reached before $\sim 8 \text{ kyr BP}$ (Dyke et al., 2014).

1195

1200

1205

1210

1215

1220

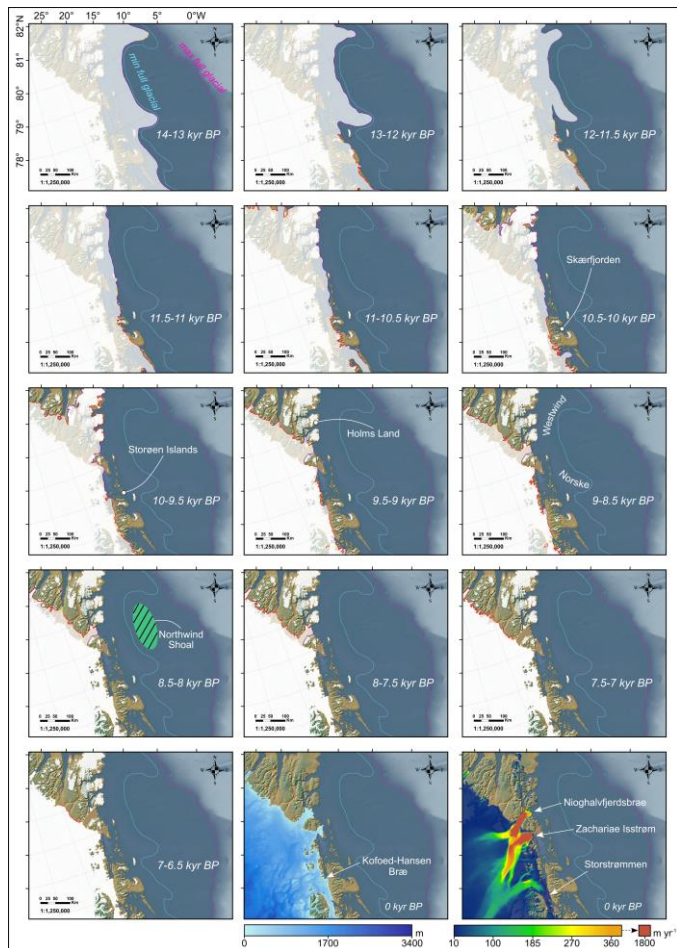
1225

1230

1235

1240

1245



1250 **Figure 9.** Time slice maps of the PaleoGrIS 1.0 isochrone reconstruction in the Nioghalvfjærdsfjorden and Jøkelbugten region. The
 1255 reconstructed ice sheet areal extent for each given time slice is displayed in each sub-panel as a white transparent polygon, while the
 underlying opaque white layer is the present-day ice cover from BedMachine v4. The reconstructed ice sheet margins are highlighted
 by our isochrone polylines, which feature different colour schemes (see Fig. 8 for key) relating to our four isochrone confidence levels
 (see section 2.3.5). Bottom panels also feature present-day ice-sheet thickness (Morlighem et al., 2017) and surface velocity data
 (Joughin et al., 2018). Topography and bathymetry are from the GEBCO 2022 release. [For a more complete figure legend, the reader
 is advised to consult Figure 8.](#)

3.2.4 Ice sheet retreat in the Southeast region, and ice-margin evolution of the Sermilik outlet glacier

1260

To the South of the Kangerlussuaq Fjord and trough, a 300 km-long stretch of the Greenland coastline is characterised by rugged, steep, and high-elevation mountains displaying numerous summits reaching 2000 m a.s.l., with some acting as contemporary Nunataks. These high coastal mountains act as orographic barriers causing snow accumulations and resulting in the contemporary ice sheet reaching the shore along the entire coastline. This results in a lack of settlements, difficult access conditions, and thus a lack of paleo-glaciological field investigations. Moreover, in this region, the offshore continental shelf does not yet feature published geochronological constraints on deglacial grounded ice margin retreat, as far as our compilation suggests. Therefore, our ice-sheet margin reconstruction along this coastline displays only very-low-confidence isochrones, and retreat is crudely assumed to be monotonic in nature. 300 km further South, the next location presenting empirical constraints on past ice sheet margin evolution is the large Sermilik Fjord, in which the rapidly-flowing Helheim (up to 8000 m yr⁻¹: Joughin et al., 2018), Apuseerajik, and Nigertip Apusiia tidewater glaciers terminate. The Sermilik Fjord is bordered on its eastern side by the large Ammassalik Island and other peninsulas which feature steep mountains reaching >1000 m a.s.l. These high topographies act as orographic barriers to moisture supply and enable sustaining numerous ice caps and mountain glaciers.

1275

Today, the deep Sermilik Fjord is thus characterised by its main tidewater glacier fronts (e.g. Helheim) terminating more than ~100 km inside the Fjord, while the Fjord's terrestrial flanks remain heavily glaciated. We attempted to mimic this [miscellaneouscharacteristic](#) ice configuration when reconstructing the deglacial retreat of the ice sheet margin in this region.

1280

Based on extrapolating chronological constraints from the Kangerlussuaq trough, we map a very low confidence outermost isochrone (14-13 kyr BP) located towards the inner-to-mid continental shelf offshore the Sermilik Fjord. Soon after, by 13-12 kyr BP, we locally reconstruct an ice margin that had quickly retreated towards the mouth of the Sermilik Fjord, and onto the shore of local coastal mountains. This relatively early retreat scenario is constrained by TCN exposure ages from the southwestern tip of Ammassalik Island (Hughes et al., 2012), located East of Sermilik Fjord, and by exposure ages from the end of the Torqulertivit Imiat valley (Roberts et al., 2008), located near the western edge of the main Fjord mouth.

1285

Since deglacial radiocarbon ages from the Ammassalik Fjord further East (Long et al., 2008) give similar ages to TCN exposure dates from rock surfaces located towards the mid-to-inner Sermilik Fjord sides (Hughes et al., 2012), we reconstruct a Sermilik Fjord outlet front that had retreated ~30 km North by 11.5-11 kyr BP, while ice sheet margins remained extensive, *i.e.* near the coast and towards the Johan Petersen Fjord mouth, on the western side of Sermilik Fjord. The Sermilik outlet thus appears to have experienced a potent state of negative mass balance during the Younger Dryas-to-early Holocene rapid warming transition (GISP2 data; Alley, 2000), while ice masses occupying the Fjord side mountains either remained stable, or retreated

1290

less and slower. ~25 km further North, exposure ages from the Amanga Island (Hughes et al., 2012), situated where the Fjord splits into three, suggest the Sermilik outlet had rapidly retreated further into the inner Fjord, and started to split into the three main tidewater glaciers existing today (Helheim, Apuseerajik, Nigertiip Apusiia), by approximately 11-10.5 kyr BP. Although uncertain, this rapid retreat prompts us to reconstruct front margins for these three outlets that were as or more retreated than present after 10-9.5 kyr BP, an early timing for this event relative to other Greenland regions, we find.

1295

1300

1305

1310

1315

1320

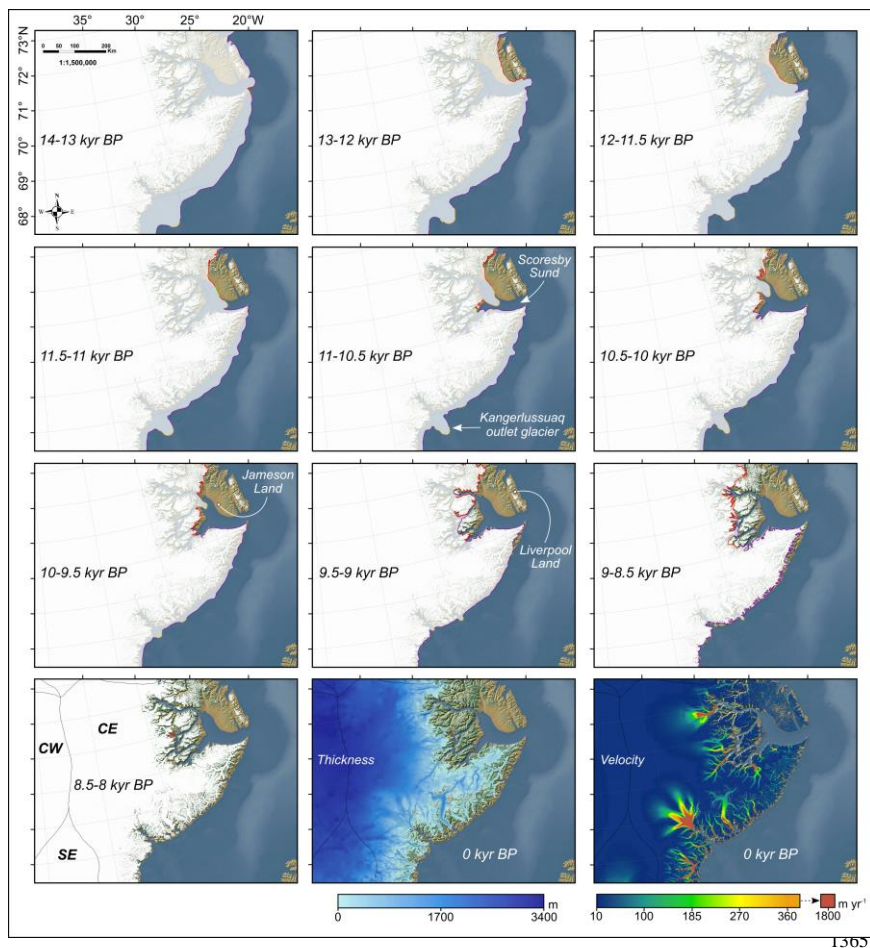


Figure 10. Time slice maps of the PaleoGrIS 1.0 isochrone reconstruction in the Scoresby Sund and Kangerlussuaq region. The reconstructed ice sheet areal extent for each given time slice is displayed in each sub-panel as a white transparent polygon, while the underlying opaque white layer is the present-day ice cover from BedMachine v4. The reconstructed ice sheet margins are highlighted by our isochrone polylines, which feature different colour schemes (see Fig. 8 for key) relating to our four isochrone confidence levels (see section 2.3.5). Bottom panels also feature present-day ice-sheet thickness (Morlighem et al., 2017) and surface velocity data (Joughin et al., 2018). Topography and bathymetry are from the GEBCO 2022 release. [For a more complete figure legend, the reader is advised to consult Figure 8.](#)

3.2.5 Ice sheet retreat in Southernmost Greenland

The southernmost region of Greenland is characterised by a relatively narrow (<70 km) and shallow (typically <200 m) continental shelf, and features high elevation coastal mountains with several summits reaching 2000 m a.s.l. The present-day ice sheet margin is generally located within 100 km of the outer coast in this region. Compared with other Greenland regions, little ice build-up was required for the ice sheet to reach the continental shelf edge during the last full glacial extent, and this scenario is considered highly likely by previous investigations (e.g. Funder et al., 2011; Andersen et al., 2020; Levy et al., 2020).

The relatively short distance to the continental shelf, combined with high local Bølling-Allerød warming and the proximity to the Irminger Current enabling warm water incursion, are thought to have caused relatively early deglaciation in southernmost Greenland (Levy et al., 2020). In fact, the well-studied N14 lake record, located on the Kitsissut Islands (-45.18°W; 59.98°N), features the oldest radiocarbon deglacial isolation age (~13.6 kyr BP) in Greenland (Bennike et al., 2002; Puleo et al., 2022). Based on these studies, southernmost Greenland is the only region where we map the oldest isochrone (14-13 kyr BP) onshore, towards the present-day outer coastline (Fig. 11). TCN event ages from Lindenows Fjord (Levy et al., 2020) suggest the series of fjords located East of the Julianehåb ice cap started deglaciating at around ~12 kyr BP. Although a lack of evidence makes isochrone mapping in adjacent northern fjords highly uncertain, our reconstruction displays outlet glaciers retreating and reaching present-day configurations earlier than most Greenland regions, by approximately 10 kyr BP. Therefore, the ice sheet margin was as or more retreated than present for most of the Holocene in this region.

To the West of Uummannarsuaq (also known as Cape Farewell), in the region of the Nanortalik and Narsarsuaq settlements, the timing of ice sheet retreat (from Qaqortoq Bay) is better constrained by empirical evidence. The majority of the local ice basin is currently drained by three fast-flowing outlet glaciers (maximum surface velocities >1000 m yr⁻¹); the Eqalorutsit Kangilliit Sermiat, Eqalorutsit Killiit Sermiat, and Qooqqup Sermia glaciers (Björk et al., 2015; Joughin et al., 2018). TCN exposure ages from Winsor et al., (2015) indicate these outlet glacier fronts had retreated ~20 km into local fjords by ~13-12 kyr BP, while TCN ages from Nelson et al. (2014) suggest retreat over the next two thousand years caused the outlet glacier fronts to be within ~15 km of present-day's before ~10 kyr BP (Fig. 11). This scenario of retreat is also consistent with a deglacial radiocarbon age produced by Weidick (1975) from the Bredefjord (the Narssaq site). To the Northwest, between Qaqortoq Bay and the large piedmont Sioqqap Sermia outlet glacier, our compilation features no geochronological constraints over a ~200 km-long stretch of ice-free coastal land. We have identified this region as a possible target for future field investigations aiming to reconstruct Holocene ice margin fluctuations. Along this region, low-confidence isochrones were thus

mapped solely by linking mapped ice marginal landforms and by extrapolating retreat timings from adjacent areas. Further North, the next site to display chronological constraints on ice sheet retreat is Kuannersooq Fjord (61.98°N), to the East of the Paamiut settlement, with TCN exposure ages from Winsor et al. (2015) dating an ice sheet margin retreating to the Fjord mouth by 12-11.5 kyr BP. Furthermore, in this valley, Carlson et al. (2014) sampled boulder and bedrock surfaces less than two km from the present-day ice-sheet margin. The resulting TCN exposure ages suggest the ice sheet had retreated towards its present-day extent by ~10 kyr BP in this sector.

1415

1420

1425

1430

1435

1440

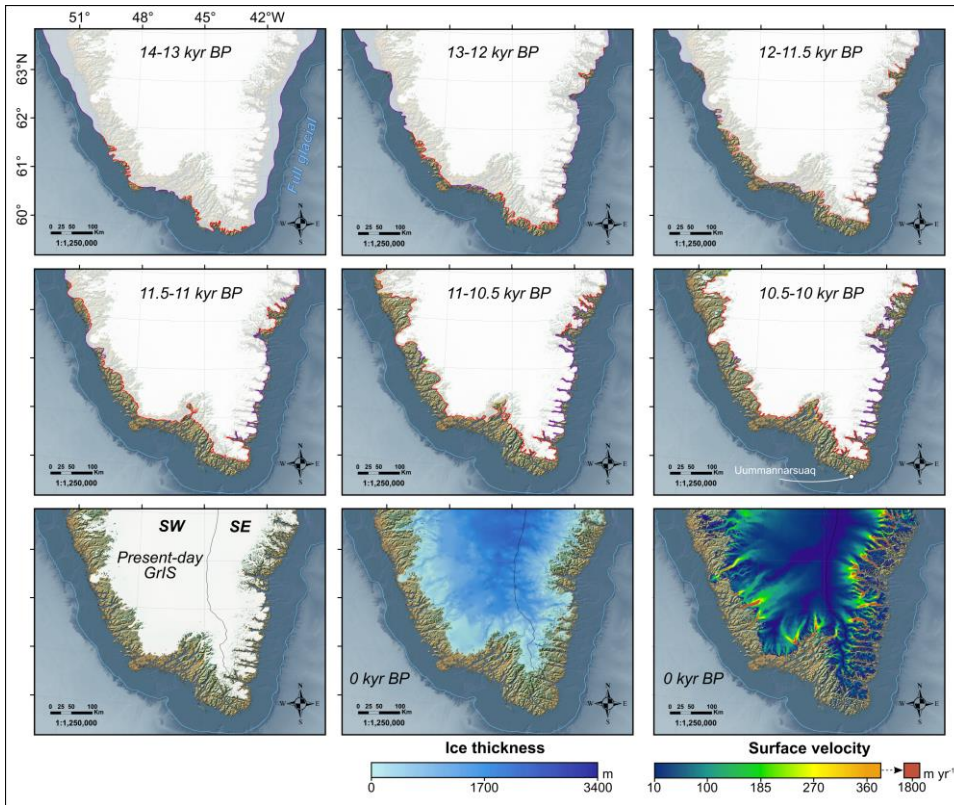


Figure 11. Time slice maps of the PaleoGrIS 1.0 isochrone reconstruction in southernmost Greenland. The reconstructed ice sheet areal extent for each given time slice is displayed in each sub-panel as a white transparent polygon, while the underlying opaque white layer is the present-day ice cover from BedMachine v4. The reconstructed ice sheet margins are highlighted by our isochrone polylines, which feature different colour schemes (see Fig. 8 for key) relating to our four isochrone confidence levels (see section 2.3.5). Bottom panels also feature present-day ice-sheet thickness (Morlighem et al., 2017) and surface velocity data (Joughin et al., 2018). Topography and bathymetry are from the GEBCO 2022 release. [For a more complete figure legend, the reader is advised to consult Figure 8.](#)

1445

¶450 ~~For a more complete figure legend, the reader is advised to consult Figure 8.~~

3.2.6 Ice sheet retreat in Southwest Greenland, and ice-margin evolution in the Nuuk region

1455

The ice-free coastal region to the East and South of Nuuk presents a complex topography with high (1500-2000 m a.s.l.) and steep-sided mountains dissected by several sinuous and deep fjords forming an archipelago. Upstream from these fjords, the majority of the ice discharge is captured by four fast-flowing outlet glaciers (maximum surface velocities: 1000-2000 m yr⁻¹). From South to North: these are the Sermeq, Kangiata Nunaata Sermia, Akullersuup Sermia, and Narsap Sermia glaciers (Björk et al., 2015). Due to easier accessibility, several investigations studying the former ice sheet evolution have taken place in this area, and the Late Glacial and early-to-mid Holocene retreat of the ice-sheet's margin is relatively well constrained. Further north, however, to the East of the Attamik settlement, a large ice-free region displaying flatter topographies with fewer overdeepenings features less geomorphological and geochronological constraints on ice margin retreat.

1460

1465

In the well-studied valleys, numerous TCN and radiocarbon dates from four parallel fjords, and from three distinct investigations (Weidick, 1976 ; Winsor et al., 2015; Larsen et al., 2014) show consistent results. These constraints enable us to map, with good levels of confidence, an ice sheet margin positioned towards the mouths of the Nuup Kangerlua, Kangerdluarsunguak, and Sermilik fjords, while positioned towards the middle of the Amelarik Fjord, at ~11-10.5 kyr BP (Fig. 12). Older isochrones (14-11 kyr BP) are less well constrained and are here reconstructed following a low-confidence and monotonic retreat pattern from a mid-shelf position at 14-13 kyr BP. Several extensive investigations sampling along the fjords and towards the modern ice margin have shown that after ~11-10.5 kyr BP, local outlets flowing into the Nuuk Fjord system likely experienced very rapid retreat, with their fronts reaching the inner fjords by ~10 kyr BP (Weidick, 1972; Larsen et al., 2014; Young et al., 2021) (Fig. 12). According to this retreat scenario, local fjords were deglaciated in less than 1000 years, which represents a retreat rate of 207 ± 69 m yr⁻¹ for the Kangiata Nunaata Sermia outlet glacier during that time. Out of the 72 Greenland outlet glaciers sampled for retreat rate analysis, this rate is the 6th highest maximum retreat rate reached over the reconstructed period. Therefore, this rapid retreat of the ice sheet margin in the Nuuk region between ~11 and ~10 kyr BP was likely a high-magnitude event at the ice-sheet scale.

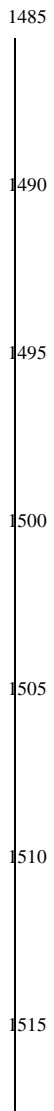
1470

1475

1480

Following this, numerous multi-nuclide TCN exposure ages from near the contemporary margins of the Kangiata Nunaata Sermia, Akullersuup Sermia, and Narsap Sermia glaciers indicate local tidewater glaciers had reached a similar-to-present extent by ~9 kyr BP (Larsen et al., 2014; Young et al., 2021). Further north, towards a plateau (> 600 m a.s.l.) lying between the Nuup Qinnua Fjord and the Saqqap Sermia outlet glacier, younger deglacial radiocarbon ages (~7.5 kyr BP; Levy et al., 2017) suggest the land-terminating ice sheet margin retreated at a slower pace. Although this hypothesis requires further

evidence for validation, our reconstruction uses this data to suggest an ice margin remaining more extensive than present until our youngest isochrone, *i.e.* 7-6.5 kyr BP (Fig. 12).



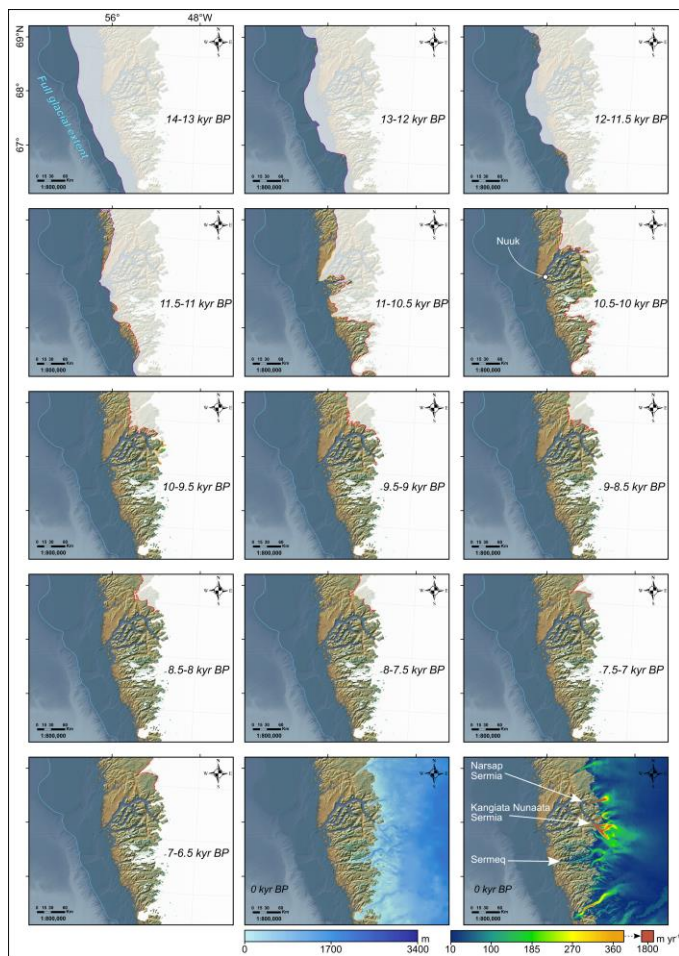


Figure 12. Time slice maps of the PaleoGrIS 1.0 isochrone reconstruction in the Nuuk region. The reconstructed ice sheet areal extent for each given time slice is displayed in each sub-panel as a white transparent polygon, while the underlying opaque white layer is the present-day ice cover from BedMachine v4. The reconstructed ice sheet margins are highlighted by our isochrone polylines, which feature different colour schemes (see Fig. 8 for key) relating to our four isochrone confidence levels (see section 2.3.5). Bottom panels also feature present-day ice-sheet thickness (Morlighem et al., 2017) and surface velocity data (Joughin et al., 2018). Topography and bathymetry are from the GEBCO 2022 release.

| [For a more complete figure legend, the reader is advised to consult Figure 8.](#)

1555

3.2.7 Ice sheet retreat in Central West Greenland, and ice-margin evolution in the Sisimiut, Disko Bay, and the Ummannaq fjord regions

1560 *Sisimiut region*

The coastal region here described as belonging to central West (CW) Greenland stretches 600 km northward from the large Maniitsoq ice cap (66°13'N; 52°11'W) to the Ummannaq Fjord region. From the Maniitsoq ice cap to the southern edge of Disko Bay (Qeqertarsuup tunua), the ice-free coast is characterised by a relatively flat bedrock plateau dissected by deep fjords and extending ~150 km from the outer coast to the contemporary ice margin (Fig. 13). This region, home to the towns of

1565 Sisimiut and Kangerlussuaq, has been the subject of numerous investigations reconstructing the evolution of the ice sheet margin during deglaciation (e.g. Ten Brink & Weidick, 1974; Eisner et al., 1995; Bennike, 2000; Roberts et al., 2009; Rinterknecht et al., 2009; Storms et al., 2012; Winsor et al., 2015; Kelley et al., 2013; 2015; Lesnek & Briner, 2018; Briner et al., 2020; Young et al., 2020). Moreover, ice-marginal landforms are well preserved and highly concentrated in this area. As a result, the Late glacial and early-to-mid Holocene retreat of the ice-sheet margin is locally well constrained. Based on this

1570 high density of geological evidence, we reconstruct with reasonable levels of confidence an ice sheet margin that had retreated to within 30 km (offshore or onshore depending on the valley) of the present-day outer coast by ~12-11.5 kyr BP (Fig. 13). After that time, the eastwards ice-sheet margin retreat appears to have been relatively monotonic in this region. Local outlets glaciers sampled, *i.e.* the South Russel, Isunnguata Sermia, Inuppaat Quuat, and Akuliarutsip Sermia glaciers (Björk et al., 2015), seem to have retreated at intermediate but steady speeds varying between 25 and 30 m yr⁻¹ once averaged. By ~9 kyr

1575 BP, we reconstruct an ice-sheet margin that was near (within 20 km) the inner end of local fjords (e.g. Kangerlussuaq, Nagssugtoq, Qasigiarssuit). Between ~9 and ~7 kyr BP, empirical evidence suggests the ice sheet started retreating slower and was located less than 30 km from the present-day margin for ~3 kyr in most locations throughout this region. This slowdown in retreat appears to have been coeval with the ice sheet margin becoming fully land-terminating in most valleys, and is thus a potential consequence of the removal of calving-related ablation. The local reconstructed retreat pattern is such that the ice

1580 sheet present-day extent was not reached until ~7-6.5 kyr BP.

Disko Bay

1585 Further North, at 68.7°N, lies Disko Bay (Qeqertarsuup tunua), formerly host to a large streaming outlet glacier (also referred as the Jakobshavn Isbræ ice stream) that flowed towards Baffin Bay. This ice stream is thought to have reached the continental shelf break during the last full glacial extent, and likely remained near such extent until ~14 kyr BP (Ó Cofaigh et al., 2013;

Rinterknecht et al., 2014). For our outermost isochrone (14-13 kyr BP), we thus reconstruct an ice sheet margin located towards the middle-to-outer continental shelf, mostly based on data from Ó Cofaigh et al. (2013) (Fig. 13). Data from McCarthy (2011) and Rinterknecht et al., (2014) enables us to tentatively draw an ice sheet margin that had retreated towards the inner continental shelf, with ice thinning causing its lateral margin to be resting against the southern coastal mountain slopes of Disko Island.

Based on offshore data by Lloyd et al. (2005) and TCN exposure ages by Kelley et al. (2013; 2015), we estimate further retreat into Disko Bay had caused the ice margin to be positioned 30 km offshore the mouth of the Ilulissat Icefjord, and towards the Akunaaq and Qasigiannuit settlements further South, by 10.5-10 kyr BP. The following phase of retreat was likely characterised by local outlet glaciers (*i.e.* Sermeq Kujalleq, Eqip Sermia, Saqqarliup Sermia, Sermeq Avannarleq, Akuliarutsip Sermia) retreating into fjords to the East of Disko Bay. These proglacial regions have been studied extensively, and are characterised by dense mapping and numerous geochronological constraints (e.g. Donner & Jungne, 1975; Long et al., 1999; 2006; Weidick & Bennike, 2007; Briner et al., 2010; Young et al., 2013; Carlson et al., 2014; Cronauer et al., 2016; Balter-Kennedy et al., 2021). This enables a high density of mid-to-high confidence isochrones to be drawn. To the South of Ilulissat Icefjord, empirical data suggests the ice sheet margin evolution was characterised by slow and steady retreat between ~10 and ~7 kyr BP. At a maximum, local outlet glacier fronts (e.g. Akuliarutsip Sermia) had retreated ~20 km during that time interval, which suggest retreat rates likely below 10 m yr⁻¹. Based on these observations, we reconstruct an ice margin that reached present-day extent by ~7.5-6.5 kyr BP in this area. For the Sermeq Kujalleq outlet glacier (also known as Jakobshavn Isbræ), extensive empirical datasets from both sides of the Ilulissat Icefjord enable us to constrain, with high levels of confidence, the position of the outlet's lateral margins through time (Briner et al., 2010; Young, et al., 2013). These data indicate that between ~10 and 8 kyr BP, the glacier calving front was either stable, or slowly retreating, and remained near the Fjord's mouth with the glacier's right lateral margins terminating on the Ilulissat peninsula (Fig. 13). After ~8 kyr BP, the calving front likely retreated to a mid-Fjord position, with lateral ice margins retreating to within ~5 km of contemporary ones by ~7 kyr BP. We estimate the Sermeq Kujalleq had retreated to near present-day extent between ~7 and ~6.5 kyr BP.

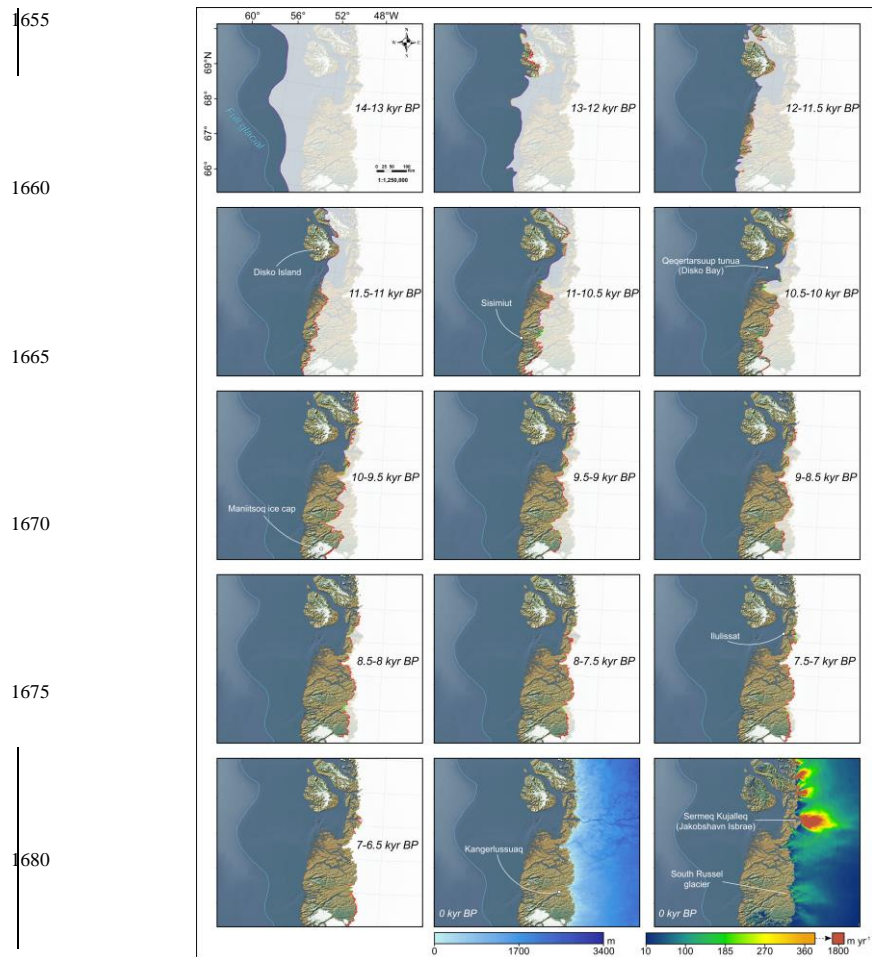
Uummannaq Fjord

Located ~250 km north from the former Jakobshavn Isbræ ice stream, a major outlet glacier, known as the Uummannaq ice stream (Lane et al., 2014), also formerly advanced towards Baffin Bay with rapid flow causing formation of streamlined subglacial bedforms (Ó Cofaigh et al., 2013). Radiocarbon ages from a marine sediment core (VC45) suggest that during the last full glacial configuration, this outlet glacier likely reached the continental shelf break, and remained in this position until ~15-14.5 kyr BP (Ó Cofaigh et al., 2013). Given this maximum-limiting constraint, we draw our outermost isochrone (14-13 kyr BP: very low confidence) in this area towards the middle-to-outer continental shelf, and map the Uummannaq ice stream margin as a protruding lobe (Fig. 14). A radiocarbon-derived event age by Bennike et al. (1994) indicates the ice-sheet margin

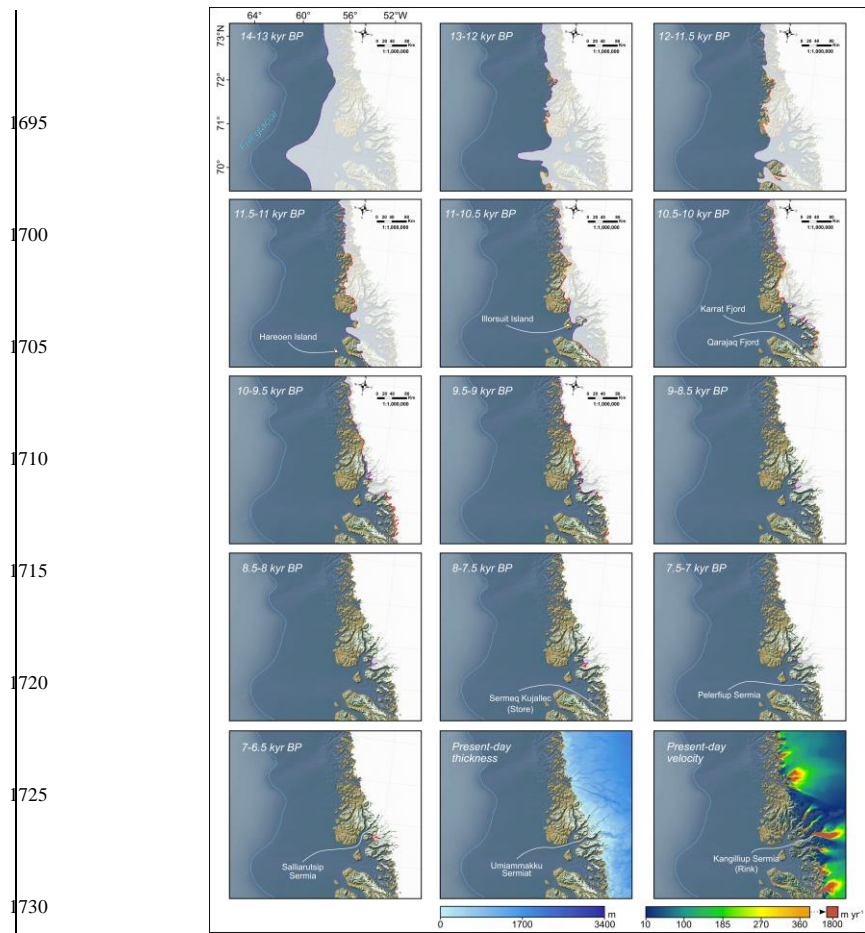
had retreated from the lower slopes of Hareoen Island prior to ~12.2 kyr BP. We thus tentatively reconstruct South and North lateral margins of the Uummannaq outlet positioned towards the outer contemporary coast between ~13 and ~12 kyr BP, while mapping a protruding lobe along the central bathymetric trough with a margin reaching a mid-shelf position. (Fig. 14).

Further East, a TCN-derived event age produced by Roberts et al. (2013) suggest the highlands of Illorsuit Island were becoming ice free by ~11.5-11 kyr BP. For this isochrone, we therefore reconstruct an ice sheet margin that separates into two distinct glaciers: with a northern glacier retreating northeastwards into Karrat Fjord, and a southern glacier retreating southeastwards into Uummannaq Fjord. (Fig. 14). Further retreat led to divisions into 12 distinct outlets retreating in a dendritic series of narrow fjords, now host to the calving fronts of several fast-flowing tidewater glaciers, such as Salliarutsip Sermia (72.0°N), Umiammakku Sermiat (71.7°N), Kangilliup Sermia (Rink Isbræ, 71.7°N), or Sermeq Kujallec (Store Gletsjer, 70.4°N). In agreement with TCN-derived event ages by Lane et al. (2014), our reconstruction suggests that by 10-9.5 kyr BP, the Umiammakku Sermiat and Kangilliup Sermia glacier fronts had retreated towards the Fjord mouths, near the western edge of Karrat Island, ~50-30 km from their present-day fronts. (Fig. 14). Therefore, in the northern sector of the Uummannaq Fjord system (Karrat area), we estimate that rapid retreat of the ice sheet margin was experienced between ~11.5 and ~9.5 kyr BP.

Informed by data from the Qarajaq Fjord further South (Simonarson, 1981; Roberts et al., 2013), our reconstruction also suggests a rapid retreat of the ice margin in the southern Uummannaq Fjord system, between ~11 and ~10 kyr BP. However, after ~10-9.5 kyr BP, northern outlet glacier fronts (Karrat area) appear to have remained relatively stable, with fronts staying more extensive than present until at least 5 kyr BP, hence for significantly longer than most other Greenland regions (Lane et al., 2014). This contrasts with the ice sheet margin evolution in the southern Uumannaq sector, for 60 km further South TCN-derived event ages from Philipps et al. (2017) suggest the lateral margins of the Perlerfiup Sermia (71.0°N) glacier were within 5 km of the present-day margin by 10.5-10 kyr BP. (Fig. 14). This dataset further indicates that after ~9.5 kyr BP, this outlet was either as or more retreated than the present-day margin. This southern sector is characterised by lower coastal mountains, more gradual slopes, wider fjords and fewer mountain glaciers today than towards the northern Uummannaq Fjord system. This setting may have caused less ice mass contribution from periphery mountain glaciers acting as tributaries, than further North. 70 km further south, our reconstruction suggests the Sermeq Kujallec (Store) glacier was more extensive than present until ~9-8 kyr BP (Roberts et al., 2013). Overall, empirical data suggest the early-to-mid Holocene margin response of individual outlet glaciers of the Uummannaq Fjord system was complex and heterogenous, and we try to capture this variability in our isochrone reconstruction.



1685 **Figure 13. Time slice maps of the PaleoGrIS 1.0 isochrone reconstruction in Sisimiut and Disko Bay region. The reconstructed ice sheet areal extent for each given time slice is displayed in each subpanel as a white transparent polygon, while the underlying opaque white layer is the present-day ice cover from BedMachine v4. The reconstructed ice sheet margins are highlighted by our isochrone polylines, which feature different colour schemes (see Fig. 8 for key) relating to our four isochrone confidence levels (see section 2.3.5). Bottom panels also feature present-day ice-sheet thickness (Morlighem et al., 2017) and surface velocity data (Joughin et al., 2018). Topography and bathymetry are from the GEBCO 2022 release. For a more complete figure legend, the reader is advised to**
 1690 **consult Figure 8.**



1695
1700
1705
1710
1715
1720
1725
1730
1735
1740

Figure 14. Time slice maps of the PaleoGrIS 1.0 isochrone reconstruction in the Ummannaq Fjord region. The reconstructed ice sheet areal extent for each given time slice is displayed in each subpanel as a white transparent polygon, while the underlying opaque white layer is the present-day ice cover from BedMachine v4. The reconstructed ice sheet margins are highlighted by our isochrone polylines, which feature different colour schemes (see Fig. 8 for key) relating to our four isochrone confidence levels (see section 2.3.5). Bottom panels also feature present-day ice-sheet thickness (Morrighem et al., 2017) and surface velocity data (Joughin et al., 2018). Topography and bathymetry are from the GEBCO 2022 release. Note that between 9-8.5 and 7-6.5 kyr BP, in this region, sections of the former ice-sheet margin may have retreated beyond its present-day extent (opaque white polygon). For a more complete figure legend, the reader is advised to consult Figure 8.

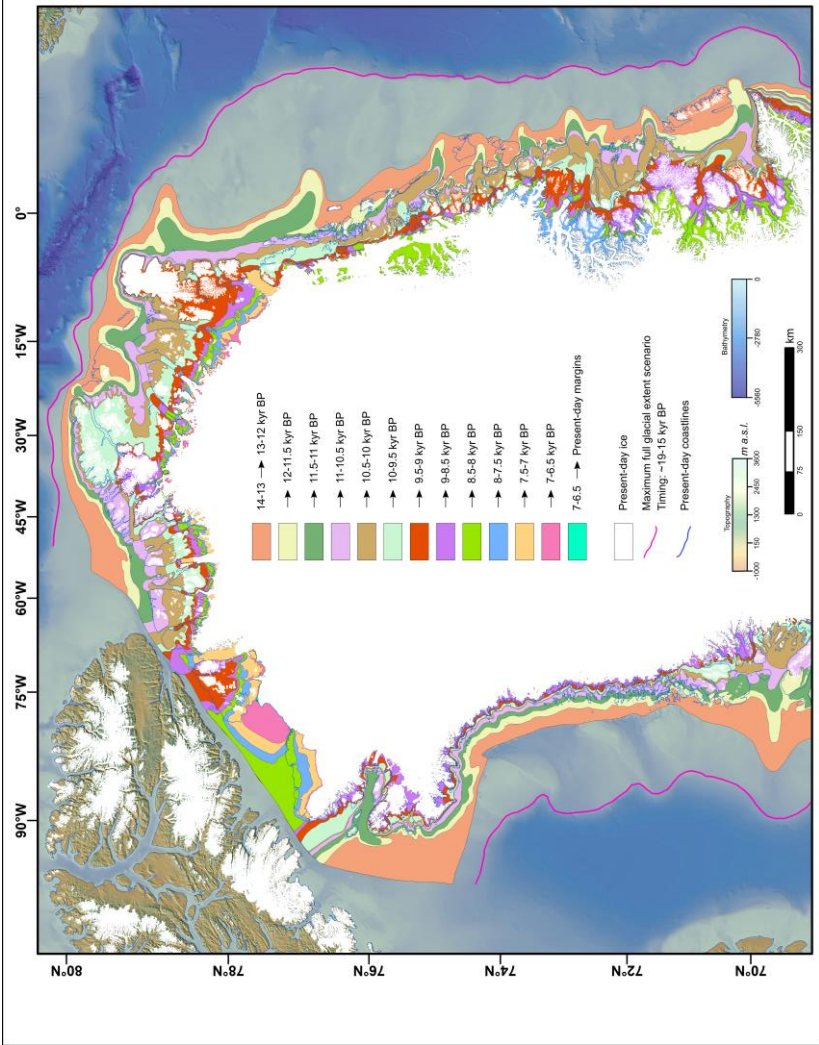
3.2.8 Ice sheet retreat in Northwest Greenland, and ice-margin evolution in the Upernavik and Aappilattup Ikera region

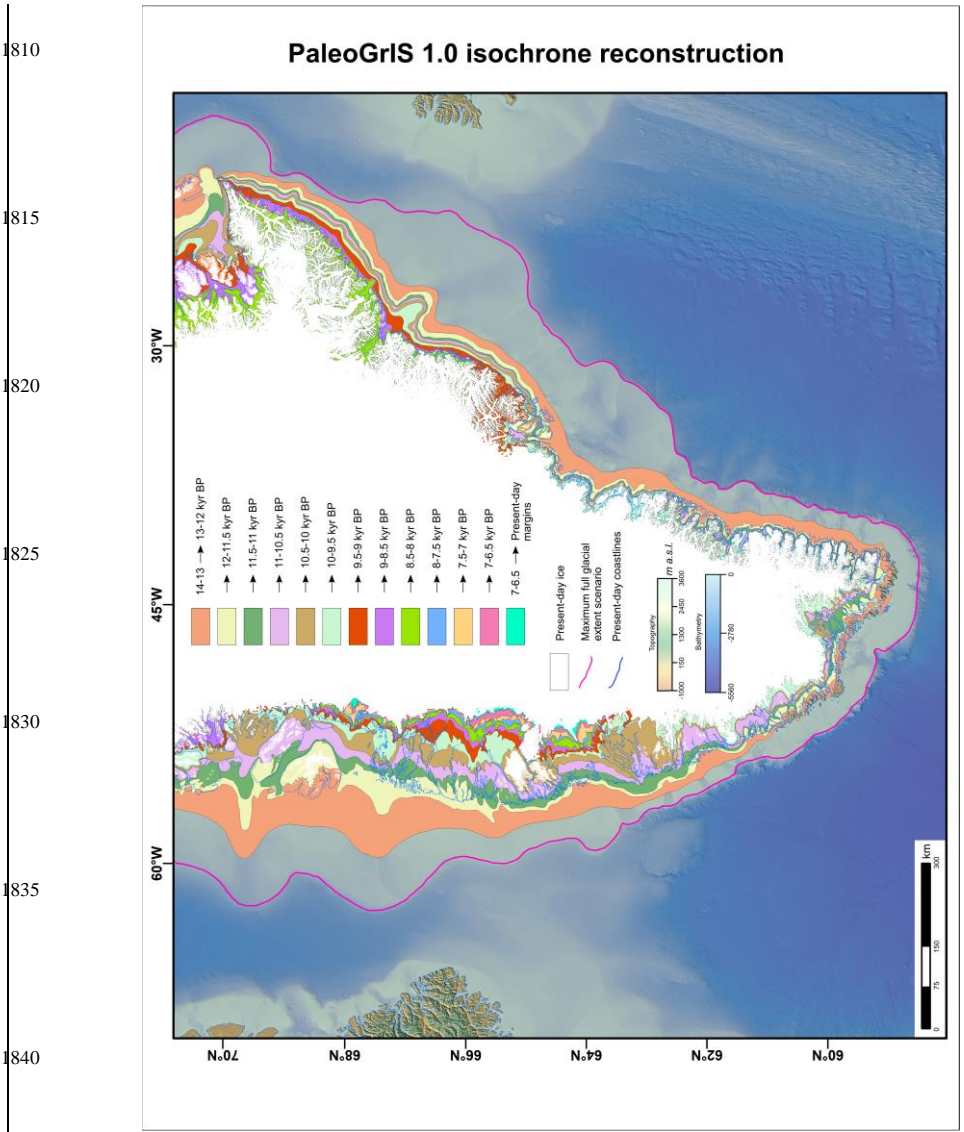
1745 To the north of the Ummannaq Fjord region, the ~800 km coastline of Greenland that stretches up to Steensby Land (77°N) is commonly described as belonging to the NW Greenland region. This coastline is characterised by little ice-free land as the present-day ice sheet margin reaches the shore along most of the coastline, and this region features relatively low-lying coastal topographies. In this sector, according to our compilation, few studies constrain the timing and positions of the former Greenland Ice Sheet margin. The exception to this is the region of Upernavik, however, where two studies (Briner et al., 2013; 1750 Corbett et al., 2013) provide numerous TCN exposure age - derived time constraints on the deglacial evolution of the Sermeq (Upernavik Isstrøm) tidewater glacier, which drains a major catchment of the NW Greenland Ice Sheet. There, we use the deglacial TCN exposure ages from westernmost Islands located 15 km offshore the Upernavik settlement (Corbett et al., 2013) to map a retreated outermost isochrone (14-13 kyr BP) located towards the inner continental shelf, approximately 30 km West of the mouth of Aappilattup Ikera (the Upernavik Isfjord). Younger TCN exposure ages and dipstick models obtained from 1755 high topographies that lie further East along the Upernavik archipelago seem to indicate a relatively monotonic and slow (~15 m yr⁻¹) ice-sheet margin retreat pattern between 14-13 and 11.5-11 kyr BP. We thus reconstruct the Sermeq outlet glacier front to rest towards the outer-to-mid Aappilattup Ikera Fjord by 11.5-11 kyr BP. Further inland, TCN exposure ages from an Island adjacent to the historical ice margin (Briner et al., 2013) indicate faster retreat likely caused the ice-sheet margin to recede towards the inner Fjord by 10-9.5 kyr BP. Moreover, according to three deglacial radiocarbon ages from lake cores sampled 1760 within 5 km of the contemporary ice front (Briner et al., 2013), we reconstruct a local ice-sheet margin that reached a similar to present-day extent shortly after ~9.5-9 kyr BP. Along the coastline located to the North of the Upernavik sector, our reconstruction mostly features very-low confidence isochrones crudely depicting a retreat pattern assumed to be monotonic, due to a lack of geochronological and land-based geomorphological evidence.

1765

1770

PaleoGIS 1.0 isochrone reconstruction





1845 Figure 1415. Ice-sheet-scale map of the PaleoGrIS 1.0 isochrone reconstruction divided in two distinct panels (North Greenland and
South Greenland) for readability purposes. The individual isochrone lines mapped as part of this study, and their four respective
confidence levels, are too detailed to be visualized at this scale. Instead, we here show a colour map of the areas located between
isochrones. Consequently, each colour-coded mask (or ‘isochrone buffer’) highlights the former location of the Greenland Ice Sheet
1850 margins between the timings of the outer and inner isochrones it is delimited by. In order to visualise the full details of the isochrone
reconstruction, along with the geomorphological and geochronological data compiled, the reader is advised to download and zoom
into the PaleoGrIS 1.0 poster (A0 format) provided in the online database. Alternatively, the reader can download the PaleoGrIS
1.0 shapefile database and visualise the reconstruction at any scale in a GIS software.

1855 3.3 Analysis of changes in areal extent of the Greenland Ice Sheet

1860 3.3.1 Ice sheet-wide areal extent evolution

Our reconstruction at 14-13 kyr BP suggests that the Greenland Ice Sheet had an approximate areal extent of 2.61 million km²
(Figs. 14, 15, 16) and lost about one third of this areal extent (0.89 million km²) as it reduced in size to its present-day extent
(1.71 million km²; Morlighem et al., 2017; Fig. 16). Between 14-13 and 9-8.5 kyr BP, our reconstruction produces a near
constant rate of ice sheet areal extent loss of 170 ± 27 km² per year (Fig. 15). Later, between 9-8.5 and 7-6.5 kyr BP, our
1865 reconstruction suggests a rate of areal extent loss that progressively decreased through time (Fig. 16). However, as our areal
extent estimates are only maximum-limiting between 10-9.5 and 7-6.5 kyr BP (see section 2.4), this potential slow down
remains hypothetical and could be a consequence of our limited knowledge regarding how far the ice-sheet margin retreated
behind the present-day position in response to the Holocene Thermal Maximum.

1870 At 7-6.5 kyr BP, we estimate the ice sheet areal extent was 1.71 million km² or less. This suggests the Greenland Ice Sheet
extent was similar or smaller than present by this time. Although highly uncertain, our literature-based maximum and minimum
full glacial extent scenarios (see section 2.6) suggest the ice sheet areal extent was likely between ~3.13 and ~2.94 million km²
during the last full glacial configuration (Figs. 5, 15, 16). We thus estimate that before the start of the Holocene (~11.7 kyr BP),
deglaciation had caused the ice sheet to lose between ~26% and ~21% of its full glacial extent. Therefore, we find that between
1875 ~57 and ~51% of the post-glacial areal extent loss occurred before the onset of the Holocene, while a significant proportion
(~49-43%) still occurred during the early-to-mid Holocene interval.

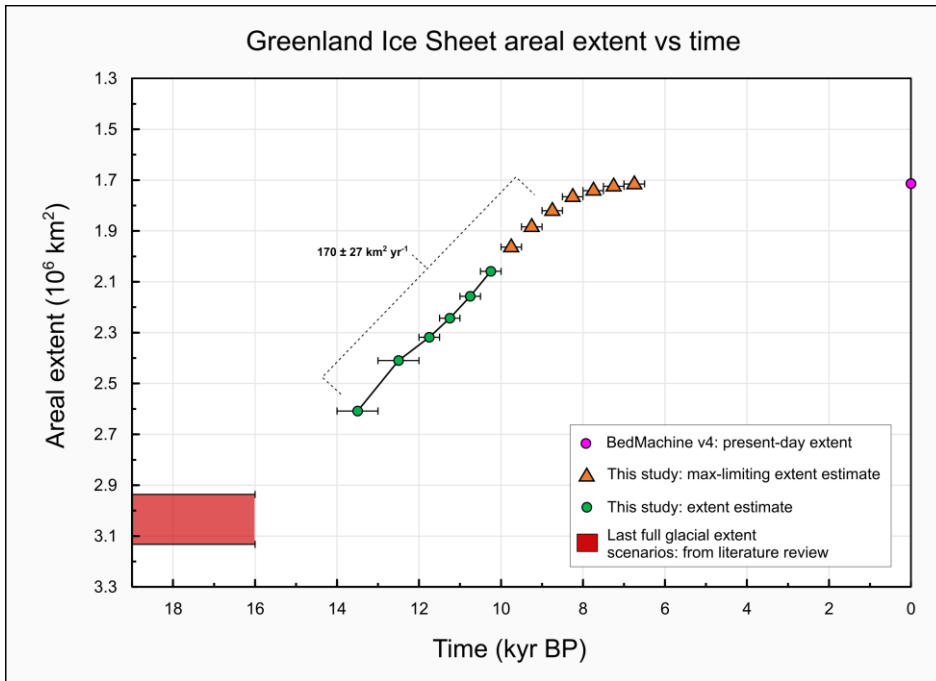
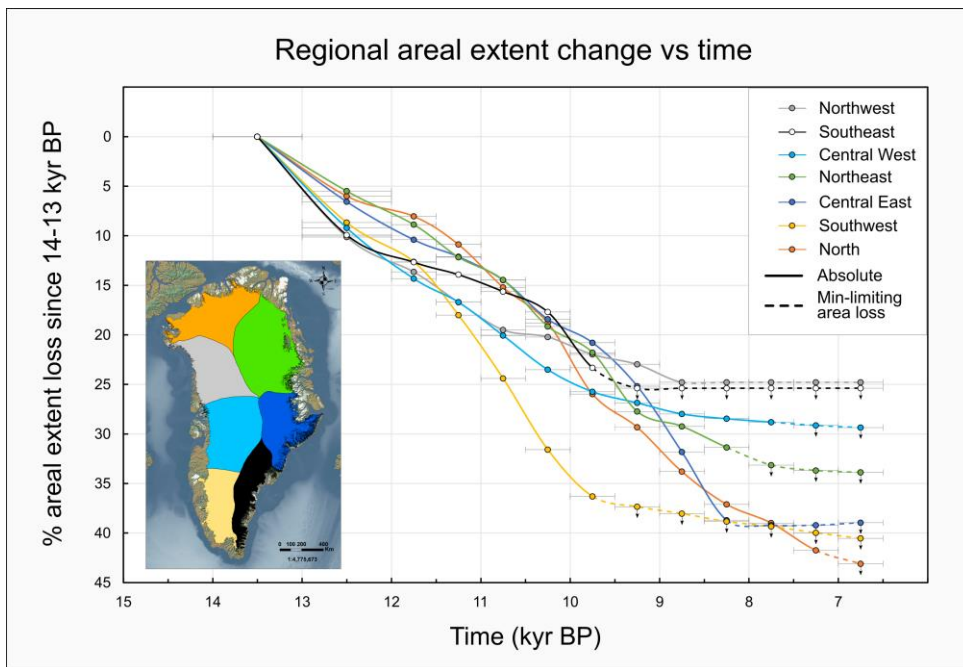


Figure 4516. Empirical estimation of the Greenland Ice Sheet areal extent evolution between ~18 kyr BP and present. The ice sheet extent during last full glacial configuration (red box) is here estimated by bracketing maximum (at continental shelf break everywhere) and minimum extent scenarios reconstructed after consulting the relevant literature, in an attempt to highlight the uncertainties in several debated or understudied regions (more details in section 2.6). The hypothetical timing of such full glacial extent is crudely associated with maximum atmospheric and oceanic cooling over Greenland during Heinrich Stadial 1 (Buizert et al., 2018), but we stress the timing of maximum extent is unknown and could have been reached before 18 kyr BP, and until Bolling-Allerod warming started after ~16 kyr BP, as highlighted by our conservative range (red box). Ice sheet areal extent estimates from the PaleoGrIS 1.0 isochrone reconstruction are shown with green circles (actual extent estimates) and orange triangles (maximum-limiting extent: pointing upwards). This differentiation is due to our isochrones not covering the full ice-sheet perimeter during the ~10-6.5 kyr BP interval, when some sections of the ice sheet margin are estimated to have been as- or more-retreated-than-present margins.

Formatted: Font: 10 pt, Not Bold

3.3.2 Region-specific areal extent change

After dividing the ice sheet into 7 major drainage basins (after Rignot & Mouginot, 2012; see section 2.4), we analysed regional patterns of areal extent change through time. While all regions lost areal extent between 14-13 and 7-6.5 kyr BP, we find the timing, rate, and magnitude of ice-sheet retreat differs substantially between regions (Fig. 4617). By 7-6.5 kyr BP, the NO, SW, and CE regions had lost at least 40% of their 14-13 kyr BP areal extent. The same figure is nearly twice as low (~25%) for the NW and SE regions. During that time, the CW and NE regions lost at the minimum ~30% and ~35% of their areal extent, respectively. Furthermore, our reconstruction suggests the rate of areal extent loss, and its evolution through time, varied significantly between regions. For instance, the SW region lost areal extent relatively quickly from the period onset (~12-8% kyr⁻¹) and reached a similar-to-present extent earlier than other regions, by 10-9.5 kyr BP. The NO region also lost areal extent at a relatively quick rate (~8-6% kyr⁻¹), but such rapid loss started later (after ~12-11.5 kyr BP), and a similar-to-present areal extent was not reached until ~7-6.5 kyr BP (Fig. 4617). In the NE region, on the other hand, empirical data suggest similar-to-present extent was reached by approximately 8-7.5 kyr BP. Before that time, the rate of percentage areal extent loss was relatively constant and at ~7-5% kyr⁻¹. In the CE region, ice sheet areal extent loss was relatively slow (~7-5% kyr⁻¹) until ~10-9.5 kyr BP, prior to accelerating substantially (~18-9% kyr⁻¹) until ~8.5-8 kyr BP, by which time it had reached a similar-to-present extent. In our reconstruction, the CE regions thus appears to have experienced rapid and delayed collapse of a significant proportion of its total areal extent, between ~10 and ~8 kyr BP (Fig. 4617). The SE region reached a similar-to-present extent relatively early, by 9.5-9 kyr BP, and experienced relatively slow areal extent loss prior to that (~7-5% kyr⁻¹). The rate of areal extent loss in the CW region decreased progressively through time, and a similar-to-present extent was reached late in this region, after ~8.5 kyr BP. The NW region follows a similar pattern, but reached near present-day extent slightly earlier, prior to ~9 kyr BP (Fig. 4617). Such comparisons should be treated with caution, as they are sometimes derived from low or very low confidence isochrones. However, the data generally suggests a latitudinal signal in the different regional retreat patterns by which southernmost regions reached a near present-day margin position earlier than northern regions, which experienced a more delayed deglaciation.



1935 **Figure 4617.** The PaleoGrIS 1.0 reconstruction of percentage ice-sheet areal extent loss between ~14 kyr BP (0%) and ~6.5 kyr BP, for each of the seven ice sheet regions spatially divided as displayed in inset map, after Rignot & Mouginot (2012). The colour code of individual time series matches the inset map polygons. Importantly, we use a different symbol to highlight whether the percentage areal extent loss, for a given region, is an absolute areal extent estimate (straight line), or a minimum-limiting areal extent loss estimate (dashed line with downward pointing arrows). The switch from straight to dashed lines thus represents, for each region, the youngest isochrone to feature a more-extensive-than-present ice-sheet extent along the full region-specific ice margin.

1940 3.4 Outlet glacier retreat rates analysis

Transects were drawn across reconstructed isochrones for 72 outlet glaciers sampled around Greenland (further methods in section 2.5) (Fig. 4718). Measuring distances along these transects allows us to estimate that overall retreat rates of glacier fronts (or of the grounding line for marine margins), ranged between 72 and 8 m yr⁻¹ during the ~14-6.5 kyr BP time period (mean & 1σ S.D.: 37 ± 16 m yr⁻¹) (Fig. 4718). Although the frequency distribution of overall retreat rates is scattered and bimodal, it is such that >80% of outlet glaciers display retreat rates between 56 and 16 m yr⁻¹. Although slightly different in nature, these overall retreat rates are comparable to calving front retreat rates observed by Carr et al. (2017) for marine-terminating glaciers across Greenland for the 1992-2000 AD period (mean & 1σ S.D.: ~42 ± 86 m yr⁻¹).

1950 Our reconstructed ice sheet Late-glacial and early-to-mid Holocene retreat rates can be compared with deglacial retreat rates from other ice sheet reconstructions. For instance, Greenland Ice Sheet outlets retreated at paces comparable, or perhaps slightly faster, to terrestrial margins of the British-Irish Ice Sheet, associated with retreat rates < 50 m yr⁻¹ for most regions during deglaciation (Clark et al., 2022). Marine calving margins of the British-Irish Ice Sheet, however, generally retreated faster than our sampled Greenland outlets (>50 and up to 451 m yr⁻¹). Greenland outlet retreat rates also appear to be slower than fast-retreating terrestrial margins of the Laurentide Ice Sheet, e.g. the Southwest margin, thought to have reached retreat rates of 380-340 m yr⁻¹ following separation from the Cordilleran Ice Sheet (Norris et al., 2022). However, the Labrador sector of the Laurentide Ice Sheet is believed to have experienced slower and similar-to-GrIS-Holocene retreat, with Lowell et al. (2021) reporting a near-constant mean retreat rate of 52 m yr⁻¹ between ~19 and ~10 kyr BP in this region. We note that our reconstructed Greenland outlet retreat rates are net rates averaged over distances and time separating 500-year resolution isochrones. Our reconstruction may thus lead to smoothing of faster pulses of retreat (>200 m yr⁻¹) which therefore should not be ruled out.

Our reconstruction further suggests overall outlet-glacier retreat rates varied significantly between regions (Fig. 4718). We find that outlet glaciers from the CW region were likely the fastest retreating in Greenland between ~14-13 and 7-6.5 kyr BP, with a regional mean retreat rate of ~50 ± 14 (1σ S.D.) m yr⁻¹. This region includes the Sermeq Kujalleq (overall rate: 49 ± 5 m yr⁻¹), Sermeq Avannarleq (72 ± 14 m yr⁻¹) and Store (70 ± 11 m yr⁻¹) glaciers, for instance. Outlet glaciers from the NE and NO regions also retreated relatively quickly during that period, with mean retreat rates of 44 ± 10 m yr⁻¹ and 44 ± 13 m yr⁻¹, respectively. The retreat of outlet glaciers from the CE and SW regions was intermediate in speed, with mean retreat rates of 35 ± 23 m yr⁻¹ and 29 ± 12 m yr⁻¹, respectively. Finally, we estimate that outlet glaciers from the SE and NW regions experienced slower retreat at the time relative to other regions, with mean retreat rates of 25 ± 5 and 24 ± 15 m yr⁻¹, respectively (Fig. 4718). The latter contrasts with present-day retreat rates, as marine-terminating outlet glaciers in SE and SW Greenland

currently show the third and fourth fastest regional mean retreat rates (136 and 117 m yr⁻¹, respectively) after NO and CW Greenland (Carr et al., 2017). Our reconstruction shows that spatial variability in outlet glacier retreat rate over the studied period is dominated by these regional patterns. Indeed, we find no statistically significant correlation between individual glacier retreat rates and their present-day front width, nor with the approximate width of over-deepened troughs along which they retreated. Moreover, we argue confidence levels in the ice-sheet-wide PaleoGrIS 1.0 isochrones are often too low to conduct quantitative analyses at the valley or outlet-glacier scale.

Our results also indicate that for most ice sheet outlet glaciers sampled, the rate of retreat is highly variable throughout the reconstructed time period, *i.e.* between 14-13 and 7-6.5 kyr BP. Indeed, the median retreat rate of all sampled glaciers (n = 72) shows intermediate values between ~14 and ~12 kyr BP (~20-10 m yr⁻¹), increases between ~11.5 and ~9.5 kyr BP (30-20 m yr⁻¹), and decreases to its lowest values between ~9.5 and ~6.5 kyr BP (~15-5 m yr⁻¹) (Fig. 4819). We thus find a significant proportion of Greenland outlet glaciers experienced acceleration in their retreat pace between ~11.5 and ~9.5 kyr BP, when our reconstruction suggests numerous glaciers retreated at speeds >100 m yr⁻¹ (Fig. 4819). These faster retreat rates are not observed as much during other time intervals of the Late-glacial and early-to-mid Holocene. The timing of this faster retreat (~11.5-9.5 kyr BP) coincides with the highest rates of atmospheric and oceanic warming reconstructed between the Younger Dryas (~13-11.7 kyr BP) and the end of the pre-industrial era (Buizert et al., 2018). Furthermore, using linear regression analyses, we find the majority of outlet glaciers (65%) indicate a decelerating retreat pace over the full reconstructed period (Fig. 4819).

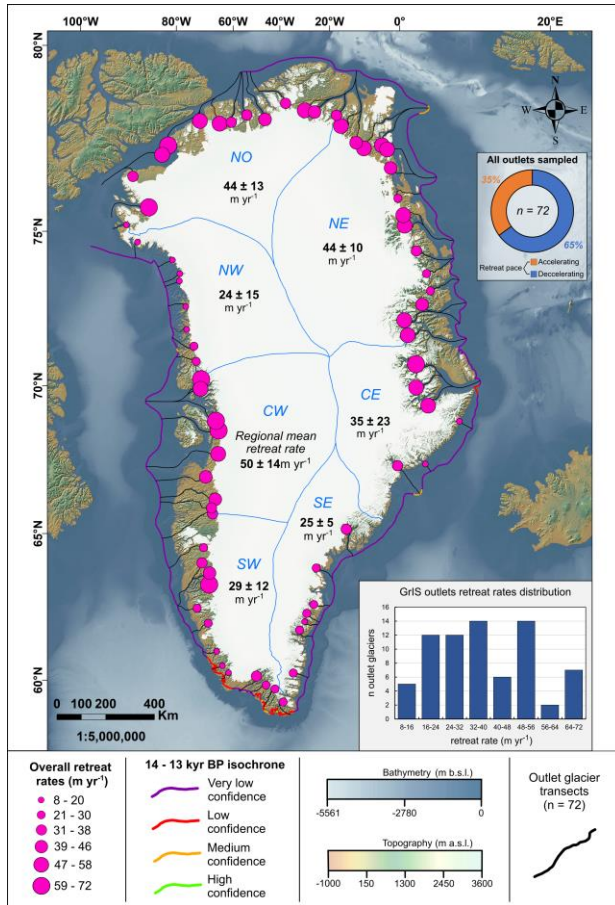


Figure 4718. Map of [GISGreenland Ice Sheet](#) outlet glacier transects (black lines, n = 72) drawn to conduct a retreat rate analysis (see section 3.4.) using [PaleoGrIS 1.0](#) isochrones, the main results of which are also shown here. Retreat rates over the full reconstruction period (~14-6.5 kyr BP) are denoted using pink circles characterised by sizes proportional to overall retreat rate magnitudes. Our outermost isochrone (14-13 kyr BP), which marks the outer edge of our transect mapping, is shown with its spatially-variable colour-coded confidence levels. Towards the bottom right-hand corner, a histogram of overall retreat rate distribution is shown as split in eight bins of retreat rate magnitude. Moreover, bold black numbers indicate the regional mean overall retreat rate ($\pm 1\sigma$ S.D.) for each of the seven ice-sheet regions sampled. Towards the top right-hand corner, a donut diagram highlights the relative proportions of outlet glacier retreat rates indicating decelerating (65%) vs accelerating (35%) trends over the full reconstruction period.

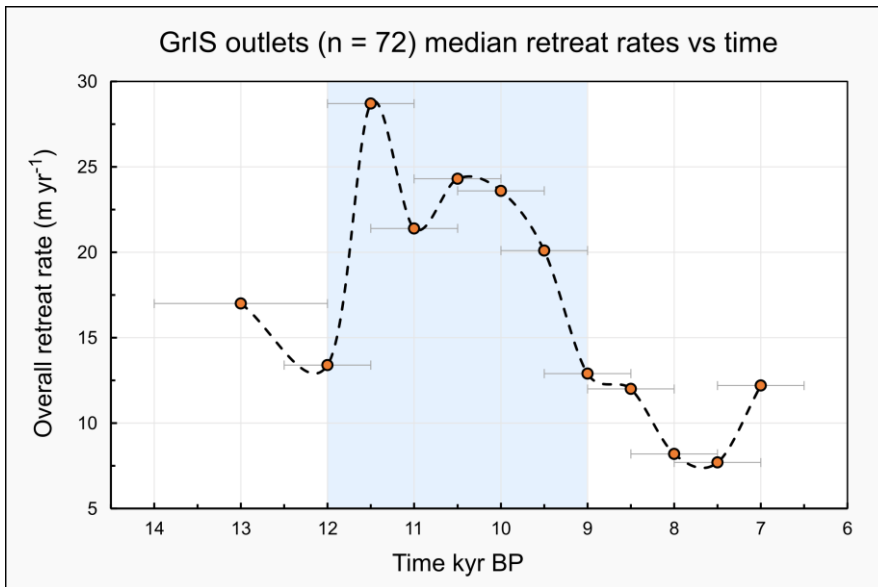


Figure 4819. Time series denoting the evolution of the median retreat rate for all outlet glaciers sampled over the full reconstruction period (14-6.5 kyr BP). The blue polygon highlights a period of general acceleration in Greenland Ice Sheet outlet glacier retreat speed (see section 3.4). It is important to note that the youngest time slices are here associated with less than 72 data points, as our reconstruction features certain outlet glacier margins reaching present-day extent before others.

4. Discussion

4.1 Progress towards a robust reconstruction of the Greenland Ice Sheet retreat, knowledge gaps, and opportunities for future investigations

PaleoGrIS 1.0 is the first attempt to merge both geochronological and geomorphological markers of former grounded ice extent to produce an ice-sheet-wide isochrone reconstruction of the Late-glacial and early-to-mid Holocene evolution of the Greenland Ice Sheet margin (Fig. 4415). It thus represents a significant improvement from previous ice-sheet-wide reviews and compilations (e.g. Dyke, 2004; Funder et al., 2011; Lecavalier et al., 2014; Sinclair et al., 2016). Another novelty of this work is that it aims to make the reconstruction and empirical database as accessible and usable as possible, whether it is to inform future empirical and model-data comparison investigations, or to provide a format suitable to the production of future versions of the reconstruction (see online database).

This first version of PaleoGrIS however remains incomplete, and has its limitations. As noted earlier (section 2.1.1), our mapping of ice-marginal landforms was conducted rapidly over a few years and deliberately at a reconnaissance level to identify only the main terrestrial landforms recording former ice margin positions. This was necessary to cover the large area and permitted us to erect the ice-sheet-wide framework we have presented. Conducting and compiling more detailed regional studies that map a wider range of ice marginal landforms, including those located offshore, is an important future task. In understudied regions displaying less empirical constraints (e.g. Fig. 4920), our reconstruction may act as a stimulus for such investigations and could represent a template that will undoubtedly require revision. We believe such revision would greatly benefit from becoming a wider community effort enabling to gather newly acquired data and knowledge on the update scenarios of local ice sheet margin history (e.g. DATED-2, Hughes et al., 2023).

To enhance confidence in the empirical record and improve our ability to quantitatively compare paleo model simulations with observations, the glaciology community requires more field data from and around Greenland. We here used our reconstruction to identify regions that would most benefit from new constraints on the timing of former grounded ice-sheet retreat. To do so, we mapped terrestrial and offshore regions displaying no or only low-confidence event ages, and thus presenting either low or very low confidence isochrones in our reconstruction. The highlighted regions are shown in Figure 4920, and shapefiles are provided in the online database. Care should be taken as this assessment does not include ongoing research efforts, data yet to be published, or data published after our census date (21/10/2022) (e.g. Weiser et al., 2023). Nonetheless, we find vast terrestrial and offshore areas displaying low or very low confidence isochrones. Offshore of present-day coastlines, we note the majority of the Greenland continental shelf remains data-scarce when compiling studies establishing the timing and pattern of grounded ice retreat from the last full glacial extent. For terrestrial regions, we also find numerous areas displaying potential

2085 for new field data collection, around the full ice sheet perimeter, with a relatively greater density and surface area coverage of
less studied sites in the northern half of the island's periphery ($>71^{\circ}\text{N}$; Fig. 19). ~~It must be noted that such data gaps are most
likely related to the increased logistical, safety, access, and financial constraints associated with field investigations in more
remote and problematic regions.~~ Furthermore, a great source of uncertainty impeding a better understanding of the
deglacial dynamics originates from the ice sheet being generally more extensive today than between ~ 6 and ~ 2 kyr BP, when
2090 responding to the Holocene Thermal Maximum. Obtaining empirical evidence of the ice sheet minimum extent during that
interval (e.g. as is attempted by the ongoing GreenDrill project: [Briner et al., 2024](#)) ~~Briner et al., 2021~~) would thus greatly
improve our capacity to reconstruct the ice-sheet deglacial evolution.

2095

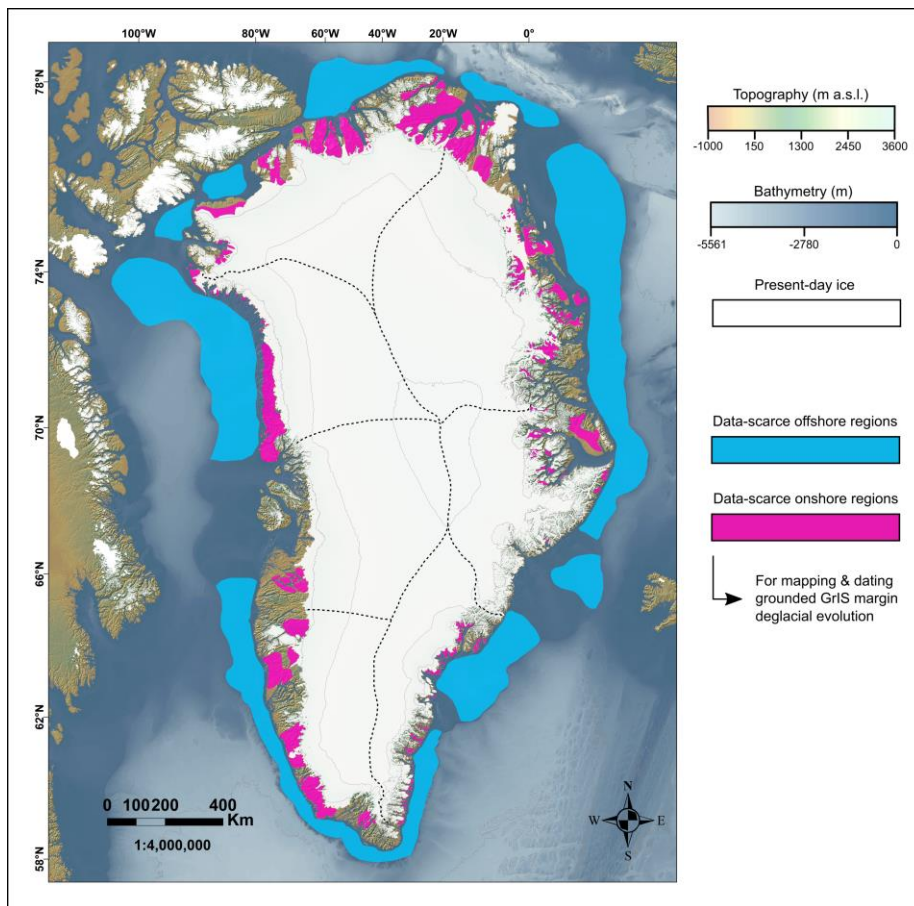


Figure 1920. Map of offshore and onshore regions that we interpret as [understudied data-scarce](#) for the specific purpose of mapping and dating the deglacial evolution of the grounded Greenland Ice Sheet margin. We thus believe these regions would most benefit from new geomorphological and geochronological data. They were identified by locating regions dominated by very low or low confidence isochrones in our PaleoGrIS 1.0 reconstruction. Two polygon shapefiles associated with these highlighted regions can be found in the online database.

4.2 Exploring controls on the varied retreat dynamics of the Greenland Ice Sheet

Our overarching interpretation of the reconstruction is that the deglacial retreat pattern and rate of the Greenland Ice Sheet, and the magnitude of the resulting mass loss, are controlled by a series of interacting mechanisms whose relative importance differs depending on the spatial and temporal scales analysed.

4.2.1 Ice-sheet-wide response

Linear response to climate and ocean forcing

Our reconstruction shows that at a Greenland-wide scale, the ice sheet mostly retreated in a simple radial pattern progressively stepping back from the continental shelf during the last deglaciation (Figs. 14, 15, 16). When analysed at a 1000 to 500-year resolution, the retreat was not found to significantly diverge from a linear retreat pattern other than with local offsets and complexity arising from lagged positioning of marine versus terrestrial margins (e.g. in and adjacent to outlet glacier tongues: Fig. 12) and where the main ice sheet left residual ice caps behind. As we here focus on the ice-sheet wide retreat signal (heterogeneous regional behaviours discussed further in section 4.2.2), and because event ages are now reasonably well distributed around Greenland's periphery, we believe this simple retreat signal would still arise even with improved spatio-temporal distribution of geochronological markers. Along with this surprisingly straightforward retreat pattern, we observe that the ice-sheet-wide reduction in areal extent reveals a simple (negative) linear relationship with atmospheric or sea surface temperatures (Buizert et al., 2018; Osman et al., 2021) during the Late-glacial and early-to-mid Holocene (Fig. 2021). These correlations suggest climate and ocean forcing were the dominating agents of former ice-sheet extent change. For instance, the overall acceleration of outlet-glacier retreat that we observe between ~11.5 and ~9.5 kyr BP is coeval with the potent atmospheric and oceanic warming that characterised the Younger-Dryas-to-early-Holocene transition in the North Atlantic and Greenland regions (Grootes et al., 1993; Fig. 20). Such observations suggest the Greenland Ice Sheet was highly sensitive to atmospheric and oceanic warming. The findings of a more retreated than present ice sheet (21). This faster retreat also coincides with significant ocean warming, with marine records indicating increasing sea surface temperatures offshore most Greenland regions from ~16 kyr BP, and reaching maximum warmth at ~10-8 kyr BP (e.g. Williams, 1993; Jennings et al., 2006; 2017; Osman et al., 2021; Fig. 21). More particularly, offshore SE, SW, and CW Greenland regions, warmer and saline sub-surface Atlantic water ingress from the Irminger current (Fig. 1) is thought to have caused rapid mass loss and initial retreat of grounded ice margins from the outer continental shelves (Knutz et al., 2011; Ó Cofaigh et al., 2013; Jennings et al., 2017). Similar forcing is thought to have occurred in NE and CE Greenland, with warmer and more saline Atlantic water advected southward from Fram Strait, along the Greenland coast, and across continental shelves to marine terminating margins.

with the establishment of the West Spitsbergen, Return Atlantic and East Greenland currents during deglaciation (Hopkins, 1991; Hebbeln et al., 1994). Furthermore, the findings of former ice-sheet margins likely located behind present-day ones during and following the Holocene Thermal Maximum (Briner et al., 2014), followed by ice margin readvances during mid-to-late Holocene cooling that peaked with the Little Ice Age (~1850 AD; Kjeldsen et al., 2015), are more evidence of this broadly linear response to climate and ocean forcing. Overall, these observations suggest the Greenland Ice Sheet was highly sensitive to atmospheric and oceanic warming.

Relative sea level change is also likely to have influenced the timing and the linear nature of the ice-sheet-wide retreat pattern during the Late-Glacial and early-to-mid Holocene periods (Figs. 15, 16). In most coastal regions, relative sea level rose rapidly after ~16 kyr BP, reaching a spatially-variable high stand of 50-120 m at around 12-10 kyr BP (Funder & Hansen 1996; Gowan, 2023; Lecavalier et al., 2014; Simpson et al., 2009). The timing of this relative sea level high-stand therefore also coincides with the observed peak in outlet glacier retreat rates (Fig. 19). More specifically, this rapid sea level rise is thought to have promoted the early deglaciation of inter-stream sectors of the marine-terminating former ice sheet, which likely presented thinner ice (<300-400 m) grounded on shallower sections of the continental shelves, and were more vulnerable to buoyant lift-off and calving-induced retreat (Roberts et al., 2009). The importance of this mechanism has moreover been confirmed by modelling studies experimenting with different sea level forcings to nudge modelled Greenland Ice Sheet extent (e.g. Lecavalier et al., 2014; Simpson et al., 2009).

Based on the observation of such broadly linear response in ice extent, we suggest that at a whole ice sheet scale, complexities in ice dynamics are less relevant at 1000 to 500-year timescales than is perhaps perceived when analysing contemporary glaciological fluctuations and feedbacks. Alternatively, our reconstructions are not yet sufficient in density and resolution to adequately constrain retreat and advance oscillations that might have existed.

'Glaciological inertia' and delay in response

Although the Greenland Ice Sheet was highly sensitive to atmospheric and oceanic warming, specific glaciological responses to a forcing may vary over different timescales. Melting or calving can happen nearly instantaneously whereas changes to ice accumulation may take thousands of years to work through the system. Dynamic changes to flow geometry and the positions of ice divides, as well as responses to glacial isostatic adjustment may take even longer still (Rogozhina et al., 2011). Consequently, significant inertia in the system may have caused delay in the ice sheet extent response to deglacial warming. The PaleoGrIS 1.0 reconstruction suggests that the Greenland Ice Sheet margins remained more extensive than present in several regions until 7-6.5 kyr BP. The minimum Holocene extent of the entire ice sheet was thus not reached until later, most likely between 6.5 and 4 kyr BP, and as was previously suggested by numerical modelling experiments (e.g. Lecavalier et al., 2014). Over Greenland, $\delta^{18}\text{O}$ ice core records (e.g. Alley, 2000; Buizert et al., 2018b) and temperature reconstructions from

2175 paleo-climate data assimilations (e.g. Buizert et al., 2018a; Erb et al., 2022) all suggest Holocene mean annual temperatures
reached maximum values between ~9 and ~6 kyr BP, followed by gradual [Neoglacial](#) cooling until the end of the pre-industrial
era (~1850 AD; [Kjær et al., 2022](#)) (Fig. [2021](#)). Therefore, our ice-sheet-wide empirical reconstruction [confirms agrees with](#)
[previous observations](#) that during the Holocene, the ice-extent response of the Greenland Ice Sheet lagged the cessation of
warming, potentially by thousands of years. ~~inertia~~[This delay in turn caused a lag in the response of the ice sheet to positive](#)
2180 [mass balances during mid-to-late Holocene cooling](#). Indeed, while both summer insolation (Berger & Loutre, 1991) and
[temperature proxy records \(e.g. Erb et al., 2022\) reveal atmospheric cooling across Greenland from 8-6 kyr BP to the pre-](#)
[industrial era, significant neoglacial glacier expansion did not occur until 2.5-1.7 kyr BP \(Kjær et al., 2022\). Finally, the](#)
[Greenland-Ice-Sheet's response to anthropogenic warming that started around 1880-1900 was also delayed by almost a](#)
[century, with mass and ice-extent loss of ice-sheet-scale significance only starting in the 1980s \(Kjeldsen et al., 2015; Yang et](#)
2185 [al., 2022\). Interestingly, the latter decadal delay was shorter than the centennial- to millennial-scale lag in ice-sheet's response](#)
[to the earlier positive mass balances associated with mid-to-late Holocene cooling, thus possibly highlighting a positive](#)
[correlation between the duration/magnitude of the climate forcing and the length of the delay in subsequent ice-extent response.](#)
[However, such a lagged response observed at the ice sheet scale was not ubiquitous across the entire ice-sheet margin, as](#)
[certain more dynamic outlet glaciers appear to be more well-coupled with short-lived early Holocene temperature changes](#)
2190 [\(e.g. Jakobshavn Isbræ; Young et al., 2013b\). Centennial to millennial-scale inertia](#) of the Greenland Ice Sheet following
warming has been previously suggested (e.g. Yang et al., 2022), and has [important](#) implications for ongoing climate warming
[generating because it results in](#) committed future mass losses, and thus sea level rise contributions, that may last for centuries
to millennia- (e.g. [Greve & Chambers, 2022](#)).

2195

2200

2205

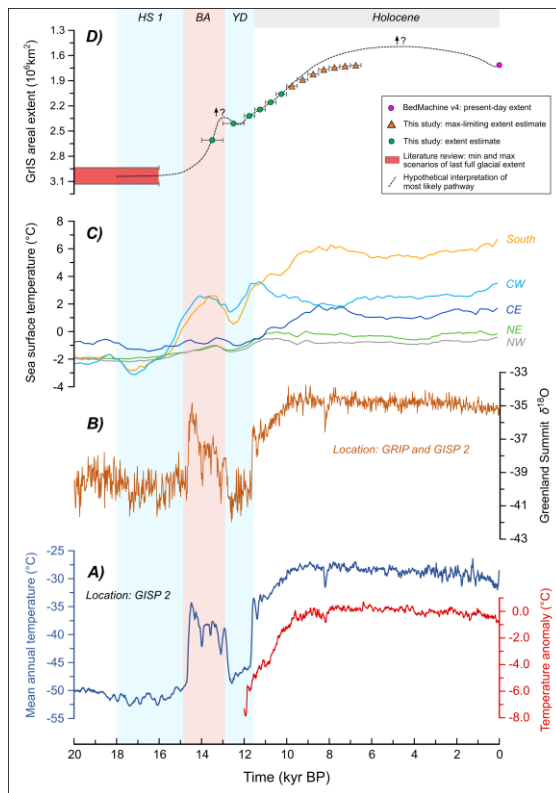


Figure 2021. Comparison between our reconstruction of Greenland Ice Sheet areal extent evolution and past atmospheric / sea surface temperature reconstructions from proxy and model data, between 20 kyr BP and present. A) Blue curve: reconstruction of mean annual near-surface temperature at location of the GISP 2 ice core (72.58°N; -38.48°W) by Buizert et al. (2018a), who merged Greenland ice core temperature reconstructions (GISP2, NGRIP, NEEM) with the TraCE-21ka simulations. Red curve: ensemble mean reconstruction of mean annual temperature anomaly (towards GISP 2 ice core location) relative to a 5-3 kyr BP reference period, by Erb et al. (2022), who use the global Holocene paleo-temperature proxy database of Kaufman et al. (2020) to conduct data assimilation on HadCM3 and TraCE-21ka simulations. B) The Greenland Summit $\delta^{18}\text{O}$ record (Buizert et al., 2018b) that averages the GISP2 and GRIP $\delta^{18}\text{O}$ records. C) Reconstructions of sea surface temperature at different locations offshore Greenland, using the ensemble mean ($n=500$) from the LGMR global dataset of Osman et al. (2021), who use a paleoclimate data assimilation scheme to correct biases in climate simulations of the iCESM (versions 1.2 and 1.3). Coordinates for time series: ‘South’ (Cape Farewell): 58.34°N; -43.25°W, ‘CW’ (Davis Strait): 64.72°N; -56.53°W, ‘CE’ (Denmark Strait): 66.64°N; -27.26°W, ‘NE’ (Nordic Sea): 72.25°N; -10.10°W, ‘NW’ (Baffin Bay): 73.17°N; -62.65°W. D) Greenland Ice Sheet areal extent reconstruction from literature review (LGM - HS 1 period), the PaleoGrIS 1.0 isochrones (this study: ~14-6.5 kyr BP), and BedMachine v4 (Morlighem et al., 2017).

4.2.2 Regional responses

2250 Moving from ice-sheet wide to a focus on individual regions (the ice catchments of Rignot & Mouginot, 2012), we find heterogeneous retreat patterns with apparent differences in both the magnitude of regional areal extent loss and the speed of ice margin retreat (Figs. 16, 17, 18). Spatially variable climate and ocean forcings (Fig. 2021) may have caused some of these differences. For instance, the saline Irminger Current transporting warm Atlantic waters offshore South Greenland (Fig. 1), likely caused this region to experience early, more intense oceanic and atmospheric warming (Levy et al., 2020; Fig. 20e). Such warm water inflow likely induced faster and earlier deglacial retreat of the ice sheet, crucial in causing sub-shelf melt near the grounding lines of marine-terminating ice-sheet margins, relative to northern regions (Knutz et al., 2011; Jennings et al., 2014). It has been argued that significant leads and lags in early deglaciation across Greenland may be partly related to the complex advection patterns of this water mass, enabled by the Irminger and West Greenland current (Fig. 1), influencing ice retreat in SE, SW and CW Greenland. Similar mechanisms are regarded to have caused the intermediate Return Atlantic current to influence ice-margin retreat across the NE and CE Greenland shelves (Hebbeln et al., 1994; Nørgaard-Pedersen et al., 2003; Hansen et al., 2022). However, at the regional to valley scales, we believe non-climatic and oceanic factors also help explain the variability. We discuss and hypothesise some of these mechanisms in the following sections, with a particular focus on ice-sheet- and sector-scale topographic heterogeneities and asymmetries. Whilst numerous other non-climatic factors, such as spatial heterogeneities in ice shelf loss and sea-ice cover, for instance, may also play roles in controlling such regional heterogeneities, we here only focus on what we believe to be main or first-order drivers.

Influence of heterogeneous continental-shelf topographies

2270 During Heinrich Stadial 1 (~18–15 kyr BP), when the Greenland Ice Sheet reached its maximum extent (between 24 and 16 kyr BP; Fig. 20), depending on regions (Funder et al., 2011), and when local atmospheric- and more importantly sea surface-temperatures decreased were lowest (Grootes et al., 1993; Osman et al., 2021), Greenland Ice Sheet the ice sheet's margins generally had advanced across continental shelves (e.g. CW Greenland: Ó Cofaigh et al., 2013). Such advances were facilitated by the soft and unlithified nature of continental shelf surface sediments promoting shear deformation of subglacial sediments, high basal sliding velocities, and ice streaming in some cases (Evans et al., 2009). Certain regions have wider continental shelves providing grounded ice considerable distances across which to advance during build-up phases, while other sectors only feature a narrow shelf to traverse before the continental slope, deep ocean and high calving losses are attained. For example, assuming grounded ice reached the continental shelf break in the NE, offshore of NEGIS, the ice sheet had a distance to advance of ~280-300 km relative to present-day positions. In southernmost Greenland however, this distance to attain the shelf break was instead only ~80-100 km.

2285 During full glacial conditions, precipitation and ice accumulation were very low in Greenland due to cold atmospheric and oceanic temperatures (Buizert et al., 2018). The GISP2 ice core record (Cuffey & Clow, 1997) suggests accumulations <10 cm yr^{-1} between 20 and 15 kyr BP, and the latest simulations of the water isotope - enabled Community Earth System Model (iCESM) suggest values of around 5 cm yr^{-1} for that location (He et al., 2021). Therefore, in sectors experiencing larger lateral ice-sheet expansion across wider continental shelves (e.g. NE and CW regions), ice accumulation was less likely to be able to compensate the required mass transfer to lower elevations during extensive margin advance. This potentially caused greater ice-sheet thinning and lower surface slopes than in other sectors experiencing less expansion across the continental shelf (e.g. SW, NW and CE regions).

2290 Relative to a steeper ice-sheet profile, a thinner sector of the ice sheet with a gentler surface slope should experience increased melting for a given rise in Equilibrium Line Altitude because a greater surface area is now below that altitude (Edwards et al., 2014). [WarmingsWarm periods](#) such as [duringthe](#) the Bølling-Allerød and early Holocene intervals may therefore have had varied effects on mass balance arising from regional differences in ice surface slope attained during build-up across continental shelves of different widths. Hypothetically, such mechanisms may have caused Greenland sectors with wider continental shelves and more extensive last full glacial advances (e.g. offshore CW Greenland) to have experienced faster grounding line retreat during the initial phase of deglaciation, under still predominantly marine-terminating conditions (e.g. Fig. [24b22b](#), scenario 2). [Such a response would be an example of geographically induced ice sheet hysteresis \(Garbe et al., 2020\).](#) Another [locationsector](#) where such effects may have played a role is in NE Greenland, which experienced rapid and extensive deglaciation of a wide continental shelf, while NW Greenland on the opposite side of the main ice divide instead experienced slower and more limited retreat of ice margins (Fig. [24e22c](#)). Consequently, during the Late-Glacial and early Holocene periods, a significant ice divide migration may have occurred in NE Greenland. The recent findings of a possible re-configuration of NEGIS during the early Holocene (Franke et al., 2022) could perhaps be linked to such regional adjustments in ice-flow. [Around Greenland more generally, the ~12 to ~8 kyr BP window may have been critical for ice-stream re-adjustments, as the ice sheet margin stepped back and thinned from mid/inner shelf positions into more topographically confined coastal fjords. Such confinement increased the fixing in position and channelising of ice flow, and pre-existing overdeepenings may have induced some stepped behaviour in retreat. The early Holocene interval was thus likely associated with a stronger topographic control on ice stream position and behaviour throughout the Greenland Ice Sheet \(Roberts et al., 2009\).](#)

Influence of heterogeneous onshore bed topography

The present-day onshore Greenland topography is spatially heterogeneous, with the CE, SE, and SW regions characterised by prominent coastal mountain ranges, while other regions generally feature lower-lying beds, in some places resting below

2315 modern sea level, such as underneath NEGIS or the Jakobshavn and Humboldt ice streams, for instance (Morlighem et al.,
2017). The latter can [in some cases](#) enhance margin retreat speed and magnitude, and promote outlet glacier instability
(Jamieson et al., 2012). [This may help explain why the CW Greenland Ice Sheet region likely experienced more retreat behind
contemporary margins in response to the Holocene Thermal Maximum \(Simpson et al., 2009; Larsen et al., 2015\), although
this remains a hypothesis.](#)

2320 Higher and more rugged topographies near the coast present orographic obstacles to precipitation from offshore. They promote
ice accumulations sustaining coastal glaciers which can contribute ice flux to the main ice sheet, and locally decrease the
impact of negative mass balances on ice-margin retreat during warming phases. Higher coastal topographies enable steeper
surface slopes near ice-sheet margins, and less accumulation area loss for a given rise in Equilibrium Line Altitude during
2325 warming (Fig. [24b22b](#), scenario 2). Moreover, high coastal mountains likely promote less slippery bed conditions, with a
rougner bed and more bedrock areas at higher elevations potentially enabling more cold-based conditions. These mechanisms
could together explain why the SE sector of the Greenland Ice Sheet is characterised by a margin located closer to the shore
than other more deglaciated regions, despite significantly warmer local atmospheric and sea surface temperatures (Fig. [2021](#);
Osman et al., 2021). Indeed, while greater ocean and atmospheric warming likely caused this region to lose its former marine-
2330 terminating margins earlier and more rapidly than in other sectors, this high coastal topography feedback may have caused the
ice sheet to stabilise when becoming predominantly land-terminating, with local margins remaining near the shore throughout
the Holocene.

2335 Generally, we observe a pattern of stabilisation of ice-sheet margins during their marine-to-terrestrial transition in several
regions. Indeed, an abundance of prominent moraines and other ice-marginal landforms close to present-day coasts can often
be observed where present-day topography reaches above the marine limit. This is common in the Ilulissat, Sisimiut, and Nuuk
regions (e.g. the Kapisigdlit stade moraines; Young et al., 2021) (Fig. 12), for example, but also in NE Greenland, onshore of
major fjords (e.g. Danmarks Fjord). These landforms imply stillstands of the margin once floatation and calving fronts were
lost, suggesting that calving and sub-shelf melt caused more ablation than subaerial processes in these regions, during the Late-
2340 Glacial to mid-Holocene retreat of the ice sheet. Here again, the role of bed topography is critical as the width, depth, and
length of Fjord systems control how much margin retreat is required prior to ice becoming fully grounded. Due to the added
ablation effect of calving, topographic heterogeneities between Fjords and inter-Fjord sectors can generate different modes of
deglaciation for adjacent outlet glaciers, as observed [for example](#) in North Greenland (Larsen et al., 2020). Therefore, the
transition from marine to land-terminating margins, which ~~likely~~ occurred at different times in different regions [due to
2345 variabilities in uplift from glacial isostatic adjustment and valleys, thus in relative sea level change \(Long et al., 2011\)](#), is an
essential factor influencing the dynamics of former ice sheet margin retreat in Greenland. We note the spatial and temporal
uncertainties of the PaleoGrIS 1.0 reconstruction are likely too large to assess such valley-scale feedback quantitatively.
Moreover, [current empirical reconstructions of relative sea level whilst numerous regions feature robust paleo sea-level change in](#)

Greenland are too uncertain records (e.g. the Disko Bugt area; Long et al., 2006), it remains a challenge to establish an accurate, time-dependent, and Greenland-wide map of paleo sea levels at the ice-sheet/valley scale (Gowan, 2023). In most Greenland regions, our ability to test the impact of this mechanism requires thorough modelling experiments (with a coupled glacial-isostatic-adjustment model) that are calibrated against observations and ran at high (<1 km) spatial resolutions.

Finally, we argue that when subglacial topography is asymmetrical on opposite sides of an ice sheet, it can cause potent ice-divide migrations during ice-sheet build up and demise phases and lead to geographically-induced hysteresis (Larsen et al., 2016). In central Greenland, for instance, significantly higher coastal topographies (up to 2500 m a.s.l.) lie underneath and around the eastern ice-sheet margin relative to the western margin, which features a wide, low-lying subglacial drainage basin (Fig. 2422). During strong cooling phases and ice build-up towards full glacial extent, the ice sheet in CE Greenland draining towards Scoresby Sund would have required thicker ice to overflow mountains and become unconstrained, than in CW Greenland where ice feeding the Jakobshavn Ice Stream faces no such obstacle. This asymmetrical thickness build-up may have generated an ice-sheet dome increasingly skewed towards the East during advance/build-up to full glacial extent, resulting in a potent eastwards migration of the main ice divide in central Greenland. Conversely, during deglaciation, when eastern margins retreated towards or behind present-day positions and became increasingly constrained by coastal mountains impeding ice evacuation, a westward migration of the divide may have occurred in this region (as drawn in Fig. 2422). In fact, one could argue that westward migration of the main ice divide in central Greenland might continue and possibly accelerate in the future, as the ice sheet margin thins, retreats, and becomes increasingly blocked by higher topographies and reversed bed slopes to the East. We therefore speculate that ice divide migrations likely play an important role in controlling the position of ice streams and influencing ice margin retreat dynamics as noted for other paleo ice sheets (e.g. Greenwood & Clark, 2009). The influence of such mechanisms could be further tested by running high order/resolution model simulations constrained by ice extent observations.

To summarise, we here raise the hypothesis that at the regional scale, the heterogeneous and sometimes asymmetric nature of Greenland's terrestrial and continental-shelf topographies may be responsible for:

- Skewed ice-sheet profiles in surface elevation
- Regional variability in thickness and surface slope
- Regional variability in mass-balance response to warming as a consequence of the above
- Re-arrangements of major/certain ice streams and of surface velocities/velocity fields during retreat
- Spatial variability in the timing of marine-to-terrestrial transitions resulting in non-synchronous margin stabilisations
- Major ice-divide migrations during both advance and retreat phases

Together, these re-arrangements may cause inter-regional variability in the speed and magnitude of Greenland Ice Sheet margin retreat during deglaciation.

2385

2390

2395

2400

2405

2410

2415

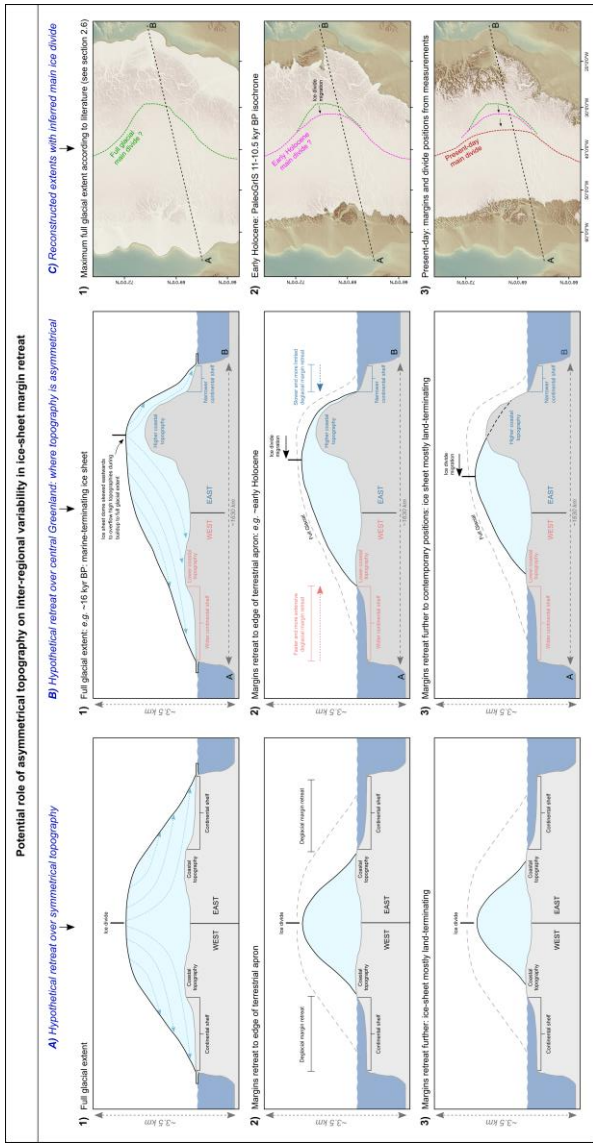


Figure 2422. Schematic model describing the hypotheses raised in section 4.2.2, which explore the potential roles of asymmetrical continental shelf- and coastal bed topographies on the observed inter-regional variability in ice-sheet margin retreat dynamics in Greenland during deglaciation. Perhaps these ideas help explain the regional variability in both rate and magnitude of retreat. The subglacial topography and bathymetry data displayed on right-hand panels is a merged product of the BedMachine v4 and GEBCO (2022 release) DEMs.

5. Summary and conclusions

- We present PaleoGrIS 1.0, an ice-sheet wide reconstruction of the Late-Glacial and Holocene Greenland Ice Sheet margin evolution, documenting the deglacial back-stepping of ice margins to the present-day ice sheet edge. This new reconstruction is based on around 194,000 geomorphological and 1,450 geochronological markers of former ice extent. It yields ice marginal isochrones at a temporal resolution of 500 years and spans ~7.5 kyr from approximately 14 to 6.5 kyr BP.
- This reconstruction of the ice sheet margin evolution through time, based on our Greenland-wide mapping of ice-marginal landforms combined with a synthesis of published geochronological data, enables us to pinpoint the timing and dynamics of key glaciological events, such as the unzipping of the Innuitian and Greenland Ice Sheets and subsequent opening of Nares Strait for example, here estimated to have occurred at ~8.5-8 kyr BP.
- The PaleoGrIS 1.0 isochrones enable us to quantify the Late-Glacial and Holocene areal extent change of the entire Greenland Ice Sheet. We find that between 14-13 kyr BP until the present day, the ice sheet has lost approximately one third of its areal extent (0.89 million km²). Between 14-13 and 9-8.5 kyr BP, the ice sheet experienced a near constant rate of areal extent loss of $170 \pm 27 \text{ km}^2 \text{ yr}^{-1}$. We also find Greenland outlet glaciers experienced faster retreat rates between ~12 and ~9 kyr BP, while both rates of areal extent loss and margin retreat decreased markedly after ~9 kyr BP. The timing of such faster retreat coincides with the most potent local climate warming to have occurred between the Younger Dryas (~13-11.7 kyr BP) and the end of the pre-industrial era (~1850 AD). In spite of local glaciological complexities, the deglacial evolution of ice margins at the ice-sheet scale is strongly correlated to, and controlled by, changes in atmospheric and oceanic temperatures. These results imply the Greenland Ice Sheet was highly sensitive to climate warming in its recent history, and will likely remain so in the future.
- We find the Greenland Ice Sheet minimum Holocene extent was reached later than ~6.5 kyr BP, which is hundreds to thousands of years after the peak warming of the Holocene Thermal Maximum. We conclude that 'inertia' in the

2485 ice-sheet system (a mix of fast and slow glaciological responses) has caused a centennial to millennial-scale time lag
in its response to the cessation of Holocene warming. Understanding and quantifying such inertia, by better calibrating
numerical ice sheet models against data for instance, is of crucial importance to anticipating the magnitude of
committed mass loss and the response of the ice sheet to ongoing global warming over the next few centuries.

2490 - When quantifying retreat in different Greenland regions, we find heterogeneous responses in the magnitude and rate
of the ice-sheet areal extent loss, and in outlet glacier retreat rates. While some of this heterogeneity may be related
to spatial variability in climate and ocean forcing, other non-climatic factors likely play important roles in determining
the regional-to-valley scale dynamics of deglacial ice margin retreat. In particular, we hypothesise that in certain
2495 Greenland regions, the asymmetrical configurations of continental shelf- and onshore bed- topographies on opposite
sides of the ice sheet may be responsible for inter-regional variability in the magnitude and timing of margin evolution,
with implications for both advance and retreat phases. Ice sheet modelling experiments could usefully explore these
hypothesised controls, which may continue to be relevant regarding future ice loss and sea level rise contributions.

- Despite remarkable and accelerating efforts from the empirical community to produce an extensive library of ice
2500 extent markers around the periphery of the Greenland Ice Sheet, we find vast onshore and offshore regions with sparse
data, and which yield isochrones of low confidence. There is therefore much potential for improving our knowledge
of deglacial Greenland Ice Sheet margin evolution by producing new robust paleo-glaciological investigations ~~from~~
[key-understudied in less well-constrained](#) regions. We believe the PaleoGrIS 1.0 reconstruction and database can prove
useful for identifying important study sites and motivating future onshore and offshore field activities.

2505 - PaleoGrIS 1.0 is made available as an open-access database which may prove useful to both the empirical and ice
sheet modelling communities, and for data-modelling comparison exercises. To reduce data-processing tasks and
make our database usable by both communities we provide isochrone-related datasets in both GIS (geotiff/shapefile)
and NetCDF formats. The database also aims to be in a format suitable to the production of improved future versions
2510 of the reconstruction.

2515 **Data availability.**

The PaleoGrIS 1.0 database will be made open access on the PANGAEA® Data platform. It will include the geomorphological mapping dataset (shapefile format), the geochronological compilation (2 Excel spreadsheets and numerous shapefiles for various products, including for both raw ages and summary event ages), a A0 poster of the reconstruction, and the PaleoGrIS 1.0 isochrone reconstruction in both [shapefile](#) and NetCDF formats, for both the empirical and modelling communities to use. [The database features several READ ME files to ease navigation through the various products.](#)

Data online repository.

2525 The PaleoGrIS 1.0 database will be made open access on the PANGAEA® Data platform. It will be freely available online, as long as original publication is cited when used and/or referred to. The online repository is accessible using this DOI:

2530 **Author contributions.**

C.D.C. conceived and guided the study. Input from J.C.E. and T.P.M.L. contributed to the design of the investigation. S.J., C.H., C.D.C., and T.P.M.L. conducted geomorphological mapping of ice marginal landforms from remote sensing (in relative order of contribution). T.P.M.L. compiled and filtered the geochronology with input from C.H.'s MSc thesis work. T.P.M.L. created the isochrone reconstruction with feedback from C.D.C. and J.C.E. and T.P.M.L. conducted the subsequent quantitative analyses. T.P.M.L. wrote the manuscript with feedback from C.D.C. and J.C.E. primarily, and other co-authors for subsequent drafts. T.P.M.L. produced all maps, figures, tables, and prepared/formatted the PaleoGrIS 1.0 database. C.D.C, J.C.E. and C.D. helped with providing feedback and ideas on figures, along with other co-authors to a lesser extent.

2540 **Competing interest.**

We (the authors) hereby declare that this scientific investigation presents no known competing financial interests or personal conflicts influencing research output.

2545 **Disclaimer.**

2550 **Acknowledgements.**

We express our gratitude towards all individuals who contributed informal ideas and feedback to this work, including Prof. Lev Tarasov, Prof. Jason Briner, Prof. David H. Roberts, and members of the PALGLAC team Remy L.J. Veness, Dr. Helen E. Dulfer, and Dr. Benjamin M. Boyes.

2555

Financial support.

This study benefited from the PALGLAC team of researchers with funding from the European Research Council (ERC) under the European Union's Horizon 2020 research and innovation programme to C.D.C. (Grant Agreement No. 787263), which
2560 supported T.P.M.L., S.J., S.L.B. and C.D. J.C.E. acknowledges support from a NERC independent fellowship award (NE/R014574/1).

Review statement.

2565

2570

2575

1620
1625
1630
1635
1640
1645
1650
1655
1660

[Bennike, O., & Björck, S. \(2002\). Chronology of the last recession of the Greenland Ice Sheet. *Journal of Quaternary Science, J. Quat. Sci.*, 17\(3\), 211–219. <https://doi.org/10.1002/jqs.670>. <https://doi.org/10.1002/jqs.670>, 2002.](#)

[Bennike, O. and Björck, S., Böcher, J., Hansen, L., Heinemeier, J., & Wohlfarth, B. \(1999\). Early Holocene plant and animal remains from North-east Greenland. In *Journal of Biogeography* \(Vol. 26\).](#)

[Bennike, O., Björck, S., & Lambeck, K. \(2002\). Estimates of South Greenland late-glacial ice limits from a new relative sea level curve. *Earth and Planetary Science Letters*, 197\(3–4\), 171–186. \[https://doi.org/10.1016/S0012-821X\\(02\\)00478-8\]\(https://doi.org/10.1016/S0012-821X\(02\)00478-8\)](#)

[Bennike, O., Hansen, K. B., Knudsen, K. L., Penney, D. N., & Rasmussen, K. L. \(1994\). Quaternary marine stratigraphy and geochronology in central West Greenland. *Boreas*, 23\(2\), 194–215. <https://doi.org/10.1111/j.1502-3885.1994.tb00599.x>](#)

[Bennike, O., & Kelly, M. \(1987\). Radiocarbon dating of samples collected during the 1984 expedition to North Greenland. *Rapport, Rapp. Grönlands Geologiske Geol. Undersøgelse*, 135\(14\), 8–10. <https://doi.org/10.34194/rapgu.v135.7991>, 8–10, <https://doi.org/10.34194/rapgu.v135.7991>, 1987.](#)

[Bennike, O., & Wagner, B. \(2012\). Deglaciation chronology, sea-level changes and environmental changes from Holocene lake sediments of Germania Havn Sø, Sabine Ø, northeast Greenland. *Quaternary Research, Quat. Res.* \(United States\), 78\(4\), 103–109. <https://doi.org/10.1016/j.yqres.2012.03.004>. <https://doi.org/10.1016/j.yqres.2012.03.004>, 2012.](#)

[Bennike, O., & Weidick, A. \(2001\). Late Quaternary history around Nioghalvfjærdsfjorden and Jøkelbugten, North-East Greenland. In *Boreas* \(Vol. 30\), 300–9483 pp., 2001.](#)

[Bennike, O., Hansen, K. B., Knudsen, K. L., Penney, D. N., and Rasmussen, K. L.: Quaternary marine stratigraphy and geochronology in central West Greenland. *Boreas*, 23, 194–215. <https://doi.org/10.1111/j.1502-3885.1994.tb00599.x>, 1994.](#)

[Bennike, O., Björck, S., Böcher, J., Hansen, L., Heinemeier, J., and Wohlfarth, B.: Early Holocene plant and animal remains from North-east Greenland. *Journal of Biogeography*, 667–677 pp., 1999.](#)

[Bennike, O., Björck, S., and Lambeck, K.: Estimates of South Greenland late-glacial ice limits from a new relative sea level curve. *Earth Planet. Sci. Lett.*, 197, 171–186. \[https://doi.org/10.1016/S0012-821X\\(02\\)00478-8\]\(https://doi.org/10.1016/S0012-821X\(02\)00478-8\), 2002.](#)

[Bentley, M. J., Ó Cofaigh, C., Anderson, J. B., Conway, H., Davies, B., Graham, A. G. C., Hillenbrand, C.-D., Hodgson, D. A., Jamieson, S. S. R., Larter, R. D., Mackintosh, A., Smith, J. A., Verleyen, E., Ackert, R. P., Bart, P. J., Berg, S., Brunstein, D., Canals, M., Colhoun, E. A., Crosta, X., Dickens, W. A., Domack, E., Dowdeswell, J. A., Dunbar, R., Ehrmann, W., Evans, J., Favier, V., Fink, D., Fogwill, C. J., Glasser, N. F., Gohl, K., Gollgede, N. R., Goodwin, I., Gore, D. B., Greenwood, S. L., Hall, B. L., Hall, K., Hedding, D. W., Hein, A. S., Hocking, E. P., Jakobsson, M., Johnson, J. S., Jomelli, V., Jones, R. S., Klages, J. P., Kristoffersen, Y., Kuhn, G., Leventer, A., Licht, K., Lilly, K., Lindow, J., Livingstone, S. J., Massé, G., McGlone, M. S., McKay, R. M., Melles, M., Miura, H., Mulvaney, R., Nel, W., Nitsche, F. O., O'Brien, P. E., Post, A. L., Roberts, S. J., Saunders, K. M., Selkirk, P. M., Simms, A. R., Spiegel, C., Stollendorf, T. D., Sugden, D. E., van der Putten, N., van Ommen, T., Verfaillie, D., Vyverman, W., Wagner, B., White, D. A., Zwartz, D. \(2014\). Witus, A. E., and Zwartz, D.: A community-based geological reconstruction of Antarctic Ice Sheet deglaciation since the Last Glacial Maximum. *Quaternary Science Reviews*, 100, 1–9. <https://doi.org/10.1016/j.quascirev.2014.06.025>, *Quat. Sci. Rev.*, 100, 1–9, <https://doi.org/10.1016/j.quascirev.2014.06.025>, 2014.](#)

Formatted: Font: Times New Roman, English (United Kingdom)

Formatted ...

Formatted: Space After: 8 pt

Formatted: Font: Times New Roman, English (United Kingdom)

Formatted: Font: Times New Roman, English (United Kingdom)

Formatted: Font: Times New Roman, English (United Kingdom)

Formatted: Font: Times New Roman, English (United Kingdom)

Formatted ...

Formatted: Space After: 8 pt

Formatted: Font: Times New Roman, English (United Kingdom)

Formatted: Font: Times New Roman

Formatted ...

Formatted: Space After: 8 pt

Formatted: Font: Times New Roman, English (United Kingdom)

Formatted: Font: Times New Roman, English (United Kingdom)

Formatted: Space After: 8 pt, Line spacing: Multiple 1.15 li

Formatted: Font: Times New Roman, English (United Kingdom)

Formatted: Font: Times New Roman, English (United Kingdom)

Formatted: Font: Times New Roman, English (United Kingdom)

Formatted ...

Formatted ...

Formatted ...

Formatted ...

2665 [Berger, A. and Loutre, M. F.: Insolation values for the climate of the last 10 million years. *Quat. Sci. Rev.*, 10, 297–317. \[https://doi.org/10.1016/0277-3791\\(91\\)90033-Q\]\(https://doi.org/10.1016/0277-3791\(91\)90033-Q\), 1991.](#)

[Bevington, P.-\(1969\).; Data reduction and error analysis for the physical sciences.; McGraw Hill Book Co, New York, 1969.](#)

2670 [Bick, H.-\(1978\).; A Postglacial Pollen Diagram From Angmagssalik, East Greenland. *Medd. Gr Nonoland; DNK; DA.*, 204\(1\), 1–22. 1978.](#)

[Björck, S., Wohlfarth, B., Bennike, O., Hjort, C., & Persson, T.-\(1994\).; Revision of the early Holocene lake sediment based chronology and event stratigraphy on Hochstetter Forland, NE Greenland–*Boreas*, 23\(4\), 513–523. <https://doi.org/10.1111/j.1502-3885.1994.tb00619.x>, *Boreas*, 23, 513–523. <https://doi.org/10.1111/j.1502-3885.1994.tb00619.x>, 1994.](#)

2675 [Björk, A. A., Kruse, L. M., & Michaelsen, P. B.-\(2015\).; Brief communication: Getting Greenland’s glaciers right – a new data set of all official Greenlandic glacier names–*The Cryosphere*, 9\(6\), 2215–2218. <https://doi.org/10.5194/tc-9-2215-2015>, *Cryosph.*, 9, 2215–2218. <https://doi.org/10.5194/tc-9-2215-2015>, 2015.](#)

[Blake, W., J.-\(1987\).; Geological Survey of Canada radiocarbon dates XXVI–*Geological Survey of Geol. Surv. Canada*, 86, 1987.](#)

2680 [Blake, W., Ruth Jackson, H., Currie, C. G., and Jackson, J.: Seafloor evidence for glaciation, northernmost Baffin Bay, *Bull. Geol. Soc. Denmark*, 43, 157–168, 1996.](#)

[Blake, W. J., Bouchierle, M., Fredskild, B., Janssens, J., & Smol, J.-\(1992\).; The geomorphological setting, glacial history and Holocene development of Kap Inglefield Sø , Inglefield Land, North-West Greenland–*Geological Survey of Geol. Surv. Canada*, 27, 1–42, 1992.](#)

2685 [Blake, W., Ruth Jackson, H., Currie, C. G., & Jackson, J. \(1996\). Seafloor evidence for glaciation, northernmost Baffin Bay. *Bulletin of the Geological Society of Denmark*, 43, 157–168.](#)

[Bradley, S. L., Reerink, T. J., Van De Wal, R. S. W., & Helsen, M. M.-\(2018\).; Simulation of the Greenland Ice Sheet over two glacial-interglacial cycles: investigating a sub-ice-shelf melt parameterization and relative sea level forcing in an ice-sheet-ice-shelf model–*Climate of the Past*, 14\(5\), 619–635. <https://doi.org/10.5194/cp-14-619-2018>, *Clim. Past*, 14, 619–635. <https://doi.org/10.5194/cp-14-619-2018>, 2018.](#)

2690 [Briner, J., Schaefer, J., Young, N., Keisling, B., Anandakrishnan, S., Kuhl, T., Boeckmann, G., MacGregor, J., Deconto, R., Morlighem, M., Winckler, G., & Walcott, C.-\(2021\).; Introducing GreenDrill: Retrieving sub-glacial bedrock cores in North Greenland to test ice sheet response to interglacial warmth \(and supporting your research?\). in AGU Fall Meeting Abstracts, 2021, C31A-07-, 2021.](#)

2695 [Briner, J. P., Stewart, H. A. M., Young, N. E., Philipps, W., and Losee, S.: Using proglacial-threshold lakes to constrain fluctuations of the Jakobshavn Isbræ ice margin, western Greenland, during the Holocene, *Quat. Sci. Rev.*, 29, 3861–3874. <https://doi.org/10.1016/j.quascirev.2010.09.005>, 2010.](#)

[Briner, J. P., Håkansson, L., and Bennike, O.: The deglaciation and neoglaciation of upernavik isström, greenland, *Quat. Res. \(United States\)*, 80, 459–467. <https://doi.org/10.1016/j.yqres.2013.09.008>, 2013.](#)

2700 [Briner, J. P., Kaufman, D. S., Bennike, O., and Kosnik, M. A.: Amino acid ratios in reworked marine bivalve shells constrain Greenland Ice Sheet history during the holocene, *Geology*, 42, 75–78. <https://doi.org/10.1130/G34843.1>, 2014.](#)

Formatted: Font: Times New Roman, English (United Kingdom)

Formatted

Formatted: Space After: 8 pt

Formatted: Font: Times New Roman, English (United Kingdom)

Formatted

Formatted: Space After: 8 pt

Formatted: Font: Times New Roman, English (United Kingdom)

Formatted

Formatted: Space After: 8 pt

Formatted: Font: Times New Roman, English (United Kingdom)

Formatted

Formatted: Font: Times New Roman, English (United Kingdom)

Formatted: Space After: 8 pt

Formatted: Font: Times New Roman

Formatted: Font: Times New Roman, English (United Kingdom)

Formatted

Formatted: Space After: 8 pt

Formatted: Default Paragraph Font, Font: Times New Roman, 10 pt, English (United Kingdom)

Formatted: Font: Times New Roman, English (United Kingdom)

Formatted: Space After: 8 pt

Formatted

Formatted

Formatted

Carr, J. R., Stokes, C. R., & Vieli, A. (2017). Threefold increase in marine-terminating outlet glacier retreat rates across the Atlantic Arctic: 1992–2010. *in: Annals of Glaciology*, 58(74), 72–91. <https://doi.org/10.1017/aog.2017.3>, <https://doi.org/10.1017/aog.2017.3>, 2017.

2750 Carrivick, J. L., Yde, J., Russell, A. J., Quincey, D. J., Ingeman-Nielsen, T., & Mallalieu, J. (2017). Ice-margin and meltwater dynamics during the mid-Holocene in the Kangerlussuaq area of west Greenland. *Boreas*, 46(3), 369–387. <https://doi.org/10.1111/bor.12199>, <https://doi.org/10.1111/bor.12199>, 2017.

2755 Cartapanis, O., Jonkers, L., Moffa-Sanchez, P., Jaccard, S. L., & de Vernal, A. (2022). Complex spatio-temporal structure of the Holocene Thermal Maximum. *Nature Communications, Nat. Commun.*, 13(4), 5662. <https://doi.org/10.1038/s41467-022-33362-1>, <https://doi.org/10.1038/s41467-022-33362-1>, 2022.

2760 Ceperley, E. G., Marcott, S. A., Reusche, M. M., Barth, A. M., Mix, A. C., Brook, E. J., & Caffee, M. (2020). Widespread early Holocene deglaciation, Washington Land, northwest Greenland. *Quaternary Science Reviews, Quat. Sci. Rev.*, 231. <https://doi.org/10.1016/j.quascirev.2020.106181>, <https://doi.org/10.1016/j.quascirev.2020.106181>, 2020.

2765 Chandler, B. M. P., Lovell, H., Boston, C. M., Lukas, S., Barr, I. D., Benediktsson, Í. Ö., Benn, D. I., Clark, C. D., Darvill, C. M., Evans, D., J. A., Ewertowski, M. W., Loibl, D., Margold, M., Otto, J. C., Roberts, D. H., Stokes, C. R., Storrar, R. D., & Stroeven, A. P. (2018). Glacial geomorphological mapping: A review of approaches and frameworks for best practice. *In Earth Science Reviews (Vol. 185, pp. 806–846)*. <https://doi.org/10.1016/j.earscirev.2018.07.015>, <https://doi.org/10.1016/j.earscirev.2018.07.015>, 2018.

Christiansen, H. H., Bennike, O., Böcher, J., Elberling, B., Humlum, O., & Jakobsen, B. H. (2002). Holocene environmental reconstruction from deltaic deposits in northeast Greenland. *Journal of Quaternary Science, J. Quat. Sci.*, 17(2), 145–160. <https://doi.org/10.1002/jqs.665>, <https://doi.org/10.1002/jqs.665>, 2002.

2770 Clark, C. D., Hughes, A. L. C., Greenwood, S. L., Jordan, C., and Sejrup, H. P.: Pattern and timing of retreat of the last British-Irish Ice Sheet. *Quat. Sci. Rev.*, 44, 112–146. <https://doi.org/10.1016/j.quascirev.2010.07.019>, 2012.

2775 Clark, C. D., Ely, J. C., Hindmarsh, R. C. A., Bradley, S., Ignénczi, A., Fabel, D., Ó Cofaigh, C., Chiverrell, R. C., Scourse, J., Benetti, S., Bradwell, T., Evans, D. J. A., Roberts, D. H., Burke, M., Callard, S. L., Medialdea, A., Saher, M., Small, D., Smedley, R. K., Gasson, E., Gregoire, L., Gandy, N., Hughes, A. L. C., Ballantyne, C., Bateman, M. D., Bigg, G. R., Doole, J., Dove, D., Duller, G. A. T., Jenkins, G. T. H., Livingstone, S. L., McCarron, S., Moreton, S., Pollard, D., Praeg, D., Sejrup, H. P., Van Landeghem, K. J., & Wilson, P. (2022). J. and Wilson, P.: Growth and retreat of the last British–Irish Ice Sheet, 31 000 to 15 000 years ago: the BRITICE-CHRONO reconstruction. *Boreas*, 51(4), 699–758. <https://doi.org/10.1111/bor.12594>, <https://doi.org/10.1111/bor.12594>, 2022.

2780 Clark, C. D., Hughes, A. L. C., Greenwood, S. L., Jordan, C., & Sejrup, H. P. (2012). Pattern and timing of retreat of the last British-Irish Ice Sheet. *Quaternary Science Reviews*, 44, 112–146. <https://doi.org/10.1016/j.quascirev.2010.07.019>

2785 Corbett, L. B., Bierman, P. R., Graly, J. A., Neumann, T. A., & Rood, D. H. (2013). Constraining landscape history and glacial erosivity using paired cosmogenic nuclides in upernavik, northwest greenland. *Bulletin of the Geological Society of America*, 125(9–10), 1539–1553. <https://doi.org/10.1130/B30813-1>

Corbett, L. B., Bierman, P. R., Lasher, G. E., & Rood, D. H. (2015). Landscape chronology and glacial history in Thule, northwest Greenland. *Quaternary Science Reviews*, 109, 57–67. <https://doi.org/10.1016/j.quascirev.2014.11.019>

Formatted: Font: Times New Roman, English (United Kingdom)

Formatted

Formatted: Space After: 8 pt

Formatted: Font: Times New Roman, English (United Kingdom)

Formatted: Font: Times New Roman, English (United Kingdom)

Formatted

Formatted: Space After: 8 pt

Formatted: Font: Times New Roman, English (United Kingdom)

Formatted: Font: Times New Roman, English (United Kingdom)

Formatted

Formatted: Space After: 8 pt

Formatted: Font: Times New Roman, English (United Kingdom)

Formatted

Formatted

Formatted: Space After: 8 pt

Formatted

Formatted

Formatted: Space After: 8 pt

Formatted

Formatted

Formatted

Formatted: Space After: 8 pt

Formatted

Formatted

Formatted: Space After: 8 pt

Formatted

Formatted

Formatted

Formatted

Formatted

Formatted

Formatted

Formatted

Formatted

Formatted

Formatted

Formatted

2790 Corbett, L. B., Young, N. E., Bierman, P. R., Briner, J. P., Neumann, T. A., Rood, D. H., & Galy, J. A. (2011). Paired bedrock and boulder ¹⁰Be concentrations resulting from early Holocene ice retreat near Jakobshavn Isfjord, western Greenland. *Quaternary Science Reviews*, 30(13–14), 1739–1749. <https://doi.org/10.1016/j.quascirev.2011.04.004>, *Quat. Sci. Rev.*, 30, 1739–1749. <https://doi.org/10.1016/j.quascirev.2011.04.001>, 2011.

2795 Corbett, L. B., Bierman, P. R., Lasher, G. E., and Rood, D. H.: Landscape chronology and glacial history in Thule, northwest Greenland. *Quat. Sci. Rev.*, 109, 57–67. <https://doi.org/10.1016/j.quascirev.2014.11.019>, 2015.

Couette, P.-O., Lajeunesse, P., Ghienne, J.-F., Dorschel, B., Gebhardt, C., Hebbeln, D., & Brouard, E. (2022). Evidence for an extensive ice shelf in northern Baffin Bay during the Last Glacial Maximum. *Communications, Commun. Earth & Environment Environ.*, 3(1), 225. <https://doi.org/10.1038/s43247-022-00559-7>, <https://doi.org/10.1038/s43247-022-00559-7>, 2022.

2800 Crane, H. R., & Griffin, J. B. (1959). University of Michigan Radiocarbon Dates IV. *Radiocarbon*, 1, 173–198. <https://doi.org/10.1017/S0033822200020452>, <https://doi.org/10.1017/S0033822200020452>, 1959.

2805 Cremer, H., Wagner, B., Melles, M., & Hubberten, H.-W. (2001). The postglacial environmental development of Raffles Sø, East Greenland: inferences from a 10,000 year diatom record. In *Journal of Paleolimnology* (Vol. 26). <https://doi.org/10.1023/A:1011179321529>, 67–87 pp., <https://doi.org/10.1023/A:1011179321529>, 2001.

Cronauer, S. L., Briner, J. P., Kelley, S. E., Zimmerman, S. R. H., & Morlighem, M. (2016). ¹⁰Be dating reveals early-middle Holocene age of the Drygalski Moraines in central West Greenland. *Quaternary Science Reviews*, *Quat. Sci. Rev.*, 147, 59–68. <https://doi.org/10.1016/j.quascirev.2015.08.034>, <https://doi.org/10.1016/j.quascirev.2015.08.034>, 2016.

2810 Cuffey, K. M., & Clow, G. D. (1997). Temperature, accumulation, and ice sheet elevation in central Greenland through the last deglacial transition. *Journal of Geophysical Research: Oceans*, 102(C12), 26383–26396. <https://doi.org/10.1029/96JC03981>, *J. Geophys. Res. Ocean.*, 102, 26383–26396. <https://doi.org/10.1029/96JC03981>, 1997.

2815 Dalton, A. S., Margold, M., Stokes, C. R., Tarasov, L., Dyke, A. S., Adams, R. S., Allard, S., Arends, H. E., Atkinson, N., Attig, J. W., Barnett, P. J., Barnett, R. L., Batterson, M., Bernatchez, P., Borns, H. W., Breckenridge, A., Briner, J. P., Brouard, E., Campbell, J. E., Carlson, A. E., Clague, J. J., Curry, B. B., Daigneault, R. A., Dubé-Loubert, H., Easterbrook, D. J., Franzi, D. A., Friedrich, H. G., Funder, S., Gauthier, M. S., Gowan, A. S., Harris, K. J., Héту, B., Hoover, T. S., Jennings, C. E., Johnson, M. D., Kehew, A. E., Kelley, S. E., Kerr, D., King, E. L., Kjeldsen, K. K., Knaeble, A. R., Lajeunesse, P., Lakeman, T. R., Lamothe, M., Larson, P., Lavoie, M., Loope, H. M., Lowell, T. V., Lusardi, B. A., Manz, L., McMartin, I., Nixon, F. C., Occhietti, S., Parkhill, M. A., Piper, D. J. W., Pronk, A. G., Richard, P. J. H., Ridge, J. C., Ross, M., Roy, M., Seaman, A., Shaw, J., Stea, R. R., Teller, J. T., Thompson, W. B., Thorleifson, L. H., Wright, H. E. (2020). Utting, D. J., Veillette, J. J., Ward, B. C., Weddle, T. K., and Wright, H. E.; An updated radiocarbon-based ice margin chronology for the last deglaciation of the North American Ice Sheet Complex. In *Quaternary Science Reviews* (Vol. 234). Elsevier Ltd. <https://doi.org/10.1016/j.quascirev.2020.106223>, <https://doi.org/10.1016/j.quascirev.2020.106223>, 15 April 2020.

2825 Davies, B. J., Darvill, C. M., Lovell, H., Bendle, J. M., Dowdeswell, J. A., Fabel, D., García, J.-L., Geiger, A., Glasser, N. F., Gheorghiu, D. M., Harrison, S., Hein, A. S., Kaplan, M. R., Martin, J. R. V., Mendelova, M., Palmer, A., Pelto, M., Rodés, Á., Sagredo, E. A., Smedley, R., Smellie, J. L., and Thorndycraft, V. R. (2020). The evolution of the Patagonian Ice Sheet from 35 ka to the present day (PATICE). *Earth-Science Reviews*, 103152. <https://doi.org/10.1016/j.earscirev.2020.103152>, <https://doi.org/10.1016/j.earscirev.2020.103152>, 2020.

2830

Formatted: Font: Times New Roman, English (United Kingdom)

Formatted

Formatted: Space After: 8 pt

Formatted: Font: Times New Roman, English (United Kingdom)

Formatted: Font: Times New Roman, English (United Kingdom)

Formatted

Formatted: Space After: 8 pt

Formatted

Formatted

Formatted: Space After: 8 pt

Formatted

Formatted: Space After: 8 pt

Formatted

Formatted

Formatted: Space After: 8 pt

Formatted

Formatted

Formatted: Space After: 8 pt

Formatted

Formatted

Formatted: Space After: 8 pt

Formatted

Formatted

Formatted: Space After: 8 pt

Formatted

Formatted

Funder, S. (1978). Holocene stratigraphy and vegetation history in the Scoresby Sund area, East Greenland. *Grønlands Geologiske Undersøgelser*, 129, 1–76, 1978.

2915 Funder, S. (1982). 14C-dating of samples collected during the 1979 expedition to North Greenland. *Rapport, Rapp, Grønlands Geologiske Undersøgelser*, 110, 9–14. <https://doi.org/https://doi.org/10.34194/rapggv.v110.7787>, <https://doi.org/https://doi.org/10.34194/rapggv.v110.7787>, 1982.

2920 Funder, S. (1990). Late Quaternary stratigraphy and glaciology in the Thule area, Northwest Greenland. *Kommissionen for Videnskabelige Undersøgelser i Grønland, Grønl.*, 22, 1990.

Funder, S., & Abrahamson, N. (1988). Palynology in a polar desert, eastern North Greenland. *Boreas*, 17(2), 195–207. <https://doi.org/10.1111/j.1502-3885.1988.tb00546.x>, <https://doi.org/10.1111/j.1502-3885.1988.tb00546.x>, 1988.

2925 Funder, S., & Hansen, L. (1996). The Greenland ice sheet—a model for its culmination and decay during and after the last glacial maximum. *Meddelelser Fra Dansk Geologisk Forening, Geol. Foren.*, 42, 137–152, 1996.

2930 Funder, S., Kjeldsen, K. K., Kjær, K. H., & O Cofaigh, C. (2011). The Greenland Ice Sheet During the Past 300,000 Years: A Review. In *Developments in Quaternary Science (Vol. 15)*. <https://doi.org/10.1016/B978-0-444-53447-7.00050-7>, 699–713 pp. <https://doi.org/10.1016/B978-0-444-53447-7.00050-7>, 2011.

Garbe, J., Albrecht, T., Levermann, A., Donges, J. F., & Winkelmann, R. (2020). The hysteresis of the Antarctic Ice Sheet. *Nature*, 585(7826), 538–544. <https://doi.org/10.1038/s41586-020-2727-5>

2935 Garcia-Oteyza, J., Oliva, M., Palacios, D., Fernández-Fernández, J. M., Schimmelpfennig, I., Andrés, N., Antoniadis, D., Christiansen, H., Humlum, O., Léanni, L., Jomelli, V., Ruiz-Fernández, J., Rinterknecht, V., Lane, T. P., Adamson, K., Aumaître, G., Bourlès, D., & Keddadouche, K. (2022). Late Glacial deglaciation of the Zackenberg area, NE Greenland. *Geomorphology*, 401. <https://doi.org/10.1016/j.geomorph.2022.108125>, <https://doi.org/10.1016/j.geomorph.2022.108125>, 2022.

2940 Georgiadis, E., Giraudeau, J., Martinez, P., Lajeunesse, P., St-Onge, G., Schmidt, S., & Massé, G. (2018). Deglacial to postglacial history of Nares Strait, Northwest Greenland: A marine perspective from Kane Basin. *Climate of the Past*, 14(12), 1991–2010. <https://doi.org/10.5194/cp-14-1991-2018>, <https://doi.org/10.5194/cp-14-1991-2018>, 2018.

2945 Goelzer, H., Nowicki, S., Payne, A., Larour, E., Seroussi, H., Lipscomb, W. H., Gregory, J., Abe-Ouchi, A., Shepherd, A., Simon, E., Agosta, C., Alexander, P., Aschwanden, A., Barthel, A., Calov, R., Chambers, C., Choi, Y., Cuzzone, J., Dumas, C., ... Van Den Broeke, M. (2020). Edwards, T., Felikson, D., Fettweis, X., Gолledge, N. R., Greve, R., Humbert, A., Huybrechts, P., Le Clec'H, S., Lee, V., Leguy, G., Little, C., Lowry, D., Morlighem, M., Nias, I., Quiquet, A., Rückamp, M., Schlegel, N. J., Slater, D. A., Smith, R., Straneo, F., Tarasov, L., Van De Wal, R., and Van Den Broeke, M.; The future sea-level contribution of the Greenland ice sheet: A multi-model ensemble study of ISMIP6. *Cryosphere*, 14(9), 3071–3096. <https://doi.org/10.5194/ice-14-3071-2020>, <https://doi.org/10.5194/ice-14-3071-2020>, 2020.

2950 Gowan, E. J.: Paleo sea-level indicators and proxies from Greenland in the GAPSLIP database and comparison with modelled sea level from the PaleoMIST ice-sheet reconstruction. *GEUS Bull.*, 53, 1–17, <https://doi.org/10.34194/geusb.v53.8355>, 2023.

Formatted: Font: Times New Roman, English (United Kingdom)

Formatted

Formatted: Space After: 8 pt

Formatted: Font: Times New Roman, English (United Kingdom)

Formatted

Formatted: Space After: 8 pt

Formatted: Font: Times New Roman, English (United Kingdom)

Formatted

Formatted: Font: Times New Roman, English (United Kingdom)

Formatted

Formatted: Font: Times New Roman, English (United Kingdom)

Formatted

Formatted: Space After: 8 pt

Formatted: Font: Times New Roman, English (United Kingdom)

Formatted

Formatted

Formatted: Space After: 8 pt

Formatted

Formatted

Formatted: Space After: 8 pt

Formatted

Formatted

Formatted

Formatted

Formatted: Space After: 8 pt

Formatted

Formatted

Formatted

Formatted: Space After: 8 pt

Formatted

Formatted

Formatted

Formatted

Formatted

Formatted

Formatted

2995 [Heaton, T. J., Butzin, M., Bard, E., Bronk Ramsey, C., Köhler, P., Hughen, K. A., & Reimer, P. J. \(2022\). Marine Radiocarbon Calibration in Polar Regions: A Simple Approximate Approach using Marine20. <http://calib.org/marine/>](#)

3000 [Heaton, T. J., Köhler, P., Butzin, M., Bard, E., Reimer, R. W., Austin, W. E. N., Bronk Ramsey, C., Grootes, P. M., Hughen, K. A., Kromer, B., Reimer, P. J., Adkins, J., Burke, A., Cook, M. S., Olsen, J., & Skinner, L. C. \(2020\). Marine20 - The Marine Radiocarbon Age Calibration Curve \(0-55,000 cal BP\). *Radiocarbon*, 62\(4\), 779–820. <https://doi.org/10.1017/RDC.2020.68>, <https://doi.org/10.1017/RDC.2020.68>, 2020.](#)

3005 [Heaton, T. J., Butzin, M., Bard, E., Bronk Ramsey, C., Köhler, P., Hughen, K. A., and Reimer, P. J.: Marine Radiocarbon Calibration in Polar Regions: A Simple Approximate Approach using Marine20, 2022.](#)

3010 [Hebbeln, D., Dokken, T., Andersen, E. S., Hald, M., and Elverhøi, A.: Moisture supply for northern ice-sheet growth during the Last Glacial Maximum, *Nature*, 370, 357–360. <https://doi.org/10.1038/370357a0>, 1994.](#)

3015 [Hjort, C.: Glaciation in northern East Greenland during the Late Weichselian and Early Flandrian. *Boreas*, 8\(3\), 281–296. <https://doi.org/10.1111/j.1502-3885.1979.tb00812.x>, <https://doi.org/10.1111/j.1502-3885.1979.tb00812.x>, 1979.](#)

3020 [Hjort, C. \(1981\). A glacial chronology for northern East Greenland. *Boreas*, 10\(3\), 259–274. <https://doi.org/10.1111/j.1502-3885.1981.tb00487.x>](#)

3025 [Hjort, C. \(1997\). Hjort, C.: Glaciation, climate history, changing marine levels and the evolution of the Northeast Water polynya. *Journal of Marine Systems*, 10\(1–4\), 23–33. \[https://doi.org/10.1016/S0924-7963\\(96\\)00068-1\]\(https://doi.org/10.1016/S0924-7963\(96\)00068-1\), *J. Mar. Syst.*, 10, 23–33, \[https://doi.org/10.1016/S0924-7963\\(96\\)00068-1\]\(https://doi.org/10.1016/S0924-7963\(96\)00068-1\), 1997.](#)

3030 [Hopkins, T. S.: The GIN Sea—A synthesis of its physical oceanography and literature review 1972–1985. *Earth-Science Rev.* 30, 175–318. \[https://doi.org/10.1016/0012-8252\\(91\\)90001-V\]\(https://doi.org/10.1016/0012-8252\(91\)90001-V\), 1991.](#)

3035 [Hughes, A. L. C., Gyllenreutz, R., Lohne, Ø. S., Mangerud, J., & Svendsen, J. I. \(2016\). The last Eurasian ice sheets – a chronological database and time-slice reconstruction, DATED-1. *Boreas*, 45\(1\), 1–45. <https://doi.org/10.1111/bor.12142>](#)

3040 [Hughes, A. L. C., Rainsley, E., Murray, T., Fogwill, C. J., Schnabel, C., & Xu, S. \(2012\). Rapid response of Helheim Glacier, southeast Greenland, to early Holocene climate warming. *Geology*, 40\(5\), 427–430. <https://doi.org/10.1130/G32730.1>, <https://doi.org/10.1130/G32730.1>, 2012.](#)

3045 [Hughes, A. L. C., Brendryen, J., Gyllenreutz, R., Gowan, F., Mangerud, J., Svendsen, J. I. \(2023, July 14–20\). DATED-2: An updated ice-extent chronology for the last Eurasian ice sheet complex, 40–10 ka \[Conference presentation\]. 21st INQUA Congress, Rome, Italy.](#)

3050 [Hughes, A. L. C., Gyllenreutz, R., Lohne, Ø. S., Mangerud, J., and Svendsen, J. I.: The last Eurasian ice sheets - a chronological database and time-slice reconstruction, DATED-1, *Boreas*, 45, 1–45. <https://doi.org/10.1111/bor.12142>, 2016.](#)

3055 [Ingólfsson, Ó., Frich, P., Funder, S., & Humlum, O. \(1990\). Paleoclimatic implications of an early Holocene glacier advance on Disko Island, West Greenland. *Boreas*, 19\(4\), 297–311. <https://doi.org/10.1111/j.1502-3885.1990.tb00133.x>, <https://doi.org/10.1111/j.1502-3885.1990.tb00133.x>, 1990.](#)

3060 [Ingólfsson, Ó., Lyså, A., Funder, S., Möller, P., & Björk, S. \(1994\). Late Quaternary glacial history of the central west coast of Jameson Land, East Greenland. *Boreas*, 23\(4\), 447–458. <https://doi.org/10.1111/j.1502-3885.1994.tb00612.x>, <https://doi.org/10.1111/j.1502-3885.1994.tb00612.x>, 1994.](#)

Formatted: Font: Times New Roman, English (United Kingdom)

Formatted: Font: Times New Roman

Formatted: Space After: 8 pt

Formatted

Formatted: Font: Times New Roman

Formatted: Font: Times New Roman, English (United Kingdom)

Formatted: Font: Times New Roman, English (United Kingdom)

Formatted

Formatted: Space After: 8 pt

Formatted: Font: Times New Roman, English (United Kingdom)

Formatted: Font: Times New Roman, English (United Kingdom)

Formatted: Space After: 8 pt

Formatted: Font: Times New Roman, English (United Kingdom)

Formatted: Font: Times New Roman, English (United Kingdom)

Formatted: Font: Times New Roman, No underline, Font color: Auto, English (United Kingdom)

Formatted

Formatted: Space After: 8 pt

Formatted: Default Paragraph Font, Font: Times New Roman, 10 pt, English (United Kingdom)

Formatted: Font: Times New Roman, English (United Kingdom)

Formatted: Font: Times New Roman, English (United Kingdom)

Formatted: Font: Times New Roman, English (United Kingdom)

Formatted: Font: Times New Roman, English (United Kingdom)

Formatted

Formatted: Space After: 8 pt

Formatted

Formatted

Formatted

Formatted: Space After: 8 pt

Formatted

Ives, P. C., Levin, B., Robinson, R. D., & Rubin, M. (1964). U. S. Geological Survey Radiocarbon Dates VII. *Radiocarbon*, 6, 37-76. <https://doi.org/10.1017/s0033822200010547>, <https://doi.org/10.1017/s0033822200010547>, 1964.

3040 Jamieson, S. S. R., Vieli, A., Livingstone, S. J., Cofaigh, C. Ó., Stokes, C., Hillenbrand, C.-D., & Dowdeswell, J. A. (2012). Ice-stream stability on a reverse bed slope. *Nature Geoscience*, 5(11), *Nat. Geosci.*, 5, 799-802. <https://doi.org/10.1038/ngeo1600>, <https://doi.org/10.1038/ngeo1600>, 2012.

3045 Jennings, A. E., Andrews, J. T., Knudsen, K. L., Hansen, C. V., & Hald, M. (2002). A mid-Holocene shift in Arctic sea-ice variability on the East Greenland Shelf. *Holocene*, 12(1), 49-58. <https://doi.org/10.1191/0959683602hl519rp>, <https://doi.org/10.1191/0959683602hl519rp>, 2002.

3050 Jennings, A. E., Andrews, J. T., Ó Cofaigh, C., Onge, G. S., Sheldon, C., Belt, S. T., Cabedo-Sanz, P., & Hillaire-Marcel, C. (2017). Ocean forcing of Ice Sheet retreat in central west Greenland from LGM to the early Holocene. *Earth and Planetary Science Letters*, 472, 1-13. <https://doi.org/10.1016/j.epsl.2017.05.007>

Jennings, A. E., Hald, M., Smith, M., and Andrews, J. T.: Freshwater forcing from the Greenland Ice Sheet during the Younger Dryas: Evidence from southeastern Greenland shelf cores, in: *Quaternary Science Reviews*, 282-298, <https://doi.org/10.1016/j.quascirev.2005.04.006>, 2006.

3055 Jennings, A. E., Sheldon, C., Cronin, T. M., Francus, P., Stoner, J., & Andrews, J. (2011). The holocene history of nares strait: transition from Glacial Bay to Arctic- Atlantic Throughflow. *Oceanography*, 24(3), 26-41. <https://doi.org/10.5670/oceanog.2011.52>, <https://doi.org/10.5670/oceanog.2011.52>, 2011.

3060 Jennings, A. E., Walton, M. E., Ó Cofaigh, C., Kilfeather, A., Andrews, J. T., Ortiz, J. D., De Vernal, A., & Dowdeswell, J. A. (2014). Paleoenvironments during Younger Dryas-Early Holocene retreat of the Greenland Ice Sheet from outer Disko Trough, central west Greenland. *Journal of Quaternary Science*, 29(1), 27-40. <https://doi.org/10.1002/jqs.2652>, *J. Quat. Sci.*, 29, 27-40, <https://doi.org/10.1002/jqs.2652>, 2014.

3065 Jennings, A. E., Andrews, J. T., Ó Cofaigh, C., Onge, G. S., Sheldon, C., Belt, S. T., Cabedo-Sanz, P., and Hillaire-Marcel, C.: Ocean forcing of Ice Sheet retreat in central west Greenland from LGM to the early Holocene, *Earth Planet. Sci. Lett.*, 472, 1-13, <https://doi.org/10.1016/j.epsl.2017.05.007>, 2017.

Jones, R. S., Whitehouse, P. L., Bentley, M. J., Small, D., & Dalton, A. S. (2019). Impact of glacial isostatic adjustment on cosmogenic surface-exposure dating. *Quaternary Science Reviews*. <https://doi.org/10.1016/j.quascirev.2019.03.012>, *Quat. Sci. Rev.*, <https://doi.org/10.1016/j.quascirev.2019.03.012>, 2019.

3070 Joughin, I., Smith, B., Howat, I., & Scambos, T. (2018). MEaSURES Greenland Ice Sheet Velocity Map from InSAR Data, Version 2 (No. 2). NASA National Snow and Ice Data Center Distributed Active Archive Center, 2018.

Kaufman, D. S., & Williams, K. M. (1992). Radiocarbon date list VII: Baffin Island, NWT, Canada, including marine dates from adjacent seas and East Greenland. *Occasional Paper - Institute of Arctic & Alpine Research*, 48, *Occas. Pap. - Inst. Arct. Alp. Res.*, 48, 1992.

3075 Kelley, S. E., Briner, J. P., & Young, N. E. (2013). Babonis, G. S., and Csatho, B.: Maximum late Holocene extent of the western Greenland Ice Sheet during the late 20th century. *Quat. Sci. Rev.*, 56, 89-98, <https://doi.org/10.1016/j.quascirev.2012.09.016>, 2012.

Formatted: Font: Times New Roman

Formatted

Formatted: Space After: 8 pt

Formatted: Font: Times New Roman

Formatted: Font: Times New Roman, English (United Kingdom)

Formatted

Formatted: Space After: 8 pt

Formatted: Font: Times New Roman, English (United Kingdom)

Formatted: Font: Times New Roman, English (United Kingdom)

Formatted

Formatted: Space After: 8 pt

Formatted: Font: Times New Roman, English (United Kingdom)

Formatted: Font: Times New Roman, English (United Kingdom)

Formatted

Formatted: Space After: 8 pt

Formatted: Font: Times New Roman, English (United Kingdom)

Formatted: Font: Times New Roman, English (United Kingdom)

Formatted

Formatted: Space After: 8 pt

Formatted: Font: Times New Roman, English (United Kingdom)

Formatted: Font: Times New Roman, English (United Kingdom)

Formatted

Formatted: Space After: 8 pt

Formatted: Font: Times New Roman, English (United Kingdom)

Formatted

Formatted: Space After: 8 pt

Formatted

Formatted: Space After: 8 pt

Formatted

Formatted: Space After: 8 pt

Formatted

3080 [Kelley, S. E., Briner, J. P., and Young, N. E. \(2013\). Rapid ice retreat in Disko Bugt supported by ¹⁰Be dating of the last recession of the western Greenland Ice Sheet. *Quaternary Science Reviews*, 82, 13–22. <https://doi.org/10.1016/j.quascirev.2013.09.018>. *Quat. Sci. Rev.*, 82, 13–22. <https://doi.org/10.1016/j.quascirev.2013.09.018>, 2013.](#)

3085 [Kelley, S. E., Briner, J. P., Young, N. E., Babonis, G. S., & Csatho, B. \(2012\). Maximum late Holocene extent of the western Greenland Ice Sheet during the late 20th century. *Quaternary Science Reviews*, 56, 89–98. <https://doi.org/10.1016/j.quascirev.2012.09.016>](#)

3090 [Kelley, S. E., Briner, J. P., & Zimmerman, S. R. H. \(2015\). The influence of ice marginal setting on early Holocene retreat rates in central West Greenland. *Journal of Quaternary Science*, *J. Quat. Sci.*, 30\(3\), 271–280. <https://doi.org/10.1002/jqs.2778>. <https://doi.org/10.1002/jqs.2778>, 2015.](#)

3095 [Kelly, M. \(1973\). Radiocarbon dated shell samples from Nordre Strømfjord, West Greenland, with comments on models of glacio-isostatic uplift. *Rapport, Rapp. Grønlands GeologiskeGeol. Undersøgelse*, 59, 1–20. <https://doi.org/10.34194/rapggu.v59.7369>. <https://doi.org/10.34194/rapggu.v59.7369>, 1973.](#)

3100 [Kelly, M. \(1979\). Comments on the implications of new radiocarbon dates from the Holsteinsborg region, central West Greenland. *Rapport, Rapp. Grønlands GeologiskeGeol. Undersøgelse*, 95, 35–42. <https://doi.org/10.34194/rapggu.v95.7642>. <https://doi.org/10.34194/rapggu.v95.7642>, 1979.](#)

3105 [Kelly, M. \(1980\). Preliminary investigations of the Quaternary of Melville Bugt and Dundas, North-West Greenland. *Rapport, Rapp. Grønlands GeologiskeGeol. Undersøgelse*, 100\(100\), 33–38. <https://doi.org/10.34194/rapggu.v100.7691>. <https://doi.org/10.34194/rapggu.v100.7691>, 1980.](#)

3110 [Kelly, M., & Bennike, O. \(1985\). Quaternary geology of parts of central and western North Greenland: a preliminary account. *Rapport, Rapp. Grønlands GeologiskeGeol. Undersøgelse*, 126, 111–116. <https://doi.org/10.34194/rapggu.v126.7917>. <https://doi.org/10.34194/rapggu.v126.7917>, 1985.](#)

3115 [Kelly, M., & Bennike, O. \(1992\). Quaternary geology of western and central North Greenland. *Rapport, Rapp. Grønlands GeologiskeGeol. Undersøgelse*, 153, 1–34. <https://doi.org/https://doi.org/10.34194/rapggu.v153.8164>. <https://doi.org/https://doi.org/10.34194/rapggu.v153.8164>, 1992.](#)

[Kelly, M., & Funder, S. \(1974\). The pollen stratigraphy of late Quaternary lake sediments of South-West Greenland. *Rapport, Rapp. Grønlands GeologiskeGeol. Undersøgelse*, 64\(64\), 1–26. <https://doi.org/10.34194/rapggu.v64.7374>. <https://doi.org/10.34194/rapggu.v64.7374>, 1974.](#)

[Kelly, M., Funder, S., Houmark-nielsen, M., Knudsen, K. L., Kronborg, C., Landvik, J., & Sorby, L. \(1999\). Quaternary glacial and marine environmental history of northwest Greenland: a review and reappraisal. *Quaternary Science Reviews*, 18\(3\), 373–392. \[https://doi.org/10.1016/S0277-3791\\(98\\)00004-3\]\(https://doi.org/10.1016/S0277-3791\(98\)00004-3\). *Quat. Sci. Rev.*, 18, 373–392. \[https://doi.org/10.1016/S0277-3791\\(98\\)00004-3\]\(https://doi.org/10.1016/S0277-3791\(98\)00004-3\), 1999.](#)

[Kjær, K. H., Bjørk, A. A., Kjeldsen, K. K., Hansen, E. S., Andresen, C. S., Siggaard-Andersen, M.-L., Khan, S. A., Søndergaard, A. S., Colgan, W., Schomacker, A., Woodroffe, S., Funder, S., Rouillard, A., Jensen, J. F., and Larsen, N. K.: Glacier response to the Little Ice Age during the Neoglacial cooling in Greenland, *Earth-Science Rev.*, 227, 103984, <https://doi.org/10.1016/j.earscirev.2022.103984>, 2022.](#)

Formatted: Font: Times New Roman, English (United Kingdom)

Formatted: Space After: 8 pt

Formatted: Font: Times New Roman, English (United Kingdom)

Formatted: Font: Times New Roman, English (United Kingdom)

Formatted

Formatted: Space After: 8 pt

Formatted: Font: Times New Roman, English (United Kingdom)

Formatted

Formatted: Space After: 8 pt

Formatted: Font: Times New Roman, English (United Kingdom)

Formatted

Formatted

Formatted: Space After: 8 pt

Formatted

Formatted

Formatted: Space After: 8 pt

Formatted

Formatted

Formatted: Space After: 8 pt

Formatted

Formatted

Formatted: Space After: 8 pt

Formatted

Formatted: Font: Times New Roman

Formatted

Formatted: Space After: 8 pt

Formatted

120

Kjeldsen, K. K., Korsgaard, N. J., Bjørk, A. A., Khan, S. A., Box, J. E., Funder, S., Larsen, N. K., Bamber, J. L., Colgan, W., Van Den Broeke, M., Siggaard-Andersen, M. L., Nuth, C., Schomacker, A., Andresen, C. S., Willerslev, E., & Kjær, K. H. (2015). Spatial and temporal distribution of mass loss from the Greenland Ice Sheet since AD 1900. *Nature*, 528(7582), 396-400. <https://doi.org/10.1038/nature16183>, <https://doi.org/10.1038/nature16183>, 2015.

125

Knutz, P. C., Sicre, M. A., Ebbesen, H., Christiansen, S., & Kuijpers, A. (2011). Multiple-stage deglacial retreat of the southern Greenland Ice Sheet linked with Irminger Current warm water transport. *Paleoceanography*, 26(3). <https://doi.org/10.1029/2010PA002053>, <https://doi.org/10.1029/2010PA002053>, 2011.

130

Kuijpers, A., Troelstra, S. R., Prins, M. A., Linthout, K., Akhmetzhanov, A., Bouryak, S., Bachmann, M. F., Lassen, S., Rasmussen, S., & Jensen, J. B. (2003). Late Quaternary sedimentary processes and ocean circulation changes at the Southeast Greenland margin. *Marine Geology*, 195(1-4), 109-129. [https://doi.org/10.1016/S0025-3227\(02\)00684-9](https://doi.org/10.1016/S0025-3227(02)00684-9), *Mar. Geol.*, 195, 109-129, [https://doi.org/10.1016/S0025-3227\(02\)00684-9](https://doi.org/10.1016/S0025-3227(02)00684-9), 2003.

135

Laberg, J. S., Forwick, M., & Husum, K. (2017). New geophysical evidence for a revised maximum position of part of the NE sector of the Greenland ice sheet during the last glacial maximum. *Arktos*, 3(1), 3. <https://doi.org/10.1007/s41063-017-0029-4>, *arktos*, 3, 3, <https://doi.org/10.1007/s41063-017-0029-4>, 2017.

140

Landvik, J. Y., Weidick, A., & Hansen, A. (2001). The glacial history of the Hans Tausen Iskappe and the last glaciation of Peary Land, North Greenland Reconstructions of the glacial dynamics from spatial data mining View project Glacial history of Svalbard View project. *Meddelelser Omøn Grønland, Geoscience, Geosci.*, 39(May), 27-44. <https://www.researchgate.net/publication/230709679>, 2001.

145

Lane, T. P., Roberts, D. H., Rea, B. R., Cofaigh, C., Vieli, A., & Rodés, A. (2014). Controls upon the Last Glacial Maximum deglaciation of the northern Uummannaq Ice Stream System, West Greenland. *Quaternary Science Reviews*, 92, 324-344. <https://doi.org/10.1016/j.quascirev.2013.09.013>, *Quat. Sci. Rev.*, 92, 324-344, <https://doi.org/10.1016/j.quascirev.2013.09.013>, 2014.

150

Larsen, E., Fredin, O., Lyså, A., Amantov, A., Fjeldskaar, W., & Ottesen, D. (2016). Causes of time-transgressive glacial maxima positions of the last Scandinavian Ice Sheet. *Norwegian Journal of Geology, Nor. J. Geol.*, 96(2), 159-170. <https://doi.org/10.17850/njg96-2-06>, <https://doi.org/10.17850/njg96-2-06>, 2016.

155

Larsen, N. K., Funder, S., Kjær, K. H., Kjeldsen, K. K., Knudsen, M. F., & Linge, H. (2014). Rapid early Holocene ice retreat in West Greenland. *Quaternary Science Reviews, Quat. Sci. Rev.*, 92, 310-323. <https://doi.org/10.1016/j.quascirev.2013.05.027>, <https://doi.org/10.1016/j.quascirev.2013.05.027>, 2014.

160

Larsen, N. K., Kjær, K. H., Lecavalier, B., Bjørk, A. A., Colding, S., Huybrechts, P., Jakobsen, K. E., Kjeldsen, K. K., Knudsen, K. L., Odgaard, B. V., & Olsen, J. (2015). The response of the southern Greenland ice sheet to the Holocene thermal maximum. *Geology*, 43(4), 291-294. <https://doi.org/10.1130/G36476-1>, <https://doi.org/10.1130/G36476-1>, 2015.

Larsen, N. K., Levy, L. B., Carlson, A. E., Buizert, C., Olsen, J., Strunk, A., Bjørk, A. A., & Skov, D. S. (2018). Instability of the Northeast Greenland Ice Stream over the last 45,000 years. *Nature Communications, Nat. Commun.*, 9(1). <https://doi.org/10.1038/s41467-018-04312-7>, <https://doi.org/10.1038/s41467-018-04312-7>, 2018.

[Larsen, N. K., Søndergaard, A. S., Levy, L. B., Olsen, J., Strunk, A., Bjørk, A.](#)

Formatted

Formatted

Formatted

Formatted

Formatted

Formatted

Formatted

Formatted

Formatted

Formatted

Formatted

Formatted

Formatted

Formatted

Formatted

Formatted

Formatted

Formatted

Formatted

Formatted

Formatted

Formatted

Formatted

Formatted

Formatted

Formatted

Formatted

Formatted

Formatted

Formatted

Formatted

Formatted

Formatted

Formatted

Formatted

Formatted

Formatted

Formatted

Formatted

Formatted

[A., and Skov, D.: Contrasting modes of deglaciation between fjords and inter-fjord areas in eastern North Greenland. *Boreas*, 49, 903–917. <https://doi.org/10.1111/bor.12475>, 2020.](#)

[Larsen, N. K., Søndergaard, A. S., Levy, L. B., Laursen, C. H., Bjørk, A. A., Kjeldsen, K. K., Funder, S., Strunk, A., Olsen, J., & Kjær, K. H. \(2021\). Cosmogenic nuclide inheritance in Little Ice Age moraines - A case study from Greenland. *Quaternary Geochronology, Quat. Geochronol.*, 65. <https://doi.org/10.1016/j.quageo.2021.101200>, <https://doi.org/10.1016/j.quageo.2021.101200>, 2021.](#)

[Larsen, N. K., Søndergaard, A. S., Levy, L. B., Olsen, J., Strunk, A., Bjørk, A. A., & Skov, D. \(2020\). Contrasting modes of deglaciation between fjords and inter-fjord areas in eastern North Greenland. *Boreas*, 49\(4\), 903–917. <https://doi.org/10.1111/bor.12475>](#)

[Larsen, N. K., Søndergaard, A. S., Levy, L. B., Strunk, A., Skov, D. S., Bjørk, A., Khan, S. A., & Olsen, J. \(2022\). Late glacial and Holocene glaciation history of North and Northeast Greenland. *Arctic, Antarctic, and Alpine Research, Antarct. Alp. Res.*, 54\(1\), 294–313. <https://doi.org/10.1080/15230430.2022.2094607>, <https://doi.org/10.1080/15230430.2022.2094607>, 2022.](#)

[Lecavalier, B. S., Milne, G. A., Simpson, M. J. R., Wake, L., Huybrechts, P., Tarasov, L., Kjeldsen, K. K., Funder, S., Long, A. J., Woodroffe, S., Dyke, A. S., & Larsen, N. K. \(2014\). A model of Greenland ice sheet deglaciation constrained by observations of relative sea level and ice extent. *Quaternary Science Reviews, Quat. Sci. Rev.*, 102, 54–84. <https://doi.org/10.1016/j.quascirev.2014.07.018>, <https://doi.org/10.1016/j.quascirev.2014.07.018>, 2014.](#)

[Leger, T. P. M., Hein, A. S., Bingham, R. G., Martini, M. A., Soteres, R. L., Sagredo, E. A., & Martínez, O. A. \(2020\). The glacial geomorphology of the Río Corcovado, Río Huemul and Lago Palena / General Vintter valleys, northeastern Patagonia \(43° S, 71° W\). *Journal of Maps*, 16\(2\), 651–668. <https://doi.org/10.1080/17445647.2020.1794990>, *J. Maps*, 16, 651–668, <https://doi.org/10.1080/17445647.2020.1794990>, 2020.](#)

[Lesnek, A. J., & Briner, J. P. \(2018\). Response of a land-terminating sector of the western Greenland Ice Sheet to early Holocene climate change: Evidence from 10Be dating in the Søndre Isortoq region. *Quaternary Science Reviews, Quat. Sci. Rev.*, 180, 145–156. <https://doi.org/10.1016/j.quascirev.2017.11.028>, <https://doi.org/10.1016/j.quascirev.2017.11.028>, 2018.](#)

[Levy, L. B., Kelly, M. A., Howley, J. A., and Virginia, R. A., Levy, L. B., Kelly, M. A., Applegate, P. A., Howley, J. A., & Virginia, R. A. \(2018\). Middle to late Holocene chronology of the western margin of the Greenland Ice Sheet: A comparison with Holocene temperature and precipitation records. *Arctic, Antarctic, and Alpine Research*, 50\(1\). <https://doi.org/10.1080/15230430.2017.1414477>](#)

[Levy, L. B., Kelly, M. A., Howley, J. A., & Virginia, R. A. \(2012\). Age of the Ørkendalen moraines, Kangerlussuaq, Greenland: Constraints on the extent of the southwestern margin of the Greenland Ice Sheet during the Holocene. *Quaternary Science Reviews, Quat. Sci. Rev.*, 52, 1–5. <https://doi.org/10.1016/j.quascirev.2012.07.021>, <https://doi.org/10.1016/j.quascirev.2012.07.021>, 2012.](#)

[Levy, L. B., Kelly, M. A., Lowell, T. V., Hall, B. L., Howley, J. A., & Smith, C. A. \(2016\). Coeval fluctuations of the Greenland ice sheet and a local glacier, central East Greenland, during late glacial and early Holocene time. *Geophysical Research Letters*, 43\(4\), 1623–1631. <https://doi.org/10.1002/2015GL067108>, *Geophys. Res. Lett.*, 43, 1623–1631, <https://doi.org/10.1002/2015GL067108>, 2016.](#)

[Levy, L. B., Larsen, N. K., Davidson, T. A., Strunk, A., Olsen, J., & Jeppesen, E. \(2017\). Contrasting evidence of Holocene ice margin retreat, south-western Greenland. *Journal of Quaternary Science, J. Quat. Sci.*, 32\(5\), 604–616. <https://doi.org/10.1002/jqs.2957>, <https://doi.org/10.1002/jqs.2957>, 2017.](#)

[Levy, L. B., Kelly, M. A., Applegate, P. A., Howley, J. A.,](#)

Formatted: Font: Times New Roman, English (United Kingdom)

Formatted

Formatted: Space After: 8 pt

Formatted: Font: Times New Roman, English (United Kingdom)

Formatted: Font: Times New Roman, English (United Kingdom)

Formatted: Font: Times New Roman, English (United Kingdom)

Formatted

Formatted: Space After: 8 pt

Formatted: Font: Times New Roman, English (United Kingdom)

Formatted: Font: Times New Roman, English (United Kingdom)

Formatted: Space After: 8 pt

Formatted

Formatted: Font: Times New Roman, English (United Kingdom)

Formatted: Font: Times New Roman, English (United Kingdom)

Formatted

Formatted: Space After: 8 pt

Formatted

Formatted

Formatted

Formatted: Space After: 8 pt

Formatted

Formatted

Formatted

Formatted

Formatted: Space After: 8 pt

Formatted

Formatted

Formatted

Formatted: Space After: 8 pt

Formatted

Formatted

Formatted

Formatted: Space After: 8 pt

Formatted

205 [and Virginia, R. A.: Middle to late Holocene chronology of the western margin of the Greenland Ice Sheet: A comparison with Holocene temperature and precipitation records, Arctic, Antarct. Alp. Res., 50, <https://doi.org/10.1080/15230430.2017.1414477>, 2018.](#)

210 [Levy, L. B., Larsen, N. K., Knudsen, M. F., Egholm, D. L., Bjørk, A. A., Kjeldsen, K. K., Kelly, M. A., Howley, J. A., Olsen, J., Tikhomirov, D., Zimmerman, S. R. H., & Kjær, K. H. \(2020\). Multi-phased deglaciation of south and southeast Greenland controlled by climate and topographic setting. *Quaternary Science Reviews*, 242. <https://doi.org/10.1016/j.quascirev.2020.106454>, *Quat. Sci. Rev.*, 242, <https://doi.org/10.1016/j.quascirev.2020.106454>, 2020.](#)

215 [Lifton, N., Sato, T., & Dunai, T. J. \(2014\). Scaling in situ cosmogenic nuclide production rates using analytical approximations to atmospheric cosmic-ray fluxes. *Earth and Planetary Science Letters*, 386, 149–160. <https://doi.org/10.1016/j.epsl.2013.10.052>, *Earth Planet. Sci. Lett.*, 386, 149–160, <https://doi.org/10.1016/j.epsl.2013.10.052>, 2014.](#)

220 [Lin, Y., Hibbert, F. D., Whitehouse, P. J., Woodroffe, S. A., Purcell, A., Shennan, I., & Bradley, S. L. \(2021\). A reconciled solution of Meltwater Pulse 1A sources using sea-level fingerprinting. *Nature Communications*, 12\(1\). <https://doi.org/10.1038/s41467-021-21990-y>](#)

225 [Lloyd, J. M., Park, L. A., Kuijpers, A., & Moros, M. \(2005\). Early Holocene palaeoceanography and deglacial chronology of Disko Bugt, West Greenland. *Quaternary Science Reviews*, *Quat. Sci. Rev.*, 24\(14–15\), 1741–1755. <https://doi.org/10.1016/j.quascirev.2004.07.024>, <https://doi.org/10.1016/j.quascirev.2004.07.024>, 2005.](#)

230 [Lloyd, J. M., Ribeiro, S., Weckström, K., Callard, L., Ó Cofaigh, C., Leng, M. J., Gulliver, P., & Roberts, D. H. \(2023\). Ice-ocean interactions at the Northeast Greenland Ice stream \(NEGIS\) over the past 11,000 years. *Quaternary Science Reviews*, *Quat. Sci. Rev.*, 308, <https://doi.org/10.1016/j.quascirev.2023.108068>, <https://doi.org/10.1016/j.quascirev.2023.108068>, 2023.](#)

235 [Long, A. J., & Roberts, D. H. \(2002\). A revised chronology for the “Fjord Stade” moraine in Disko Bugt, west Greenland. *Journal of Quaternary Science*, *J. Quat. Sci.*, 17\(5–6\), 561–579. <https://doi.org/10.1002/jqs.705>, <https://doi.org/10.1002/jqs.705>, 2002.](#)

240 [Long, A. J., & Roberts, D. H. \(2003\). Late Weichselian deglacial history of Disko Bugt, West Greenland, and the dynamics of the Jakobshavns Isbrae ice stream. *Boreas*, 32\(1\), 208–226. <https://doi.org/10.1111/j.1502-3885.2003.tb01438.x>, *Boreas*, 32, 208–226, <https://doi.org/10.1111/j.1502-3885.2003.tb01438.x>, 2003.](#)

245 [Long, A. J., Roberts, D. H., & Dawson, S. \(2006\). Early Holocene history of the west Greenland Ice Sheet and the GH-8.2 event. *Quaternary Science Reviews*, 25\(9–10\), 904–922. <https://doi.org/10.1016/j.quascirev.2005.07.002>](#)

[Long, A. J., Roberts, D. H., & Rasch, M. \(2003\). New observations on the relative sea-level and deglacial history of Greenland from Innaarsuit, Disko Bugt. *Quaternary Research*, 60\(2\), 162–171. \[https://doi.org/10.1016/S0033-5894\\(03\\)00085-1\]\(https://doi.org/10.1016/S0033-5894\(03\)00085-1\)](#)

[Long, A. J., Roberts, D. H., Simpson, M. J. R., Dawson, S., Milne, G. A., & Huybrechts, P. \(2008\). Late Weichselian relative sea-level changes and ice sheet history in southeast Greenland. *Earth and Planetary Science Letters*, 272\(1–2\), 8–18. <https://doi.org/10.1016/j.epsl.2008.03.042>](#)

[Long, A. J., Roberts, D. H., & Wright, M. R. \(1999\). Isolation basin stratigraphy and Holocene relative sea-level change on Arveprinsen Eiland, Disko Bugt, West Greenland. *JOURNAL OF QUATERNARY SCIENCE*, 14\(4\), 323–345. \[https://doi.org/10.1002/\\(SICI\\)1099-1417\\(199907\\)14:4<323::AID-JQS442>3.0.CO;2-0\]\(https://doi.org/10.1002/\(SICI\)1099-1417\(199907\)14:4<323::AID-JQS442>3.0.CO;2-0\), *J. Quat. Sci.*, 14, 323–345, \[https://doi.org/10.1002/\\(SICI\\)1099-1417\\(199907\\)14:4<323::AID-JQS442>3.0.CO;2-0\]\(https://doi.org/10.1002/\(SICI\)1099-1417\(199907\)14:4<323::AID-JQS442>3.0.CO;2-0\), 1999.](#)

Formatted: Font: Times New Roman, English (United Kingdom)

Formatted: Space After: 8 pt

Formatted ...

Formatted: Font: Times New Roman, English (United Kingdom)

Formatted: Font: Times New Roman, English (United Kingdom)

Formatted ...

Formatted: Space After: 8 pt

Formatted: Font: Times New Roman, English (United Kingdom)

Formatted: Font: Times New Roman, English (United Kingdom)

Formatted ...

Formatted: Font: Times New Roman, English (United Kingdom)

Formatted: Space After: 8 pt

Formatted: Font: Times New Roman, English (United Kingdom)

Formatted: Font: Times New Roman, English (United Kingdom)

Formatted ...

Formatted: Space After: 8 pt

Formatted: Font: Times New Roman, English (United Kingdom)

Formatted ...

Formatted ...

Formatted: Space After: 8 pt

Formatted ...

Long, A. J., Roberts, D. H., and Rasch, M.: New observations on the relative sea level and deglacial history of Greenland from Innaarsuit, Disko Bugt. *Quat. Res.*, 60, 162–171, [https://doi.org/10.1016/S0033-5894\(03\)00085-1](https://doi.org/10.1016/S0033-5894(03)00085-1), 2003.

250 Long, A. J., Roberts, D. H., and Dawson, S.: Early Holocene history of the west Greenland Ice Sheet and the GH-8.2 event. *Quat. Sci. Rev.*, 25, 904–922, <https://doi.org/10.1016/j.quascirev.2005.07.002>, 2006.

Long, A. J., Roberts, D. H., Simpson, M. J. R., Dawson, S., Milne, G. A., and Huybrechts, P.: Late Weichselian relative sea-level changes and ice sheet history in southeast Greenland. *Earth Planet. Sci. Lett.*, 272, 8–18, <https://doi.org/10.1016/j.epsl.2008.03.042>, 2008.

255 Long, A. J., Woodroffe, S. A., Roberts, D. H., and Dawson, S.: Isolation basins, sea-level changes and the Holocene history of the Greenland Ice Sheet. *Quat. Sci. Rev.*, 30, 3748–3768, <https://doi.org/10.1016/j.quascirev.2011.10.013>, 2011.

Lowell, T. V., Kelly, M. A., Howley, J. A., Fisher, T. G., Barnett, P. J., Schwartz, R., Zimmerman, S. R. H., Norris, N., & Malone, A. G. O. (2021). Near-constant retreat rate of a terrestrial margin of the Laurentide Ice Sheet during the last deglaciation. *Geology*, 49(12), 1511–1515. <https://doi.org/10.1130/G49081-1>, <https://doi.org/10.1130/G49081-1>, 2021.

260 Manley, W. F., & Jennings, A. E. (1996). Radiocarbon date list VIII: Eastern Canadian Arctic, Labrador, Northern Quebec, East Greenland shelf, Iceland shelf, and Antarctica. Institute of Arctic and Alpine Research, Occasional Paper, 50, 163.

265 Marienfeld, P. (1990). Faziesvariationen glazialmariner Sedimente im Scoresby-Sund, Ost-Grönland. *Zentralblatt Für Geologie Und für Geol. und Paläontologie*, 1(41), 1739–1749, 1990.

McCarthy, D. J. (2011). Late Quaternary ice-ocean interactions in central West Greenland. Durham University, Durham, 0–292 pp., 2011.

270 Mejdahl, V. and Funder, S.: Luminescence dating of Late Quaternary sediments from East Greenland. *Boreas*, 23, 525–535, <https://doi.org/10.1111/j.1502-3885.1994.tb00620.x>, 1994.

Meredith, M., M. Sommerkorn, S. M., Cassotta, C. S., Derksen, A. C., Ekaykin, A., Hollowed, G. A., Kofinas, A. G., Mackintosh, J. A., Melbourne-Thomas, M. M. C. I., Muelbert, G. M. M. C., Ottersen, H. G., Pritchard, H., and E. A. G. Schuur. (2019). E. A. G.; *Polar Regions: In: regions. Chapter 3 IPCC Special Report on the Ocean and Cryosphere in a Changing Climate* (H. O. Pörtner, D. C. Roberts, V. Masson-Delmotte, P. Zhai, M. Tignor, E. Poloczanska, K. Mintenbeck, A. Alegria, M. Nicolai, A. Okem, J. Petzold, B. Rama, N. M. Weyer (eds.)). Cambridge University Press, Cambridge, UK and New York, NY, USA, pp. 203–320. <https://doi.org/10.1017/9781009157964.005>, pp. 2019.

275 Mienert, J., Andrews, J. T., & Milliman, J. D. (1992). The East Greenland continental margin (65°N) since the last deglaciation: Changes in seafloor properties and ocean circulation. *Marine Geology* (Vol. 106), 217–238 pp., 1992.

280 Möller, P., Larsen, N. K., Kjær, K. H., Funder, S., Schomacker, A., Linge, H., & Fabel, D. (2010). Early to middle Holocene valley glaciations on northernmost Greenland. *Quaternary Science Reviews: Quat. Sci. Rev.*, 29(25–26), 3379–3398. <https://doi.org/10.1016/j.quascirev.2010.06.044>, <https://doi.org/10.1016/j.quascirev.2010.06.044>, 2010.

285 Mørligheim, M., Williams, C. N., Rignot, E., An, L., Arndt, J. E., Bamber, J. L., Catania, G., Chauché, N., Dowdeswell, J. A., Dorschel, B., Fenty, I., Hogan, K., Howat, I., Hubbard, A., Jakobsson, M., Jordan, T. M., Kjeldsen, K. K., Millan, R., Mayer, L., Zinglensen, K. B. (2017). Mougnot, J., Noël, B. P. Y., O’Cofaigh, C., Palmer, S., Rysgaard, S., Seroussi, H., Siegert, M. J., Slabon, P., Straneo, F., van den Broeke, M. R., Weinrebe, W., Wood, M., and Zinglensen, K. B.; BedMachine v3: Complete Bed Topography and Ocean Bathymetry

Formatted: Font: Times New Roman, English (United Kingdom)

Formatted: Font: Times New Roman, English (United Kingdom)

Formatted: Font: Times New Roman, English (United Kingdom)

Formatted

Formatted: Space After: 8 pt

Formatted: Font: Times New Roman, English (United Kingdom)

Formatted: Font: Times New Roman, English (United Kingdom)

Formatted

Formatted: Space After: 8 pt

Formatted: Font: Times New Roman, English (United Kingdom)

Formatted

Formatted: Space After: 8 pt

Formatted: Font: Times New Roman, English (United Kingdom)

Formatted

Formatted: Space After: 8 pt

Formatted: Font: Times New Roman, English (United Kingdom)

Formatted: Font: Times New Roman, English (United Kingdom)

Formatted

Formatted: Space After: 8 pt

Formatted: Font: Times New Roman, English (United Kingdom)

Formatted

Formatted: Space After: 8 pt

Formatted: Font: Times New Roman, English (United Kingdom)

Formatted: Font: Times New Roman, English (United Kingdom)

Formatted: Space After: 8 pt

Formatted: Font: Times New Roman, English (United Kingdom)

3290 Mapping of Greenland From Multibeam Echo Sounding Combined With Mass Conservation. *Geophysical Research Letters*, 44(21), 11,051–11,061. <https://doi.org/10.1002/2017GL074954>. *Geophys. Res. Lett.*, 44, 11,051–11,061. <https://doi.org/10.1002/2017GL074954>, 2017.

Nelson, A. H., Bierman, P. R., Shakun, J. D., & Rood, D. H. (2014). Using in situ cosmogenic ¹⁰Be to identify the source of sediment leaving Greenland. *Earth Surface Processes and Surf. Process. Landforms*, 39(8), 1087–1100. <https://doi.org/10.1002/esp.3565>. <https://doi.org/10.1002/esp.3565>, 2014.

3295 Newton, A. M. W., Knutz, P. C., Huuse, M., Gannon, P., Brocklehurst, S. H., Clausen, O. R., & Gong, Y. (2017). Ice stream reorganization and glacial retreat on the northwest Greenland shelf. *Geophysical Research Letters*, *Geophys. Res. Lett.*, 44(15), 7826–7835. <https://doi.org/10.1002/2017GL073690>. <https://doi.org/10.1002/2017GL073690>, 2017.

3300 Nichols, R. (1969). Geomorphology of Inglefield Land, North Greenland. *Meddelelser Om Grønland, om Grøn.*, 1, 109, 1969.

Niwano, M., Box, J. E., Wehrlé, A., Vandecrux, B., Colgan, W. T., & Cappelen, J. (2021). Rainfall on the Greenland Ice Sheet: Present-Day Climatology From a High-Resolution Non-Hydrostatic Polar Regional Climate Model. *Geophysical Research Letters*, 48(15). <https://doi.org/10.1029/2021GL092942>. *Geophys. Res. Lett.*, 48. <https://doi.org/10.1029/2021GL092942>, 2021.

3305 Nørgaard-Pedersen, N., Spielhagen, R. F., Erlenkeuser, H., Grootes, P. M., Heinemeier, J., and Knies, J.: Arctic Ocean during the Last Glacial Maximum: Atlantic and polar domains of surface water mass distribution and ice cover. *Paleoceanography*, 18, 1–19. <https://doi.org/10.1029/2002PA000781>, 2003.

Nørgaard-Pedersen, N., Mikkelsen, N., & Kristoffersen, Y. (2008). Late glacial and Holocene marine records from the Independence Fjord and Wandel Sea regions, North Greenland. *Polar Research*, 27(2), 209–221. <https://doi.org/10.1111/j.1751-8369.2008.00065.x>. *Polar Res.*, 27, 209–221. <https://doi.org/10.1111/j.1751-8369.2008.00065.x>, 2008.

3310 Norris, S. L., Tarasov, L., Monteath, A. J., Gosse, J. C., Hidy, A. J., Margold, M., & Froese, D. G. (2022). Rapid retreat of the southwestern Laurentide Ice Sheet during the Bølling-Allerød interval. *Geology*, 50(4), 417–421. <https://doi.org/10.1130/G49493.1>. <https://doi.org/10.1130/G49493.1>, 2022.

3315 Ó Cofaigh, C., Dowdeswell, J. A., Evans, J., Kenyon, N. H., Taylor, J., Mienert, J., & Wilken, M. (2004). Timing and significance of glacially influenced mass-wasting in the submarine channels of the Greenland Basin. *Marine Geology*, 207(1–4), 39–54. <https://doi.org/10.1016/j.margeo.2004.02.009>. *Mar. Geol.*, 207, 39–54. <https://doi.org/10.1016/j.margeo.2004.02.009>, 2004.

3320 Ó Cofaigh, C., Dowdeswell, J. A., Jennings, A. E., Hogan, K. A., Kilfeather, A., Hiemstra, J. F., Noormets, R., Evans, J., McCarthy, D. J., Andrews, J. T., Lloyd, J. M., & Moros, M. (2013). An extensive and dynamic ice sheet on the west Greenland shelf during the last glacial cycle. *Geology*, 41(2), 219–222. <https://doi.org/10.1130/G33759.1>. <https://doi.org/10.1130/G33759.1>, 2013.

3325 Ó Cofaigh, C., Roberts, D. H., Callard, J., Lloyd, J., Ware, G., Streuff, K., Kanszow, T. (2023). Shelf edge terminating glaciation offshore of northeast Greenland during the Last Glacial Maximum and timing of initial ice sheet retreat [Conference poster]. 21st INQUA Congress, Rome, Italy.

Formatted: Font: Times New Roman, English (United Kingdom)

Formatted: Font: Times New Roman, English (United Kingdom)

Formatted

Formatted: Space After: 8 pt

Formatted: Font: Times New Roman, English (United Kingdom)

Formatted: Font: Times New Roman, English (United Kingdom)

Formatted

Formatted: Space After: 8 pt

Formatted

Formatted

Formatted

Formatted: Space After: 8 pt

Formatted

Formatted

Formatted: Space After: 8 pt

Formatted

Formatted

Formatted

Formatted

Formatted

Formatted

Formatted

Formatted

Formatted

Formatted

Formatted

Formatted

Formatted

Formatted

Formatted

Formatted

Formatted

Formatted

Formatted

Formatted

Formatted

Formatted

3330 Osman, M. B., Tierney, J. E., Zhu, J., Tardif, R., Hakim, G. J., King, J., & Poulsen, C. J. (2021). Globally resolved surface temperatures since the Last Glacial Maximum. *Nature*, 599(7884), 239–244. <https://doi.org/10.1038/s41586-021-03984-4>, 2021.

3335 Ootaka, I. N., Shepherd, A., Ivins, E. R., Schlegel, N.-J., Amory, C., van den Broeke, M. R., Horwath, M., Joughin, I., King, M. D., Krinner, G., Nowicki, S., Payne, A. J., Rignot, E., Scambos, T., Simon, K. M., Smith, B. E., Sørensen, L. S., Velicogna, I., Whitehouse, P. L., Wouters, B. (2023). Mass balance of the Greenland and Antarctic ice sheets from 1992 to 2020. *Earth System Science Data*, 15(4), 1597–1616. <https://doi.org/10.5194/essd-15-1597-2023>

3340 A., Agosta, C., Ahlström, A. P., Blazquez, A., Colgan, W., Engdahl, M. E., Fettweis, X., Forsberg, R., Gallée, H., Gardner, A., Gilbert, L., Gourmelen, N., Groh, A., Gunter, B. C., Harig, C., Helm, V., Khan, S. A., Kittel, C., Konrad, H., Langen, P. L., Lecavalier, B. S., Liang, C.-C., Loomis, B. D., McMillan, M., Melini, D., Mernild, S. H., Mottram, R., Mouginot, J., Nilsson, J., Noël, B., Pattle, M. E., Peltier, W. R., Pie, N., Roca, M., Sasgen, I., Save, H. V., Seo, K.-W., Scheuchl, B., Schrama, E. J. O., Schröder, L., Simonsen, S. B., Slater, T., Spada, G., Sutterley, T. C., Vishwakarma, B. D., van Wessem, J. M., Wiese, D., van der Wal, W., and Wouters, B.: Mass balance of the Greenland and Antarctic ice sheets from 1992 to 2020. *Earth Syst. Sci. Data*, 15, 1597–1616. <https://doi.org/10.5194/essd-15-1597-2023>, 2023.

3345 Pados-Dibattista, T., Pearce, C., Detlef, H., Bendtsen, J., & Seidenkrantz, M. S. (2022). Holocene palaeoceanography of the Northeast Greenland shelf. *Climate of the Past*, 18(1), 103–127. <https://doi.org/10.5194/cp-18-103-2022>, 2022.

3350 Patton, H., Hubbard, A., Andreassen, K., Auriac, A., Whitehouse, P. L., Stroeven, A. P., Shackleton, C., Winsborrow, M., Heyman, J., & Hall, A. M. (2017). Deglaciation of the Eurasian ice sheet complex. *Quaternary Science Reviews*, *Quat. Sci. Rev.*, 169, 148–172. <https://doi.org/10.1016/j.quascirev.2017.05.019>, <https://doi.org/10.1016/j.quascirev.2017.05.019>, 2017.

3355 Pearce, C., Özdemir, K. S., Forchhammer, R. C., Detlef, H., and Olsen, J. (in review). The marine reservoir age of Greenland coastal waters. *Geochronology* *Geochronol. Discuss. [preprint]*. <https://doi.org/10.5194/gchron-2023-7>, 2023, 1–26. <https://doi.org/10.5194/gchron-2023-7>, 2023.

3360 Pearce, D. M., Mair, D. W. F., Rea, B. R., Lea, J. M., Schofield, J. E., Kamenos, N., & Schoenrock, K. (2018). The glacial geomorphology of upper Godthåbsfjord (Nuup Kangerlua) in southwest Greenland. *Journal of Maps*, 14(2), 45–55. <https://doi.org/10.1080/17445647.2017.1422447>, <https://doi.org/10.1080/17445647.2017.1422447>, 2018.

3365 Pedersen, M., Weng, W. L., Keulen, N., & Kokfelt, T. F. (2013). A new seamless digital 1:500 000 scale geological map of Greenland. *GEUS Bulletin*, *Geol. Surv. Denmark Green. Bull.*, 28, 65–68. www.geus.dk/publications/bull, <https://doi.org/10.34194/geusb.v28.4727>, 2013.

3370 Perner, K., Moros, M., Snowball, I., Lloyd, J. M., Kuijpers, A., & Richter, T. (2013). Establishment of modern circulation pattern at 6000 cal a BP in Disko Bugt, central West Greenland: opening of the Vaigat Strait. *Journal of Quaternary Science*, 28(5), 480–489. <https://doi.org/10.1002/jqs.2638>, *J. Quat. Sci.*, 28, 480–489, <https://doi.org/10.1002/jqs.2638>, 2013.

Philippis, W., Briner, J. P., Bennike, O., Schweinsberg, A., Beel, C., & Lifton, N. (2017). Earliest Holocene deglaciation of the central Uummannaq Fjord system, West Greenland. *Boreas*, 47(4), 311–325. <https://doi.org/10.1111/bor.12270>, <https://doi.org/10.1111/bor.12270>, 2017.

Formatted: Font: Times New Roman, English (United Kingdom)

Formatted

Formatted: Space After: 8 pt

Formatted: Font: Times New Roman, English (United Kingdom)

Formatted: Font: Times New Roman, English (United Kingdom)

Formatted: Space After: 8 pt

Formatted: Font: Times New Roman, English (United Kingdom)

Formatted: Font: Times New Roman, No underline, Font color: Auto, English (United Kingdom)

Formatted

Formatted: Space After: 8 pt

Formatted: Default Paragraph Font, Font: Times New Roman, 10 pt, English (United Kingdom)

Formatted

Formatted

Formatted: Space After: 8 pt

Formatted

Formatted

Formatted: Space After: 8 pt

Formatted

Formatted

Formatted: Space After: 8 pt

Formatted

Formatted

Formatted: Space After: 8 pt

Formatted

Formatted

Formatted: Space After: 8 pt

Formatted

Formatted

Formatted: Space After: 8 pt

Formatted

Formatted

Formatted: Space After: 8 pt

Formatted

Formatted

3375 Pittard, M. L., Whitehouse, P. L., Bentley, M. J., & Small, D. (2022). An ensemble of Antarctic deglacial simulations constrained by geological observations. *Quaternary Science Reviews*, *Quat. Sci. Rev.*, 298, 107800. <https://doi.org/10.1016/j.quascirev.2022.107800>, <https://doi.org/10.1016/j.quascirev.2022.107800>, 2022.

Porter, Morin, C., Howat, P., Noh, I., Bates, M.-J., Peterman, B., Keesey, K., Schlenk, S., Gardiner, M., & Tomko, J. (2018). ArcticDEM. *Harvard Dataverse*, 1, 0–30, 2018.

3380 Puleo, P. J. K., Masterson, A. L., Medeiros, A. S., Schellinger, G., Steigleder, R., Woodroffe, S., Osburn, M. R., & Axford, Y. (2022). Younger Dryas and early Holocene climate in south Greenland inferred from oxygen isotopes of chironomids, aquatic Moss, and Moss cellulose. *Quaternary Science Reviews*, 296, 107810. <https://doi.org/10.1016/j.quascirev.2022.107810>, *Quat. Sci. Rev.*, 296, 107810, <https://doi.org/10.1016/j.quascirev.2022.107810>, 2022.

3385 Rasmussen, T. L., Pearce, C., Andresen, K. J., Nielsen, T., & Seidenkrantz, M. S. (2022). Northeast Greenland ice-free shelf edge at 79.4°N around the Last Glacial Maximum 25.5–17.5 ka. *Boreas*. <https://doi.org/10.1111/bor.12593>, 2022.

Reimer, P. J. and Reimer, R. W.: A marine reservoir correction database and on-line interface. *Radiocarbon*, 43, 461–463. <https://doi.org/10.1017/s0033822200038339>, 2001.

3390 Reimer, P. J., Austin, W. E. N., Bard, E., Bayliss, A., Blackwell, P. G., Bronk Ramsey, C., Butzin, M., Cheng, H., Edwards, R. L., Friedrich, M., Grootes, P. M., Guilderson, T. P., Hajdas, I., Heaton, T. J., Hogg, A. G., Hughen, K. A., Kromer, B., Manning, S. W., Muscheler, R., Palmer, J. G., Pearson, C., Van Der Plicht, J., Reimer, R. W., Richards, D. A., Scott, E. M., Southon, J. R., Turney, C. S. M., Wacker, L., Adolphi, F., Büntgen, U., Capano, M., Fahrni, S. M., Fogtmann-Schulz, A., Friedrich, R., Köhler, P., Kudsk, S., Miyake, F., Olsen, J., Reinig, F., Sakamoto, M., Sookdeo, A., and Talamo, S. (2020). The IntCal20 Northern Hemisphere Radiocarbon Age Calibration Curve (0–55 cal kBP). *Radiocarbon*, 62(4), 725–757. <https://doi.org/10.1017/RDC.2020.41>, <https://doi.org/10.1017/RDC.2020.41>, 2020.

3395 Reimer, P. J., & Reimer, R. W. (2001). A marine reservoir correction database and on-line interface. *Radiocarbon*, 43(2 PART 1), 461–463. <https://doi.org/10.1017/s0033822200038339>

3400 Reusche, M. M., Marcott, S. A., Ceperley, E. G., Barth, A. M., Brook, E. J., Mix, A. C., & Caffee, M. W. (2018). Early to Late Holocene Surface Exposure Ages From Two Marine-Terminating Outlet Glaciers in Northwest Greenland. *Geophysical Research Letters*, 45(14), 7028–7039. <https://doi.org/10.1029/2018GL078266>, *Geophys. Res. Lett.*, 45, 7028–7039, <https://doi.org/10.1029/2018GL078266>, 2018.

3405 Rignot, E., & Mouginot, J. (2012). Ice flow in Greenland for the International Polar Year 2008–2009. *Geophysical Research Letters*, *Geophys. Res. Lett.*, 39(14), <https://doi.org/10.1029/2012GL051634>, <https://doi.org/10.1029/2012GL051634>, 2012.

Rinterknecht, V., Gorokhovich, Y., Schaefer, J., & Caffee, M. (2009). Preliminary 10Be chronology for the last deglaciation of the western margin of the Greenland Ice Sheet. *Journal of Quaternary Science*, 24(3), 270–278. <https://doi.org/10.1002/jqs.1226>, *J. Quat. Sci.*, 24, 270–278, <https://doi.org/10.1002/jqs.1226>, 2009.

3410 Rinterknecht, V., Jomelli, V., Brunstein, D., Favier, V., Masson-Delmotte, V., Bourlès, D., Leanni, L., & Schläppy, R. (2014). Unstable ice stream in Greenland during the Younger Dryas cold event. *Geology*, 42(9), 759–762. <https://doi.org/10.1130/G35929.1>, <https://doi.org/10.1130/G35929.1>, 2014.

Formatted: Font: Times New Roman, English (United Kingdom)

Formatted

Formatted: Space After: 8 pt

Formatted: Font: Times New Roman, English (United Kingdom)

Formatted: Font: Times New Roman, English (United Kingdom)

Formatted

Formatted: Space After: 8 pt

Formatted: Font: Times New Roman, English (United Kingdom)

Formatted

Formatted: Space After: 8 pt

Formatted

Formatted

Formatted

Formatted

Formatted: Space After: 8 pt

Formatted

Formatted

Formatted

Formatted

Formatted

Formatted

Formatted

Formatted: Space After: 8 pt

Formatted

Formatted

Formatted

Formatted: Space After: 8 pt

Formatted

Formatted

Formatted

Formatted

Formatted: Space After: 8 pt

Formatted

Formatted

Formatted

Formatted: Space After: 8 pt

Formatted

3415 [Roberts, D. H., Long, A. J., Schnabel, C., Davies, B. J., Xu, S., Simpson, M. J. R., & Huybrechts, P. \(2009\). Ice sheet extent and early deglacial history of the southwestern sector of the Greenland Ice Sheet. *Quaternary Science Reviews*, 28\(25–26\), 2760–2773. <https://doi.org/10.1016/j.quascirev.2009.07.002>](#)

3420 [Roberts, D. H., Long, A. J., Schnabel, C., Freeman, S., & Simpson, M. J. R. \(2008\). The deglacial history of southeast sector of the Greenland Ice Sheet during the Last Glacial Maximum. *Quaternary Science Reviews*, 27\(15–16\), 1505–1516. <https://doi.org/10.1016/j.quascirev.2008.04.008>, *Quat. Sci. Rev.*, 27, 1505–1516. <https://doi.org/10.1016/j.quascirev.2008.04.008>, 2008.](#)

[Roberts, D. H., Long, A. J., Schnabel, C., Davies, B. J., Xu, S., Simpson, M. J. R., & Huybrechts, P.: Ice sheet extent and early deglacial history of the southwestern sector of the Greenland Ice Sheet. *Quat. Sci. Rev.*, 28, 2760–2773. <https://doi.org/10.1016/j.quascirev.2009.07.002>, 2009.](#)

3425 [Roberts, D. H., Rea, B. R., Lane, T. P., Schnabel, C., & Rodés, A. \(2013\). New constraints on Greenland ice sheet dynamics during the last glacial cycle: Evidence from the Uummannaq ice stream system. *Journal of Geophysical Research: Earth Surface*, 118\(2\), 519–541. <https://doi.org/10.1002/jgrf.20032>, *J. Geophys. Res. Earth Surf.*, 118, 519–541. <https://doi.org/10.1002/jgrf.20032>, 2013.](#)

3430 [Rogozhina, I., Martinec, Z., Hagedoorn, J. M., Thomas, M., & Fleming, K. \(2011\). On the long-term memory of the Greenland ice sheet. *Journal of Geophysical Research: Earth Surface*, 116\(4\), 1–16. <https://doi.org/10.1029/2010JF001787>, 2011.](#)

3435 [Rootes, C. M., & Clark, C. D. \(2020\). Glacial trimlines to identify former ice margins and subglacial thermal boundaries: A review and classification scheme for trimline expression. *Earth-Science Reviews*, 210, 103355. <https://doi.org/10.1016/j.earscirev.2020.103355>, <https://doi.org/10.1016/j.earscirev.2020.103355>, 2020.](#)

[Sbarra, C. M., Briner, J. P., Graham, B. L., Poinar, K., Thomas, E. K., & Young, N. E. \(2022\). Evidence for a more extensive Greenland Ice Sheet in southwestern Greenland during the Last Glacial Maximum. *Geosphere*, 18\(4\), 1316–1329. <https://doi.org/10.1130/GES02432.1>, 2022.](#)

3440 [Seidenkrantz, M.-S., Kuijpers, A., Olsen, J., Pearce, C., Lindblom, S., Ploug, J., Przybylo, P., & Snowball, I. \(2019\). Southwest Greenland shelf glaciation during MIS 4 more extensive than during the Last Glacial Maximum. *Scientific Reports*, 9\(1\), 15617. <https://doi.org/10.1038/s41598-019-51983-3>, *Sci. Rep.*, 9, 15617. <https://doi.org/10.1038/s41598-019-51983-3>, 2019.](#)

3445 [Shotton, F. W., Williams, R. E. G., & Johnson, A. S. \(1974\). Birmingham University Radiocarbon Dates VIII. *Radiocarbon*, 16\(3\), 285–303. <https://doi.org/10.1017/s0033822200059610>, <https://doi.org/10.1017/s0033822200059610>, 1974.](#)

[Simonarson, L. A. \(1981\). Upper Pleistocene and Holocene marine deposits and faunas on the north coast of Nûgssuaq, West Greenland. *GRØNLANDS GEOLØGISKE/Geol. UNDERSØGELSE*, 140, 0–129. 1981.](#)

3450 [Simpson, M. J. R., Milne, G. A., Huybrechts, P., & Long, A. J. \(2009\). Calibrating a glaciological model of the Greenland ice sheet from the Last Glacial Maximum to present-day using field observations of relative sea level and ice extent. *Quaternary Science Reviews*, 28\(17–18\), 1631–1657. <https://doi.org/10.1016/j.quascirev.2009.03.004>, *Quat. Sci. Rev.*, 28, 1631–1657. <https://doi.org/10.1016/j.quascirev.2009.03.004>, 2009.](#)

Formatted: Font: Times New Roman, English (United Kingdom)

Formatted: Font: Times New Roman, English (United Kingdom)

Formatted

Formatted: Space After: 8 pt

Formatted: Font: Times New Roman, English (United Kingdom)

Formatted: Font: Times New Roman, English (United Kingdom)

Formatted

Formatted: Space After: 8 pt

Formatted

Formatted

Formatted

Formatted: Space After: 8 pt

Formatted

Formatted

Formatted

Formatted: Space After: 8 pt

Formatted

Formatted

Formatted: Space After: 8 pt

Formatted

Formatted

Formatted: Space After: 8 pt

Formatted

Formatted

Formatted

Formatted: Space After: 8 pt

Formatted

Formatted

Formatted: Space After: 8 pt

Formatted

Formatted

Formatted: Space After: 8 pt

Formatted

Formatted

Formatted: Space After: 8 pt

Formatted

Formatted

- 3455 Sinclair, G., Carlson, A. E., Mix, A. C., Lecavalier, B. S., Milne, G., Mathias, A., Buizert, C., & DeConto, R. (2016). Diachronous retreat of the Greenland ice sheet during the last deglaciation. *Quaternary Science Reviews, Quat. Sci. Rev.*, 145, 243–258. <https://doi.org/10.1016/j.quascirev.2016.05.040>, <https://doi.org/10.1016/j.quascirev.2016.05.040>, 2016.
- 3460 Skov, D. S., Andersen, J. L., Olsen, J., Jacobsen, B. H., Knudsen, M. F., Jansen, J. D., Larsen, N. K., & Egholm, D. L. (2020). Constraints from cosmogenic nuclides on the glaciation and erosion history of Dove Bugt, northeast Greenland. *Bulletin of the Geological Society of America*, 132(11–12), 2282–2294. <https://doi.org/10.1130/b35410.1>, *Bull. Geol. Soc. Am.*, 132, 2282–2294. <https://doi.org/10.1130/b35410.1>, 2020.
- 3465 Small, D., Clark, C. D., Chiverrell, R. C., Smedley, R. K., Bateman, M. D., Duller, G. A. T., Ely, J. C., Fabel, D., Medialdea, A., & Moreton, S. G. (2017). Devising quality assurance procedures for assessment of legacy geochronological data relating to deglaciation of the last British-Irish Ice Sheet. In *Earth Science Reviews* (Vol. 164, pp. 232–250). Elsevier B.V. <https://doi.org/10.1016/j.earscirev.2016.11.007>, <https://doi.org/10.1016/j.earscirev.2016.11.007>, 1 January 2017.
- Smith, L. M., & Licht, K. J. (2000). Radiocarbon Date List IX: Antarctica, Arctic Ocean, and the Northern North Atlantic, 2000.
- 3470 Smith, M. J., & Clark, C. D. (2005). Methods for the visualization of digital elevation models for landform mapping. *Earth Surface Processes and Landforms*, 30(7), 885–900. <https://doi.org/10.1002/esp.1210>
- 3475 Sofie Søndergaard, A., Krog Larsen, N., Steinemann, O., Olsen, J., Funder, S., Lundbek Egholm, D., & Henrik Kjær, K. (2020). Glacial history of Ingfield Land, north Greenland from combined in situ ¹⁰Be and ¹⁴C exposure dating. *Climate of the Past*, 16(5), 1999–2015. <https://doi.org/10.5194/cp-16-1999-2020>, *Clim. Past*, 16, 1999–2015, <https://doi.org/10.5194/cp-16-1999-2020>, 2020.
- Søndergaard, A. S., Larsen, N. K., Olsen, J., Strunk, A., & Woodroffe, S. (2019). Glacial history of the Greenland Ice Sheet and a local ice cap in Qaanaaq, northwest Greenland. *Journal of Quaternary Science, J. Quat. Sci.*, 34(7), 536–547. <https://doi.org/10.1002/jqs.3139>, <https://doi.org/10.1002/jqs.3139>, 2019.
- 3480 Sparrenbom, C. J., Bennike, O., Björck, S., & Lambeck, K. (2006). Holocene relative sea-level changes in the Qaqortoq area, southern Greenland. *Boreas*, 35(2), 171–187. <https://doi.org/10.1111/j.1502-3885.2006.tb01148.x>, <https://doi.org/10.1111/j.1502-3885.2006.tb01148.x>, 2006.
- 3485 Storms, J. E. A., de Winter, I. L., Overeem, I., Drijkoningen, G. G., & Lykke-Andersen, H. (2012). The Holocene sedimentary history of the Kangerlussuaq Fjord-valley fill, West Greenland. *Quaternary Science Reviews, Quat. Sci. Rev.*, 35, 29–50. <https://doi.org/10.1016/j.quascirev.2011.12.014>, <https://doi.org/10.1016/j.quascirev.2011.12.014>, 2012.
- 3490 Stroeven, A. P., Hättestrand, C., Kleman, J., Heyman, J., Fabel, D., Fredin, O., Goodfellow, B. W., Harbor, J. M., Jansen, J. D., Olsen, L., Caffee, M. W., Fink, D., Lundqvist, J., Rosqvist, G. C., Strömberg, B., & Jansson, K. N. (2016). Deglaciation of Fennoscandia. *Quaternary Science Reviews, Quat. Sci. Rev.*, 147, 91–121. <https://doi.org/10.1016/j.quascirev.2015.09.016>, <https://doi.org/10.1016/j.quascirev.2015.09.016>, 2016.
- 3495 Sugden, D. (1972). Deglaciation and Isostasy in the Sukkertoppen Ice Cap Area, West Greenland. *Arct. Alp. Res.*, 4, 97. <https://doi.org/10.1080/00040851.1972.12003631>, 1972.

Formatted: Font: Times New Roman, English (United Kingdom)

Formatted

Formatted: Space After: 8 pt

Formatted: Font: Times New Roman, English (United Kingdom)

Formatted: Font: Times New Roman, English (United Kingdom)

Formatted

Formatted: Space After: 8 pt

Formatted

Formatted

Formatted

Formatted: Space After: 8 pt

Formatted

Formatted

Formatted

Formatted

Formatted: Space After: 8 pt

Formatted

Formatted

Formatted: Space After: 8 pt

Formatted

Formatted

Formatted

Formatted: Space After: 8 pt

Formatted

Formatted: Font: Times New Roman

Formatted

Formatted: Space After: 8 pt

Formatted

Formatted

Formatted

Formatted: Space After: 8 pt

Formatted

Formatted

Formatted

Formatted: Space After: 8 pt

Formatted

Formatted

Formatted

van Tatenhove, F. G. M., van der Meer, J. J. M., — Arctic and Alpine Research, 4(2), 97-102. <https://doi.org/10.1080/00040851.1972.12003634> Koster, E. A.: Implications for Deglaciation Chronology from New AMS Age Determinations in Central West Greenland, Quat. Res., 45, 245–253. <https://doi.org/10.1006/qres.1996.0025>, 1996.

3500 Tauber, H. (1966).; Copenhagen Radiocarbon Dates VII. Radiocarbon, 8(Copenhagen IV), 213–234. <https://doi.org/10.1017/s003382220000126>, <https://doi.org/10.1017/s003382220000126>, 1966.

3505 Tauber, H. (1968).; Copenhagen Radiocarbon Dates IX. Radiocarbon, 10(2), 295–327. <https://doi.org/10.1017/s0033822200010912>, <https://doi.org/10.1017/s0033822200010912>, 1968.

Ten Brink, N. W., & Weidick, A. (1974). Greenland ice sheet history since the last glaciation. Quaternary Research, 4(4), 429–440. [https://doi.org/10.1016/0033-5894\(74\)90038-6](https://doi.org/10.1016/0033-5894(74)90038-6)

3510 The IMBIE Team. (2019).; Mass balance of the Greenland Ice Sheet from 1992 to 2018. Nature, 579(7798), 233–239. <https://doi.org/10.1038/s41586-019-1855-2>, <https://doi.org/10.1038/s41586-019-1855-2>, 2019.

Trautman, M. A. (1963).; Isotopes, Inc. Radiocarbon Measurements III. Radiocarbon, 5(1–2), 62–79. <https://doi.org/10.1017/S0033822200036794>, <https://doi.org/10.1017/S0033822200036794>, 1963.

3515 Trautman, M. A., & Willis, E. H. (1966).; Isotopes, Inc. Radiocarbon Measurements V. Radiocarbon, 8, 161–203. <https://doi.org/10.1017/S003382220000102>, <https://doi.org/10.1017/S003382220000102>, 1966.

3520 van Tatenhove, F. G. M., van der Meer, J. J. M., & Koster, E. A. (1996). Implications for Deglaciation Chronology from New AMS Age Determinations in Central West Greenland. Quaternary Research, 45(3), 245–253. <https://doi.org/10.1006/qres.1996.0025>

Wagner, B., & Melles, M. (2002).; Holocene environmental history of western Ymer Ø, East Greenland, inferred from lake sediments. Quaternary International, Quat. Int., 89(1), 165–176. [https://doi.org/10.1016/S1040-6182\(01\)00087-8](https://doi.org/10.1016/S1040-6182(01)00087-8), [https://doi.org/10.1016/S1040-6182\(01\)00087-8](https://doi.org/10.1016/S1040-6182(01)00087-8), 2002.

3525 Wagner, B., Melles, M., Hahne, J., Niessen, F., & Hubberten, H.-W. (2000).; Holocene climate history of Geographical Society Ø, East Greenland — evidence from lake sediments—Palaeogeography, Palaeoclimatology, Palaeoecology, Palaeogeogr. Palaeoclimatol. Palaeoecol., 160(1–2), 45–68. [https://doi.org/10.1016/S0031-0182\(00\)00046-8](https://doi.org/10.1016/S0031-0182(00)00046-8), [https://doi.org/10.1016/S0031-0182\(00\)00046-8](https://doi.org/10.1016/S0031-0182(00)00046-8), 2000.

3530 Washburn, A. L., & Stuiver, M. (1962).; Radiocarbon-Dated Postglacial Deleveling in Northeast Greenland and Its Implications. ARCTIC, 15(4), 66–73. <https://doi.org/10.14430/arctic3558>, 66–73. <https://doi.org/10.14430/arctic3558>, 1962.

Weidick, A. (1968).; Observations on some Holocene glacier fluctuations in West Greenland—Bulletin, Bull. Grønlands Geologiske Geol. Undersøgelse, 73(6), 1–202. <https://doi.org/10.34194/bullggu.v73.6611>, 1–202. <https://doi.org/10.34194/bullggu.v73.6611>, 1968.

3535 Weidick, A. (1971).; Short explanation to the Quaternary Map of Greenland—Rapport, Rapp. Grønlands Geologiske Geol. Undersøgelse, 36, 1–15. <https://doi.org/10.34194/rapggu.v36.7269>, <https://doi.org/10.34194/rapggu.v36.7269>, 1971.

Williams, K. M. (1993). Ice Sheet and Ocean Interactions, Margin of the East Greenland Ice Sheet (14 Ka to Present): Diatom Evidence. *Paleoceanography*, 8(1), 69–83. <https://doi.org/10.1029/92PA02594>, <https://doi.org/10.1029/92PA02591>, 1993.

Williams, K. M., Andrews, J. T., Weiner, N. J., & Mudie, P. J. (1995). Late Quaternary Paleooceanography of the Mid-to Outer Continental Shelf, East Greenland. *Arctic and Alpine Research*, 27(4), 352–363. <https://doi.org/10.1080/00040851.1995.12003132>, <https://doi.org/10.1080/00040851.1995.12003132>, 1995.

Winkelmann, R., Martin, M. A., Haseloff, M., Albrecht, T., Bueler, E., Khroulev, C., & Levermann, A. (2011). The Potsdam Parallel Ice Sheet Model (PISM-PIK) – Part 1: Model description. *The Cryosphere*, 5(3), 715–726. <https://doi.org/10.5194/tc-5-715-2011>, <https://doi.org/10.5194/tc-5-715-2011>, 2011.

Winsor, K., Carlson, A. E., and Rood, D. H., Winsor, K., Carlson, A. E., Caffee, M. W., & Rood, D. H. (2015). Rapid last deglacial thinning and retreat of the marine-terminating southwestern Greenland ice sheet. *Earth and Planetary Science Letters*, 426, 1–12. <https://doi.org/10.1016/j.epsl.2015.05.040>

Winsor, K., Carlson, A. E., & Rood, D. H. (2014). ¹⁰Be dating of the Narsarsuaq moraine in southernmost Greenland: Evidence for a late-Holocene ice advance exceeding the Little Ice Age maximum. *Quaternary Science Reviews*, 98, 135–143. <https://doi.org/10.1016/j.quascirev.2014.04.026>, *Quat. Sci. Rev.*, 98, 135–143, <https://doi.org/10.1016/j.quascirev.2014.04.026>, 2014.

Winsor, K., Carlson, A. E., Caffee, M. W., and Rood, D. H.: Rapid last-deglacial thinning and retreat of the marine-terminating southwestern Greenland ice sheet. *Earth Planet. Sci. Lett.*, 426, 1–12, <https://doi.org/10.1016/j.epsl.2015.05.040>, 2015.

Yang, H., Krebs-Kanzow, U., Kleiner, T., Sidorenko, D., Rodehacke, C. B., Shi, X., Gierz, P., Niu, L., Gowan, E. J., Hinck, S., Liu, X., Stap, L. B., & Lohmann, G. (2022). Impact of paleoclimate on present and future evolution of the Greenland Ice Sheet. *PLoS ONE*, 17(1 January), 1–21. <https://doi.org/10.1371/journal.pone.0259816>, <https://doi.org/10.1371/journal.pone.0259816>, 2022.

Yang, Q., Dixon, T. H., Myers, P. G., Bonin, J., Chambers, D., and Van Den Broeke, M. R.: Recent increases in Arctic freshwater flux affects Labrador Sea convection and Atlantic overturning circulation. *Nat. Commun.*, 7, <https://doi.org/10.1038/ncomms10525>, 2016.

Young, N. E., Briner, J. P., Axford, Y., Csatho, B., Babonis, G. S., Rood, D. H., & Finkel, R. C. (2011). Response of a marine-terminating Greenland outlet glacier to abrupt cooling 8200 and 9300 years ago. *Geophysical Research Letters*, 38(24), 1–4. <https://doi.org/10.1029/2011GL049639>, <https://doi.org/10.1029/2011GL049639>, 2011a.

Young, N. E., Briner, J. P., Stewart, H. A. M., Axford, Y., Csatho, B., Rood, D. H., and Finkel, R. C.: Response of Jakobshavn Isbrae, Greenland, to Holocene climate change. *Geology*, 39, 131–134, <https://doi.org/10.1130/G31399.1>, 2011b.

Young, N. E., Schaefer, J. M., Briner, J. P., and Goehring, B. M.: A ¹⁰Be production-rate calibration for the Arctic. *J. Quat. Sci.*, 28, 515–526, <https://doi.org/10.1002/jqs.2642>, 2013a.

Young, N. E., Briner, J. P., Rood, D. H., Finkel, R. C., Corbett, L. B., and Bierman, P. R.: Age of the Fjord Stade moraines in the Disko Bugt region, western Greenland, and the 9.3 and 8.2 ka cooling events. *Quat. Sci. Rev.*, 60, 76–90, <https://doi.org/10.1016/j.quascirev.2012.09.028>, 2013b.

Young, N. E., Briner, J. P., Miller, G. H., Lesnek, A. J., Crump, S. E., Thomas, E. K., Pendleton, S. L., Cuzzzone, J., Lamp, J., Zimmerman, S., Caffee, M., & Schaefer, J. M. (2020). Deglaciation of the Greenland and Laurentide ice sheets interrupted by glacier advance during abrupt coolings. *Quaternary Science Reviews*, 229, <https://doi.org/10.1016/j.quascirev.2019.106091>, *Quat. Sci. Rev.*, 229, <https://doi.org/10.1016/j.quascirev.2019.106091>, 2020.

Formatted: Font: Times New Roman, English (United Kingdom)

Formatted

Formatted: Space After: 8 pt

Formatted: Font: Times New Roman, English (United Kingdom)

Formatted: Font: Times New Roman, English (United Kingdom)

Formatted

Formatted: Space After: 8 pt

Formatted: Font: Times New Roman, English (United Kingdom)

Formatted: Font: Times New Roman, English (United Kingdom)

Formatted

Formatted: Space After: 8 pt

Formatted: Font: Times New Roman, English (United Kingdom)

Formatted: Font: Times New Roman, English (United Kingdom)

Formatted: Font: Times New Roman, English (United Kingdom)

Formatted: Space After: 8 pt

Formatted: Font: Times New Roman, English (United Kingdom)

Formatted: Font: Times New Roman, English (United Kingdom)

Formatted

Formatted: Space After: 8 pt

Formatted

Formatted

Formatted

Formatted

Formatted: Space After: 8 pt

Formatted

Formatted

Formatted

3620
3625
3630
3635
3640

Young, N. E., Briner, J. P., Rood, D. H., Finkel, R. C., Corbett, L. B., & Bierman, P. R. (2013). Age of the Fjord Stade moraines in the Disko Bugt region, western Greenland, and the 9.3 and 8.2 ka cooling events. Quaternary Science Reviews, 60, 76-90. <https://doi.org/10.1016/j.quascirev.2012.09.028>

Formatted: Font: Times New Roman, English (United Kingdom)

Young, N. E., Briner, J. P., Stewart, H. A. M., Axford, Y., Csatho, B., Rood, D. H., & Finkel, R. C. (2011). Response of Jakobshavn Isbrae, Greenland, to Holocene climate change. Geology, 39(2), 131-134. <https://doi.org/10.1130/G31399.1>

Formatted: Font: Times New Roman, English (United Kingdom)

Young, N. E., Lesnek, A. J., Cuzzone, J. K., Briner, J. P., Badgeley, J. A., Balter-Kennedy, A., Graham, B. L., Cluett, A., Lamp, J. L., Schwartz, R., Tuna, T., Bard, E., Caffee, M. W., Zimmerman, S. R. H., & Schaefer, J. M. (2021). In situ cosmogenic 10Be-14C-26Al measurements from recently deglaciated bedrock as a new tool to decipher changes in Greenland Ice Sheet size. *Climate of the Past*, 17(1), 419-450. <https://doi.org/10.5194/cp-17-419-2021>. *Clim. Past*, 17, 419-450. <https://doi.org/10.5194/cp-17-419-2021>, 2021.

Formatted: Font: Times New Roman, English (United Kingdom)

Formatted: Space After: 8 pt

Formatted: Font: Times New Roman, English (United Kingdom)

Young, N. E., Schaefer, J. M., Briner, J. P., & Goehring, B. M. (2013). A 10Be production rate calibration for the Arctic. *Journal of Quaternary Science*, 28(5), 515-526. <https://doi.org/10.1002/jqs.2642>

Formatted: Font: Times New Roman, English (United Kingdom)

Formatted: Font: Times New Roman, English (United Kingdom)

Formatted: Font: Times New Roman, English (United Kingdom)

Formatted: No underline, Font color: Auto

Formatted: Default Paragraph Font, Font: Times New Roman, 10 pt, English (United Kingdom)

Formatted: Line spacing: 1.5 lines

Formatted: Font: Times New Roman, 10 pt, English (United Kingdom)

Formatted: Normal